GEOLOGY OF THE INTERMOUNTAIN WEST
an open-access journal of the Utah Geological Association
ISSN 2380-7601

Volume 12 ***2025***

A RIVER RUNS THROUGH IT—THE QUARRY SANDSTONE AND ADJACENT STRATA, DINOSAUR NATIONAL MONUMENT, UTAH

Kenneth Carpenter and Louis H. Taylor

GEOLOGY OF THE INTERMOUNTAIN WEST

an open-access journal of the Utah Geological Association

ISSN 2380-7601

Volume 12 ***2025***

Production

Cover Design and Desktop Publishing
Douglas A. Sprinkel

Cover

An outcrop of the Quarry Sandstone in the Brushy Basin Member of the Upper Jurassic Morrison Formation located east of the Quarry Exhibit Hall, Dinosaur National Monument, Utah.

Become a member of the UGA to help support the work of the Association and receive notices for monthly meetings, annual field conferences, and new publications. Annual membership is $30 and annual student membership is only $5. Visit the UGA website at www.utahgeology.org for information and membership application.

The UGA board is elected annually by a voting process through UGA members. However, the UGA is a volunteer-driven organization, and we welcome your voluntary service. If you would like to participate please contact the current president or committee member corresponding with the area in which you would like to volunteer.

Utah Geological Association formed in 1970 from a merger of the Utah Geological Society, founded in 1946, and the Intermountain Association of Geologists, founded in 1949. Affiliated with the American Association of Petroleum Geologists.

GEOLOGY OF THE INTERMOUNTAIN WEST
an open-access journal of the Utah Geological Association
Volume 12 ***2025***

A River Runs Through It—The Quarry Sandstone and Adjacent Strata, Dinosaur National Monument, Utah

Kenneth Carpenter[1] and Louis H. Taylor[2]
[1]Museum of Natural History, University of Colorado, Boulder, CO 80309 USA; Kenneth.Carpenter-1@colorado.edu
[2]Littleton, CO 80128 USA; loutaylor44@aol.com

ABSTRACT

This study investigates the depositional environment, sedimentological dynamics, and tectonic influences that shaped the Quarry Sandstone within the Brushy Basin Member of the Upper Jurassic Morrison Formation in Dinosaur National Monument, Utah. Characterized by laterally extensive, multistory sandstone bodies, the origin of the Quarry Sandstone has been a subject of ongoing debate. By synthesizing new field data and revisiting existing interpretations, this research challenges prevailing hypotheses and offers new perspectives on the geological history of the Morrison Formation at the Monument. Whereas the Morrison Formation, deposited in a foreland basin setting on the Colorado Plateau, is generally well understood, the Quarry Sandstone's unique width-to-thickness ratio sets it apart from other sandstone units in the Brushy Basin Member. This distinct feature suggests a depositional history that cannot be fully explained by traditional foreland basin models. To address this anomaly, the study places the sandstone within its stratigraphic framework, emphasizing the critical role of accommodation space in shaping its deposition.

A key finding of this research is the proposed influence of a proto-Split Mountain anticline on the sedimentation patterns of the Quarry Sandstone. This minor structural feature, likely generated by oblique compressional forces associated with regional tectonics on the Colorado Plateau, appears to have played a pivotal role in reducing accommodation space during the deposition of the sandstone. Evidence for this reduction includes localized thinning of stratigraphic units and increased lateral connectivity of braided channel sandstones.

The structural uplift caused by the proto-Split Mountain anticline likely created an asymmetrical depositional setting. This uplift restricted accommodation, triggering a transition in fluvial systems from single-threaded sinuous channels to multithreaded braided rivers with frequent avulsions. The interconnected nature of these braided channels over time reshaped sediment distribution patterns, producing the distinctive characteristics of the Quarry Sandstone.

INTRODUCTION

The Morrison Formation, an extensive Upper Jurassic sedimentary succession in the Western United States, is renowned for its rich paleontological record and diverse depositional environments set within a foreland basin. Stretching from southern Alberta and Saskatchewan, Canada to New Mexico, United States, and encompassing over 1.8 million km^2, this formation offers a unique opportunity to study a variety of

Citation for this article.
Carpenter, K., and Taylor, L.H., 2025, A river runs through it—the Quarry Sandstone and adjacent strata, Dinosaur National Monument, Utah: Geology of the Intermountain West, v. 12, p. 25–74, https://doi.org/10.31711/giw.v12.pp25-74.

sedimentological processes and depositional settings. Morrison Formation stratigraphy features an array of lithologies, including fluvial sandstones, lacustrine mudstones, limestones, and overbank deposits, which collectively record the interplay of terrestrial and aquatic environments during the Late Jurassic period.

Historically, research on the Morrison Formation has focused primarily on its extraordinary dinosaur fossils since their earliest discoveries in 1877 (Cope, 1877; Marsh, 1877). However, recent advancements in sedimentology have expanded the emphasis toward understanding the depositional environments and sedimentary processes that contributed to the formation's geological complexity. These environments are interpreted to include meandering and braided river systems (e.g., Kjemperud et al., 2008; Hayden and Lamb, 2020), distributive fluvial systems (e.g., Weissmann et al., 2013; Owen et al., 2015), floodplains (e.g., Demko et al., 2004), lakes (e.g., Dunagan and Turner, 2004), and rare aeolian dunes (e.g., Peterson, 1994; Demko et al., 2004), each imparting distinct sedimentary structures and lithofacies. Detailed sedimentological analysis of these deposits reveals critical insights into the paleoclimatic conditions, paleohydrology, and tectonic influences that shaped the Morrison landscape (see papers in Carpenter et al., 1998; Turner and Peterson, 1998; Turner et al., 2004; Foster and Lucas, 2006).

A comprehensive sedimentological study involves the examination of grain size distributions, sedimentary structures, facies associations, and stratigraphic relations. These analyses help reconstruct paleoenvironments and elucidate the dynamic processes responsible for sediment deposition. With this in mind, we investigated the unusual ridge of sandstone in which the world-famous dinosaur quarry is developed at Dinosaur National Monument, Utah. The quarry originally occupied about 130 m of the 1500-m-long discontinuous sandstone ridge, which lies near the middle of the mudstone-dominated Brushy Basin Member of the Morrison Formation. This study investigated the relations among the stratigraphic architecture, sedimentary processes, accommodation, and depositional environment of the sandstone ridge in the context of the Brushy Basin. Examining how these factors interact provides a deeper understanding of the geological history and the conditions that led to the formation of the sandstone ridge and the preservation of dinosaur fossils within it.

GEOLOGICAL SETTING

The study area is on the southern side of Split Mountain, on the southeastern flank of the east-west trending Uinta Mountains in northeastern Utah (Figure 1). These mountains, also known as the Uinta arch or Uinta anticline, mark the northern boundary of the Colorado Plateau. Split Mountain is an anticline associated with the Uinta Mountains and is crossed by the Green River (Figure 2A), providing extensive exposures of Paleozoic and Mesozoic strata (Rowley et al., 1979; Sprinkel, 2019; Gregson et al., 2024).

The Morrison Formation, well exposed around the nose of the Split Mountain anticline, extends into the Yampa Plateau and Blue Mountain areas within Dinosaur National Monument, across the Utah-Colorado border (Figure 2B). The study area is specifically near the historic Carnegie Dinosaur Quarry, now housed within the Quarry Exhibit Hall (QEH), between Douglass Draw to the west and Swelter Shelter Draw to the east (Figure 2C). The famous dinosaur quarry is at the western end of the discontinuous sandstone ridge, which extends approximately 1.5 km through the Brushy Basin Member (Figure 3B). Referred to as the Quarry Sandstone here, this sandstone is the "quarry interval" of Turner and Peterson (1992a, 1992b) and "Quarry Sandstone" of Carpenter (2013) and Brezinski and Kollar (2018). Unusual for its lateral extent within the Brushy Basin Member, this sandstone and adjacent mudstone, are the focus of this study.

STUDY METHODS

We measured sections by tape and Brunton compass on both the east and west side of the QEH and through the thickest part of the remaining sandstone within the QEH (Figure 4). We integrated these sections with measured sections made by Fred ("Pete") Peterson (formerly of the U.S. Geological Survey) and shared with us (Figures 5 and 6). Peterson made his sections in 1991 using benchmark 4992.8 on the east side of the QEH for horizontal and vertical control. Peterson's sections averaged 30 m apart and connected laterally with

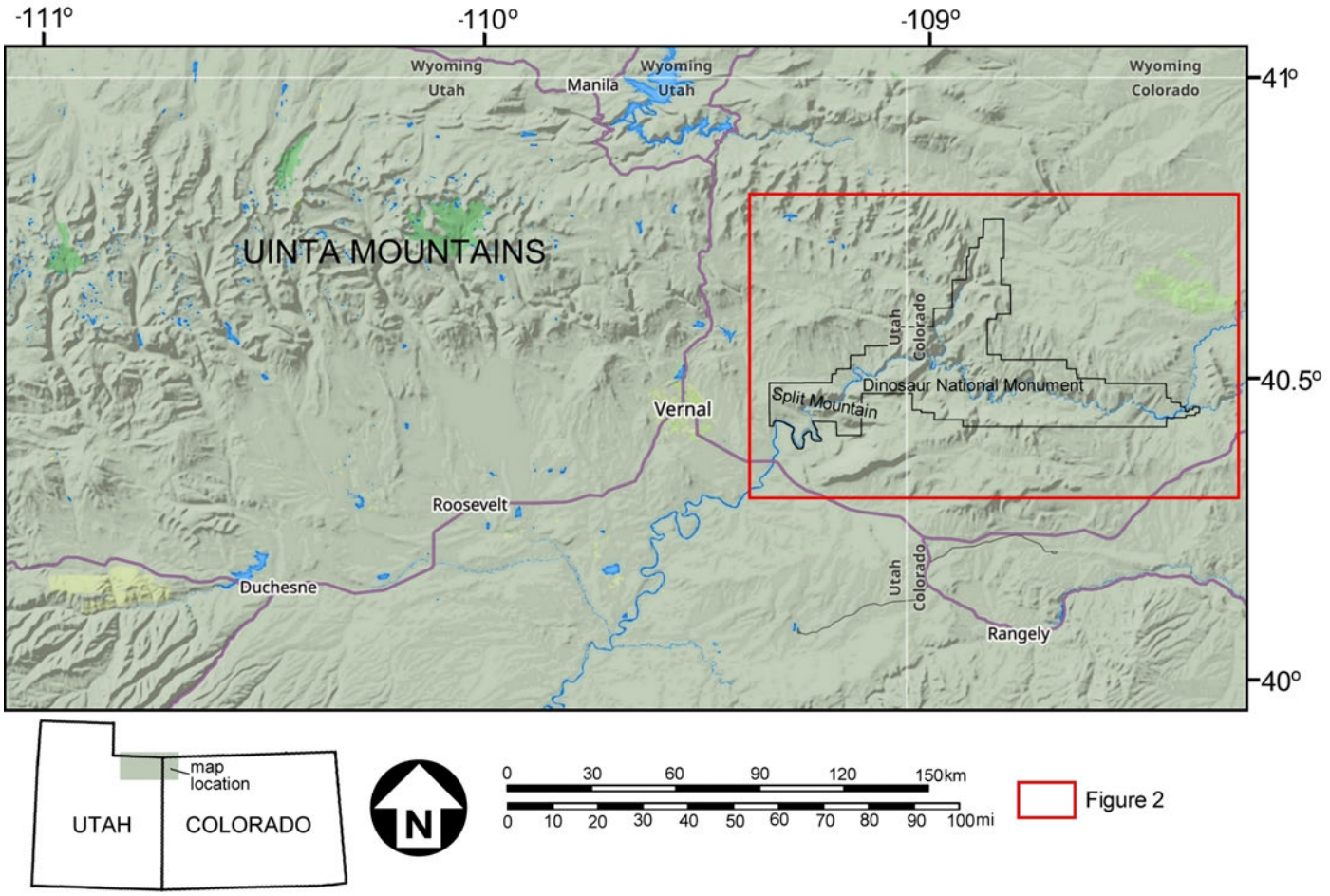

Figure 1. Map showing the Uinta Mountains of northeastern Utah and the location of Split Mountain and Dinosaur National Monument.

key beds and scour surfaces (Turner and Peterson, 1992a, 1993). Peterson made another stratigraphic section 550 m west of the QEH in Douglass Draw, which was designated as the primary or master stratigraphic reference section for the Morrison Formation by Turner and Peterson (1999) for their biostratigraphy of dinosaur localities (see STRATIGRAPHIC SETTING).

We used photographs taken at different times during the 1930s by various National Park Service employees, especially geologist Albert Boyle overseeing work crews of the Federal Emergency Relief Administration (FERA) and later the Work Progress Administration (WPA) (Carpenter, 2018), to reconstruct the now missing interval of strata that overlaid the fossil-bearing sandstone beds. This interval of strata was considered overburden and was removed from 1934–1938 by FERA and WPA crews as part of the National Park Service's early development of what was to become the dinosaur quarry exhibit. These photographs and cited reports containing strata descriptions are housed in the archives of Dinosaur National Monument. Other photographs, mostly by Boyle, are housed in the Uintah County Regional History Center, Vernal, Utah. Correspondence of Earl Douglass is in the archives of the Carnegie Museum of Natural History, Pittsburgh, Pennsylvania. Diane Iverson, granddaughter of Earl Douglass provided photographs of Earl Douglass through Sue Ann Bilbey and Evan Hall (both Uinta Paleontological Associates, Inc., Vernal, Utah).

We collected oriented hand samples in the trenches made for the measured sections on the west and east sides of the QEH, the samples are plotted on the measured sections in Figure 4. Rock color is based on the Munsell (2009) hue, value, and chroma rock color

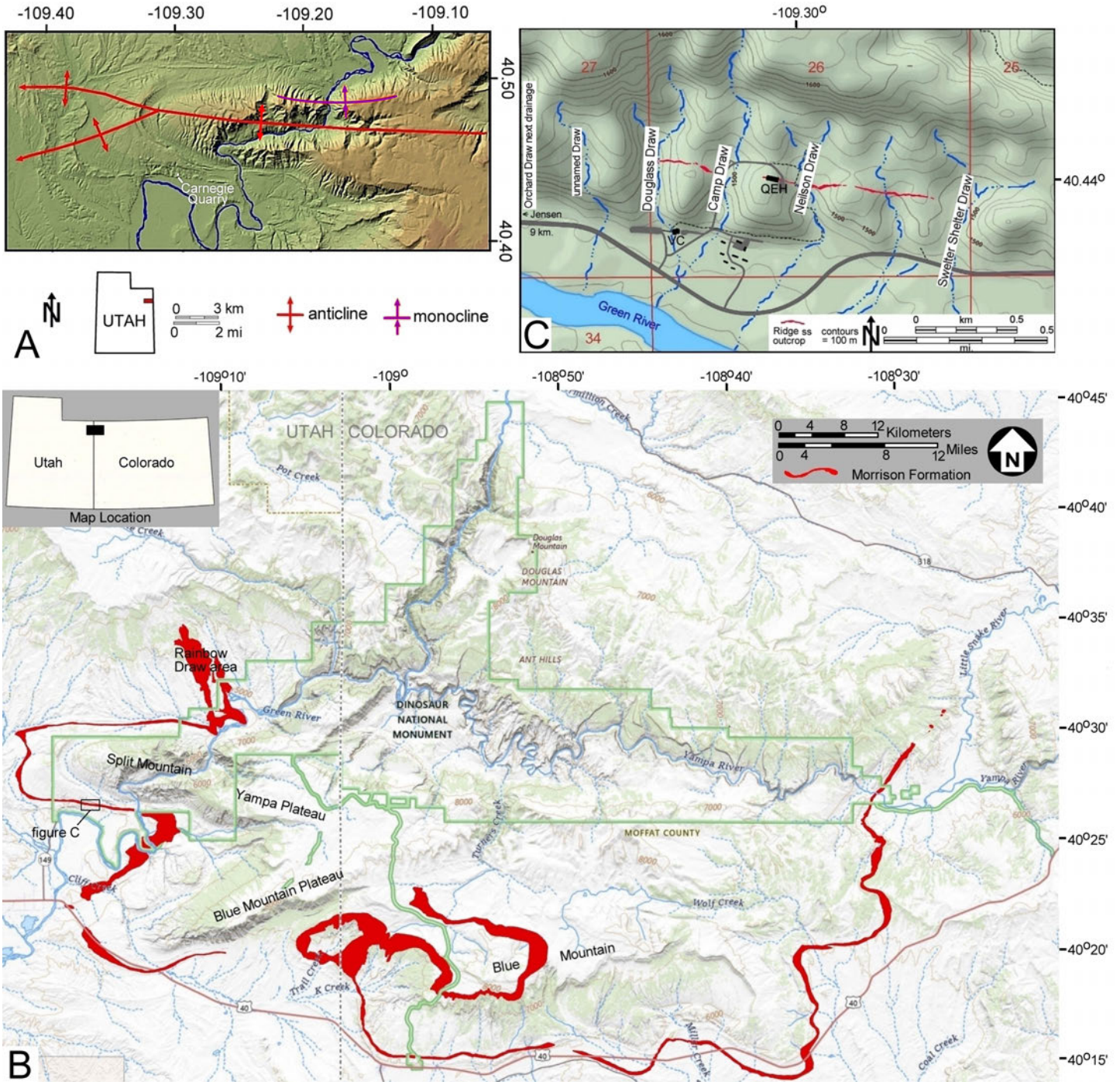

Figure 2. (A) Split Mountain anticline. (B) Outcrop map of the Morrison Formation in and around Dinosaur National Monument of Utah and Colorado. (C) Distribution of the Quarry Sandstone in relation to the Quarry Exhibit Hall (QEH) and named drainages referenced in the text.

scheme. Wagner Petrographic (Lindon, Utah) made the thin sections of these samples. These and other thin sections are referenced below by their catalog numbers prefaced by DINO. The thin sections are curated in the Dinosaur National Monument collections stored at the Utah Field House of Natural History State Park Muse-

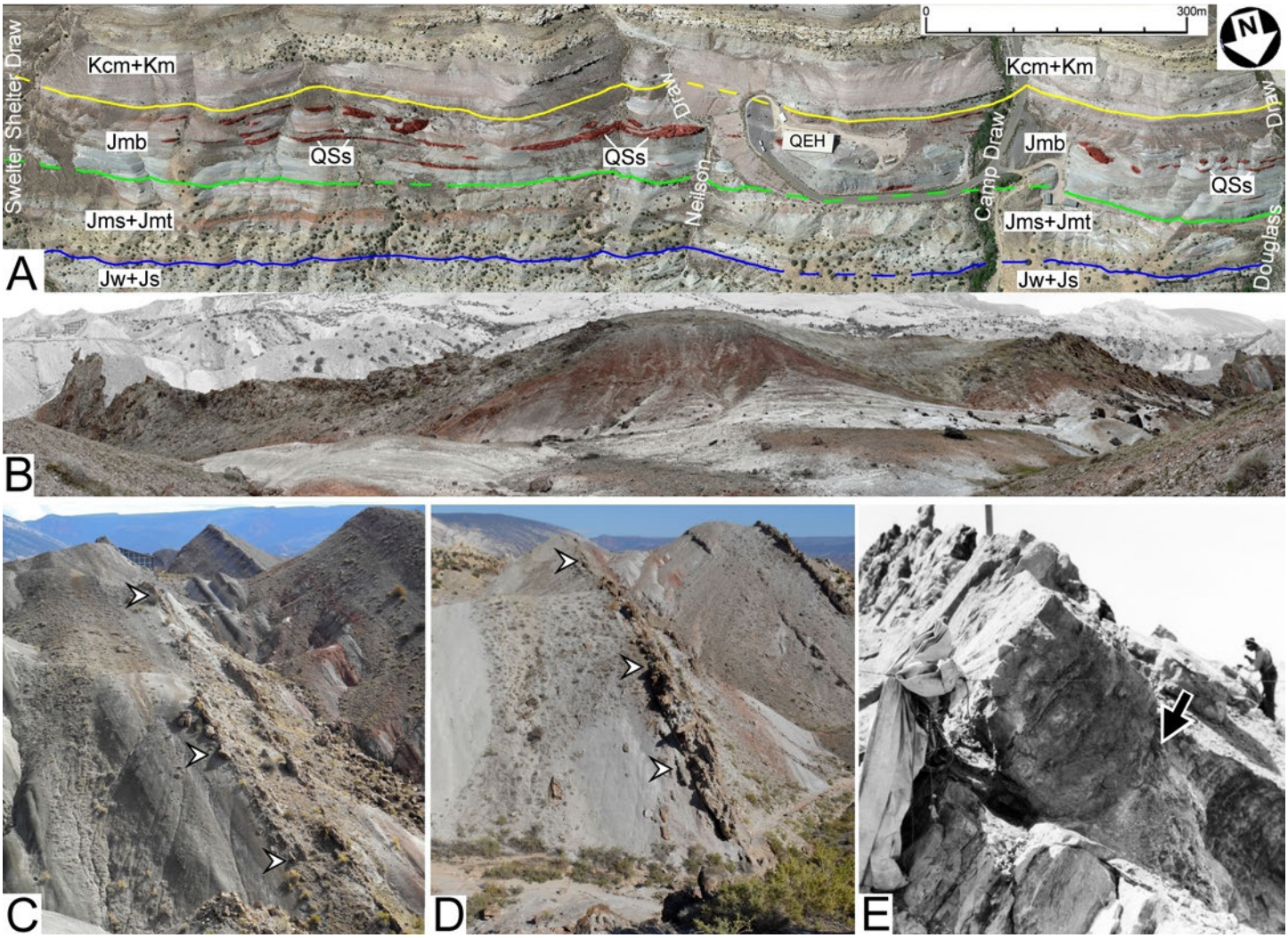

Figure 3. (A) Strata and distribution of sandstone beds in the study area. Abbreviations: Jmb – Brushy Basin Member; Jms + Jmt – Salt Wash and Tidwell Members; Jw + Js – Windy Hill and Stump Formations; Kcm + Km – Cedar Mountain and Muddy Formations; QEH – Quarry Exhibit Hall; QSs – Quarry Sandstone. Satellite view from Google Earth. (B) 180° panorama of the Quarry Sandstone from Neilson Draw to Swelter Shelter Draw. (C) Quarry Sandstone (indicated by arrows) from Douglass Draw, viewed eastward. (D) Quarry Sandstone (indicated by arrows) from the Quarry Exhibit Hall parking lot, viewed eastward (Neilson Draw). (E) Abrupt contact between the lowest Quarry Sandstone and underlying muddy sandstone beds. Photograph by Earl Douglass (Carnegie Museum) on the east-end of the quarry viewed west. Date of photograph unknown.

um in Vernal, Utah. Samples of the Quarry Sandstone were obtained from matrix still adhering to dinosaur bones collected by the Carnegie Museum crews between 1909–1922. These thin sections are listed by the bone catalog number prefaced by CM and are housed at the Carnegie Museum of Natural History, Pittsburgh. Carpenter (2013) previously described some of these thin sections. The exact stratigraphic levels of these samples are unknown, but they are assumed to be in the lower two sandstone beds from which most dinosaur bones were excavated. In addition, we collected hand samples from the Morrison Formation along the north and west sides of Split Mountain anticline during our search for the upstream part of the fluvial system that deposited the Quarry Sandstone. No thin sections of these latter samples were made.

We polished most of the cut surfaces of the samples to reveal internal texture. Mudstone samples were hand-polished dry using progressively finer grit sandpaper. The polished faces and whole mounts of thin sec-

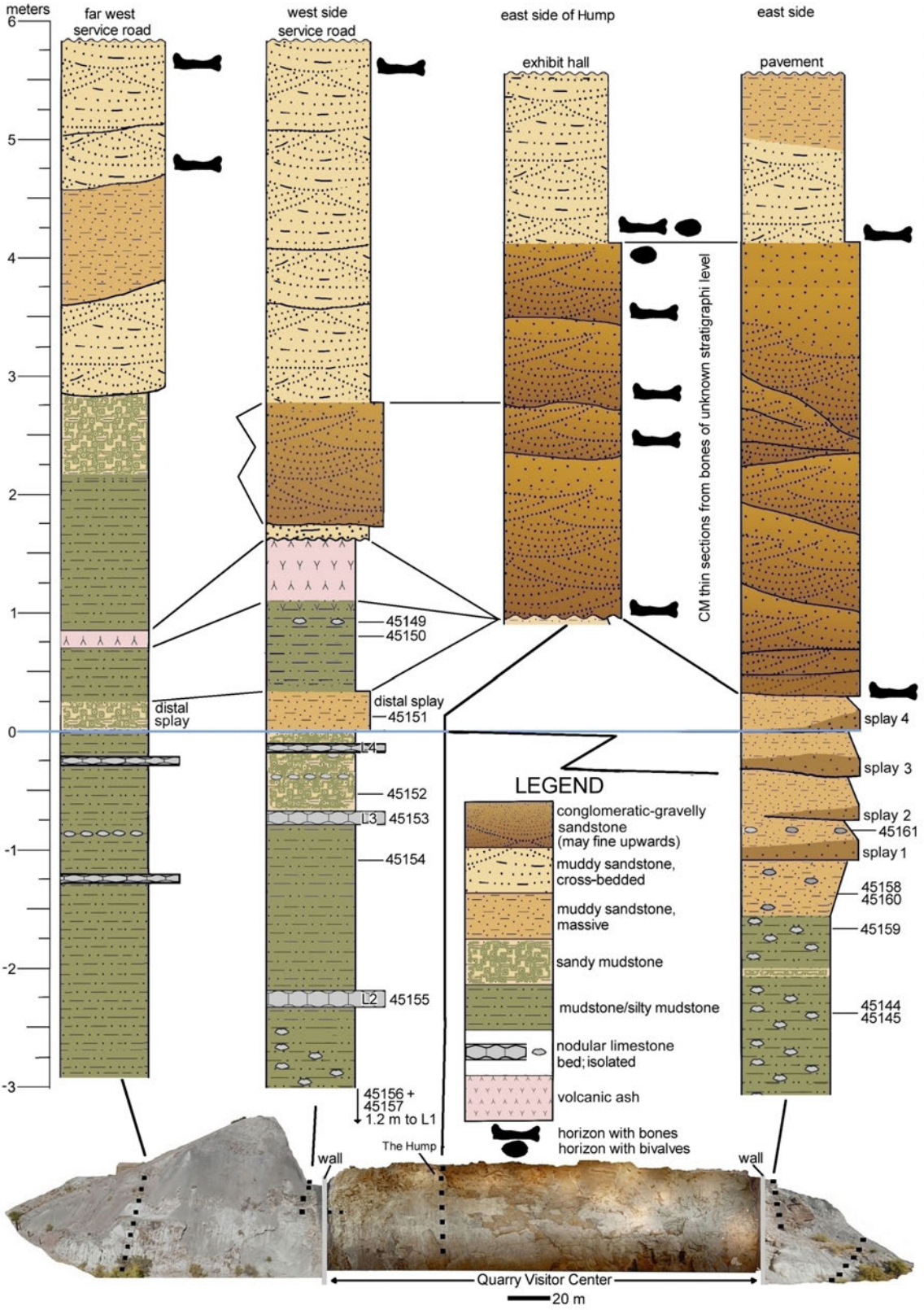

Figure 4. Stratigraphic sections in and near the QEH, showing the location of the thin sections. DINO 45156 and 45157 are 1.2 m below the bottom of the west side column. Detailed descriptions of the thin sections are included in Appendices 1 and 2. The term DINO is not shown on the stratigraphic section because of space constraints.

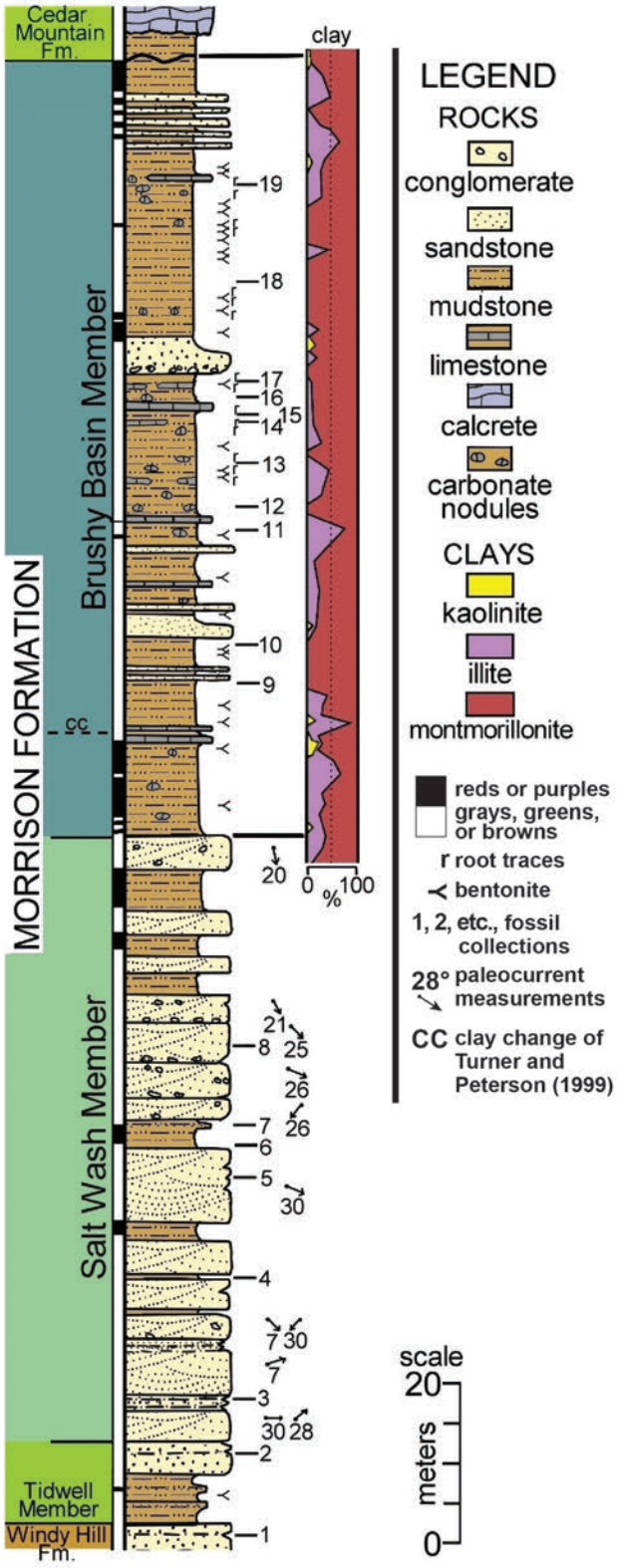

Figure 5. Stratigraphic section of the Morrison Formation and adjacent strata along Douglass Draw. Redrawn from a section provided by Fred Peterson (U.S. Geological Survey). Clay data from Bilbey (1992).

tions are illustrated to show macroscopic features (Figure 7). Usually, these are subtle in color differences and were enhanced by darkening the image and increasing contrast. Micrographs of thin sections were not enhanced. The thin sections and a portion of the associated hand samples were subjected to hydrochloric acid (HCl) and Alizarin Red-S stain to identify and enhance the presence of calcite. Potassium ferricyanide stain was used on some sandstone thin sections to reveal ferroan dolomite cement.

We conducted a petrographic examination using a Zeiss Photoscope III petrographic microscope. Thin section examinations provided overall lithology, mineralogy (including clay content), grain size, grain roundness, and sorting data. Examination of the carbonate samples provided overall lithology, crystal or allochem size, and fossil content. Petrographic examinations also included identification of diagenetic features. This information is shown in table format in the Appendices, as are figures of all of the thin sections. Mudstone with modifiers refers to a spectrum of fine-grained sedimentary rock in which 50% or more of its grains are mud (calcite, clay and silt) size (Potter et al., 2005; Lazar et al., 2022). Clay particles are 4 μm or less in diameter, whereas silt particles range from 4 to 62.5 μm in diameter. Whole rock mudstone terminology is based on Macquaker and Adams (2003) and Lazar et al. (2022). Grain size identification follows the Udden-Wentworth scale as included in Ehlers and Blatt (1982) and Blair and McPherson (1999), among others.

A Th-corrected $^{206}Pb/^{238}U$ CA-ID-TIMS zircon date reported below on a tuff we collected in the west trench was analyzed by Kevin Chamberlain, Department of Geology, University of Wyoming. Chronostratigraphic age names are those of the International Chronostratigraphic Chart v2023/09 (www.stratigraphy.org).

STRATIGRAPHIC SETTING

The Morrison Formation, prominently displayed on the Colorado Plateau, consists of the thinly bedded siltstone and mudstone beds of the Tidwell Member, which is overlain by the sandstone-dominated Salt Wash Member, and capped by the gray or variegated mudstone-dominated Brushy Basin Member (Figure 8A).

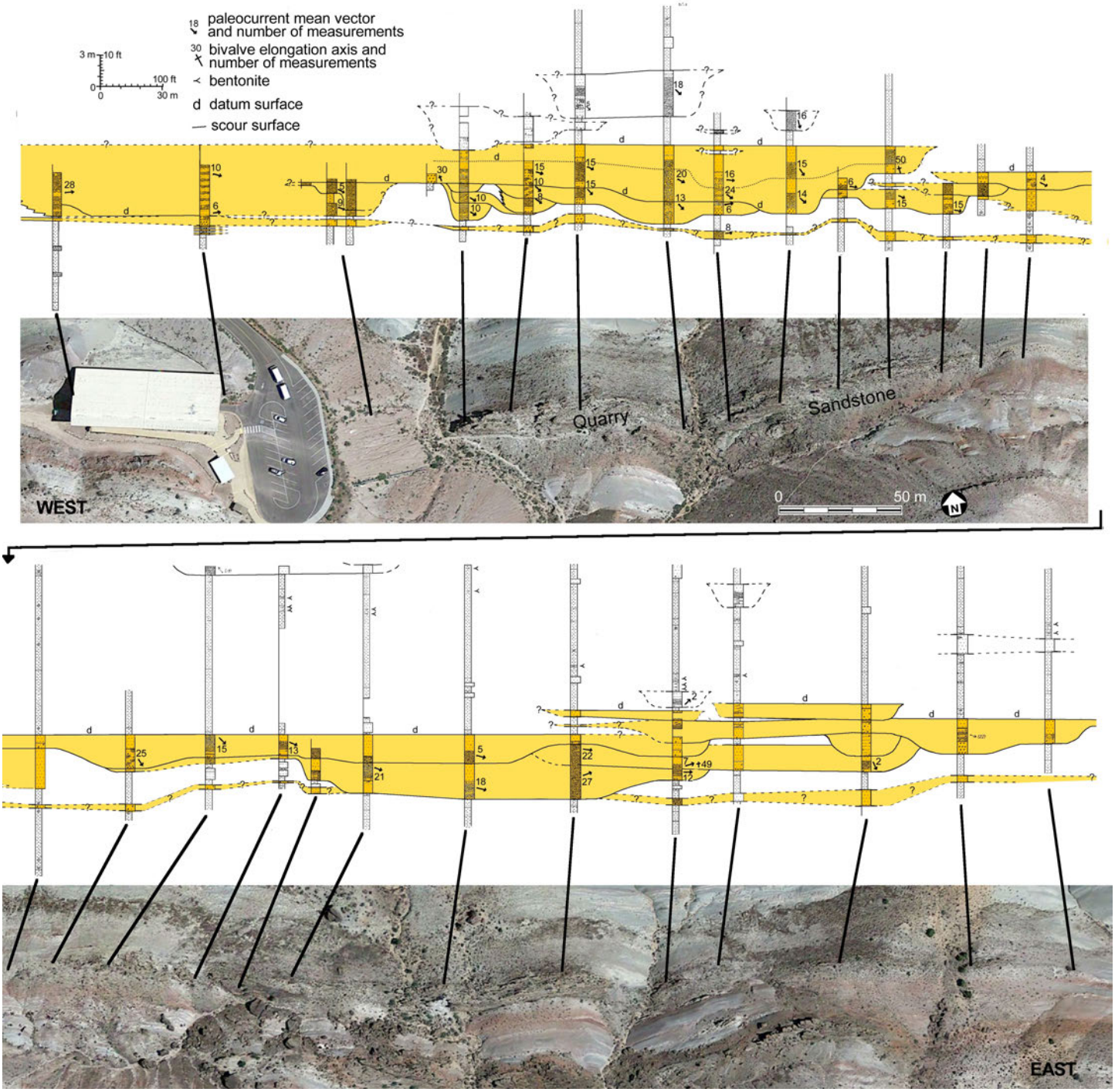

Figure 6. Stratigraphic profile of the Quarry Sandstone from the QEH to near Swelter Shelter Draw. The profile shows that the Quarry Sandstone consists of stacked and coalesced fluvial sandstone beds. Courtesy of Fred Peterson, U.S. Geological Survey

These three members are present in Dinosaur National Monument (Turner and Peterson, 1991, 1992b, 1999); however, the distinction between members can be challenging due to the scarcity of resistant sandstone beds within the Salt Wash Member as initiatlly observed by Stokes (1944) (Figures 8B and 8C), and the Tidwell Member was not recognized by Bilbey et al. (1974) in the Monument.

In the study area, the Morrison Formation is most extensively exposed in Douglass Draw, oriented per-

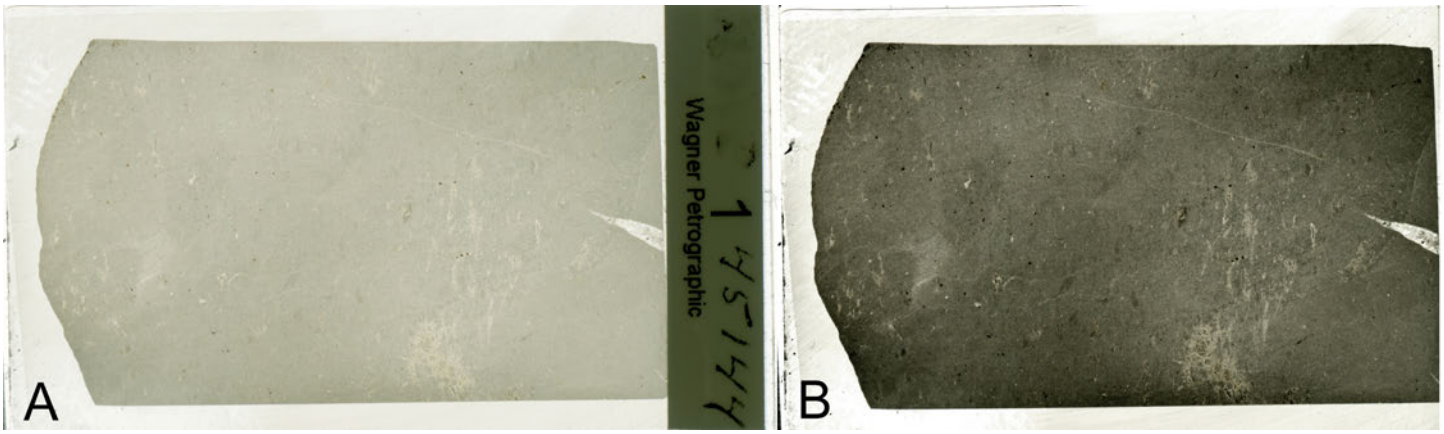

Figure 7. Comparison of unenhanced (A) and enhanced (B) miscrohotographic images, illustrating subtle macro-features as a function of color in the whole slide sample.

pendicular to the formation's strike, and designated as a primary reference section by Turner and Peterson (1999). Here, the Tidwell Member measures approximately 10 m in thickness, the Salt Wash Member approximately 74.8 m, and the Brushy Basin Member approximately 100 m thick (Figure 5).

Tidwell Member

The Tidwell Member is poorly exposed in the study area (Figures 8A and 8B). Where visible, it comprises interbedded moderate reddish-brown (10R 4/6 of the Munsell color scheme) and pale greenish-yellow (10Y 8/2) mudstone, along with white (N9) fine-grained sandstone and siltstone. Near the base, many areas feature a zone of red botryoidal authigenic chert, which Peterson (1988) identified as a widespread marker unit on the Colorado Plateau. Carpenter (2022), however, found its distribution to be inconsistent. Marine dinoflagellates reported from the Tidwell Member near the quarry (Turner and Peterson, 1999) are actually from the Redwater Member of the Stump Formation (Turner and Peterson, 1992b, p. 88; Litwin et al., 1998, p. 302). Currently, compelling evidence for a marine influence on the Tidwell Member is lacking.

The Tidwell Member serves as the base of the Morrison Formation across the Colorado Plateau (O'Sullivan, 1984; Peterson, 1988; Carpenter, 2022). In the Rainbow Draw area north of Split Mountain (Figure 2A), a volcanic ash layer within the Tidwell has a recalibrated $^{40}Ar/^{39}Ar$ age of 156.84 ± 0.59 Ma (middle Oxfordian) (Trujillo and Kowallis, 2015), closely matching the 156.77 ± 0.55 Ma age abtained 2.4 m above the base of the Tidwell near Notom, Utah, 290 km farther south on the plateau (Trujillo and Kowallis, 2015).

The Windy Hill Formation (originally the Windy Hill Member of the Sundance Formation, Pipiringos, 1968), which underlies the Tidwell Member, has at times been considered a basal member of the Morrison Formation (Peterson, 1994; Sprinkel et al., 2019). However, we regard it as a separate formation, following the reasoning put forth by Danise and Holland (2018) and Holland and Wright (2020) (see Wroblewski and Morris, 2022, for a dissenting position). Our field work in the formation has yielded a section of sauropod rib in the Orchard Draw drainage, 1250 m west of the QEH. It is the first reported dinosaur bone from this formation in the Monument; pterosaur and sauropod tracks have been reported from Wyoming (e.g., Meters et al., 2009; Meyers and Breithaupt, 2014).

Salt Wash Member

The coarse-grained sandstone beds of the Salt Wash Member exhibit greater prominence in Douglass Draw (Figure 8B) compared to east of the QEH, where rapid weathering due to higher clay content is evident (Figure 8C). These sandstone beds, ranging from white to very light gray (N9–N8), are interbedded with non-swelling, moderate orange-pink to moderate red (10R 7/4–5R 4/6) mudstone.

In Douglass Draw, the lower boundary of the Salt

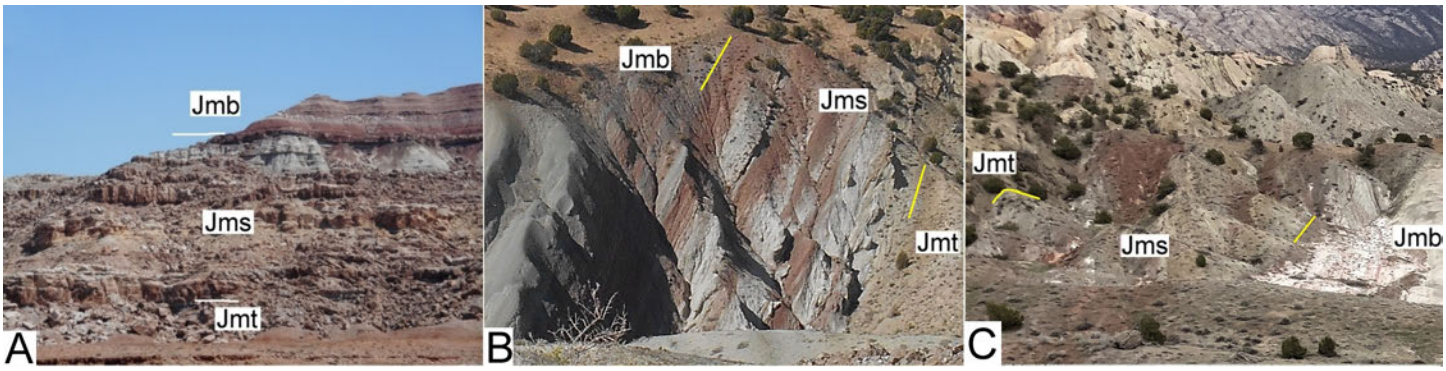

Figure 8. (A) Typical Morrison Formation on the north-central Colorado Plateau, featuring erosion-resistant, ledge-forming sandstone beds in the Salt Wash Member, positioned between the underlying siltstone of the Tidwell Member and the overlying mudstone of the Brushy Basin Member (38.7982°N., -109.9867°W.; type location of the Salt Wash Member). (B) Morrison Formation in Douglass Draw, characterized by a few ridges of erosion-resistant sandstone beds in the Salt Wash Member (40.4419°N., -109.3084°W.). (C) Salt Wash Member east of the QEH, showing the absence of resistant sandstone (40.4404°N., -109.2934°W.). Abbreviations: Jmb – Brushy Basin Member, Morrison Formation; Jms – Salt Wash Member, Morrison Formation; Jmt – Tidwell Member, Morrison Formation.

Wash Member is marked by a white to very light gray (N9–N8) muddy sandstone at the base, juxtaposed against a very pale orange (10YR 8/2) muddy sandstone of the underlying Tidwell Member (Figure 8B). The upper boundary of the Salt Wash Member is identified by a similar white to very light gray (N9–N8) muddy sandstone or a moderate red (5R 4/6) mudstone just below a moderate orange-pink to moderate reddish-orange (10R 7/4–10R 6/6) mudstone of the Brushy Basin Member (Figure 8B). Archival photographs show that the boundary between the Salt Wash and Brushy Basin Members lies in the axis of the valley currently underlying the road from the lower parking lot to the upper parking lot at the QEH.

Around Dinosaur National Monument, the Salt Wash Member is at the edge of its recognizable extent on the Colorado Plateau. Sprinkel et al. (2019) identified the northernmost recognizable occurrence of the Salt Wash Member in the Rainbow Draw area north of the Split Mountain anticline (Figure 2B). Beyond this region, sandstone beds no longer distinctly delineate the Salt Wash Member, leading to its mapping as "undifferentiated" within the Morrison Formation (Mullens and Freeman, 1957).

Within Dinosaur National Monument, the Salt Wash Member is interpreted as part of the "claystone and lenticular sandstone facies" of a distal part of an alluvial megafan (Craig et al., 1955, 1977) or more recently as a distributive fluvial system (Weissmann et al., 2013; Owen et al., 2015, 2017). However, Carpenter (2022) raised significant concerns regarding these interpretations based on paleocurrent data across the entire Colorado Plateau.

Brushy Basin Member

The Brushy Basin Member on the Colorado Plateau constitutes a thick slope-forming unit rich in clay and notably lacking in sandstone, contrasting sharply with the underlying Salt Wash Member (e.g., Figure 8A). The majority of the Brushy Basin Member mudstone beds are composed of montmorillonite clay formed through the alteration of volcanic ash (Keller, 1962). Robinson and McCabe (1998) attributed the abrupt lithofacies shift from the sandstone-dominated Salt Wash Member to the mudstone- or claystone-dominated Brushy Basin Member to changes in watershed hydrology driven by climate or tectonism, with Currie (1997) suggesting concomitant changes in fluvial dynamics. However, Heller et al. (2015) found little difference in paleochannel architecture between the Salt Wash and Brushy Basin Members in southeastern Utah, proposing that reduced channel-belt stacking in the Brushy Basin resulted from decreased avulsion frequency, potentially

linked to increased volcanic ash input as airfall or washload in rivers. Dawson (1970) also linked the abrupt decrease in clastics to volcanism, specifically the burial of clastic sources by volcanic deposits.

Despite differing causal interpretations, the transition between the Salt Wash and Brushy Basin Members is diachronous (Kjemperud et al., 2008) relative to a mid-Morrison unconformity often represented by a paleosol at the top of the Salt Wash Member (Demko et al., 2004). This paleosol or unconformity, however, is not universally present (Kjemperud et al., 2008; Heller et al., 2015; Maidment and Muxworthy, 2019), and evidence for large-scale incisions or paleovalleys (Demko et al., 2004) was not noted by Currie (1997), nor have we seen such structures in the study area.

Within Dinosaur National Monument, the Brushy Basin Member may be informally subdivided into a discontinuous lower unit exhibiting red and white weathering and an upper unit exhibiting gray weathering (Figure 9; Turner and Peterson, 1999). The lower unit, approximately 12 m thick, predominantly exhibits hues ranging from grayish-pink (5R 8/2) to light-red (5R 6/6) and lacks the popcorn or frothy texture of weathered smectitic clay. This unit is overlain by an upper unit, 83 m thick, weathering from light-gray (N8) to medium-gray (N5) mudstone characterized by the popcorn texture of weathered smectite, the predominant clay in the Brushy Basin Member (Keller, 1962; Bilbey et al., 1974; Owen et al., 1989; Heller et al., 2015). In its unweathered state, this silty clay-rich mudstone appears grayish-black (N2). The sandstone housing the dinosaur quarry is about 43 m above the Salt Wash Member.

The color and texture distinctions in the lower Brushy Basin Member observed by Turner and Peterson (1992a, 1999) seem to correlate with their hypothesized Morrison clay change marker representing a shift from non-swelling illitic clays to swelling smectitic clays. However, such a clay change was not confirmed by X-ray diffraction analysis of clays near the QEH by Bilbey (1992), which revealed a mix of montmorillonite-illite (smectite-illite) clays in this interval (Figure 5). Trujillo (2006) suggested that the differing weathering patterns observed by Turner and Peterson are a reflection of the proportion of silt and sand grains, with amounts greater in the "illitic"-looking weather profile. This seems to be the case in the study area, where the lower unit is associated with multiple thin gravelly crevasse splays or levee deposits traceable laterally into channel sandstone beds along the road to the QEH (Figure 9B).

The upper contact (K-1 unconformity) of the Brushy Basin Member across much of the western part of the northern Colorado Plateau is marked by the base of the chert-rich, cobble- to boulder-containing Buckhorn Conglomerate Member of the Lower Cretaceous Cedar Mountain Formation (Kirkland et al., 2016). In areas where the conglomerate is absent, this boundary is identified at the top of a mottled yellow-orange mudstone paleosol bearing chert pebbles below the lowermost calcrete bed, separating smectitic, generally red or gray mudstone of the Brushy Basin Member, from the non-smectitic, pastel-colored mudstone of the Cedar Mountain Formation (Figure 10A; Sprinkel et al., 2012; Kirkland et al., 2016). Near the QEH, where the conglomerate is absent, the contact is found at the top of yellow-orange to moderate red mudstone, typically situated 1 to 3 m below a sporadically occurring calcrete paleosol (Figure 10B; Kirkland and Madsen, 2007; Chure et al., 2010; Sprinkel et al., 2012, 2019).

Currie (1997) identified the top of this calcrete as the K-1 contact, indicating that a Cretaceous paleosol developed within the top of the Brushy Basin Member during a hiatus in sediment deposition. In contrast, Brezinski and Kollar (2018) placed the K-1 boundary at the base of the calcrete, positioning the paleosol and its host sediments entirely within the Cedar Mountain Formation, implying a second hiatus with calcrete formation in earliest Cretaceous sediments. This calcrete, discontinuous and thinning out approximately 600 m east and 320 m west of the QEH, is insufficient evidence alone to determine the boundary placement, as the lower Cedar Mountain Formation contains several discontinuous calcrete beds (Kirkland et al., 2016). At least three such beds are present in the lower Cedar Mountain Formation along Douglass Draw (Figure 10C). Locating the yellow-orange to moderate red mudstone K-1 contact at Dinosaur National Monument can be challenging due to soil creep on steep slopes, though visible where erosion maintains clean exposures.

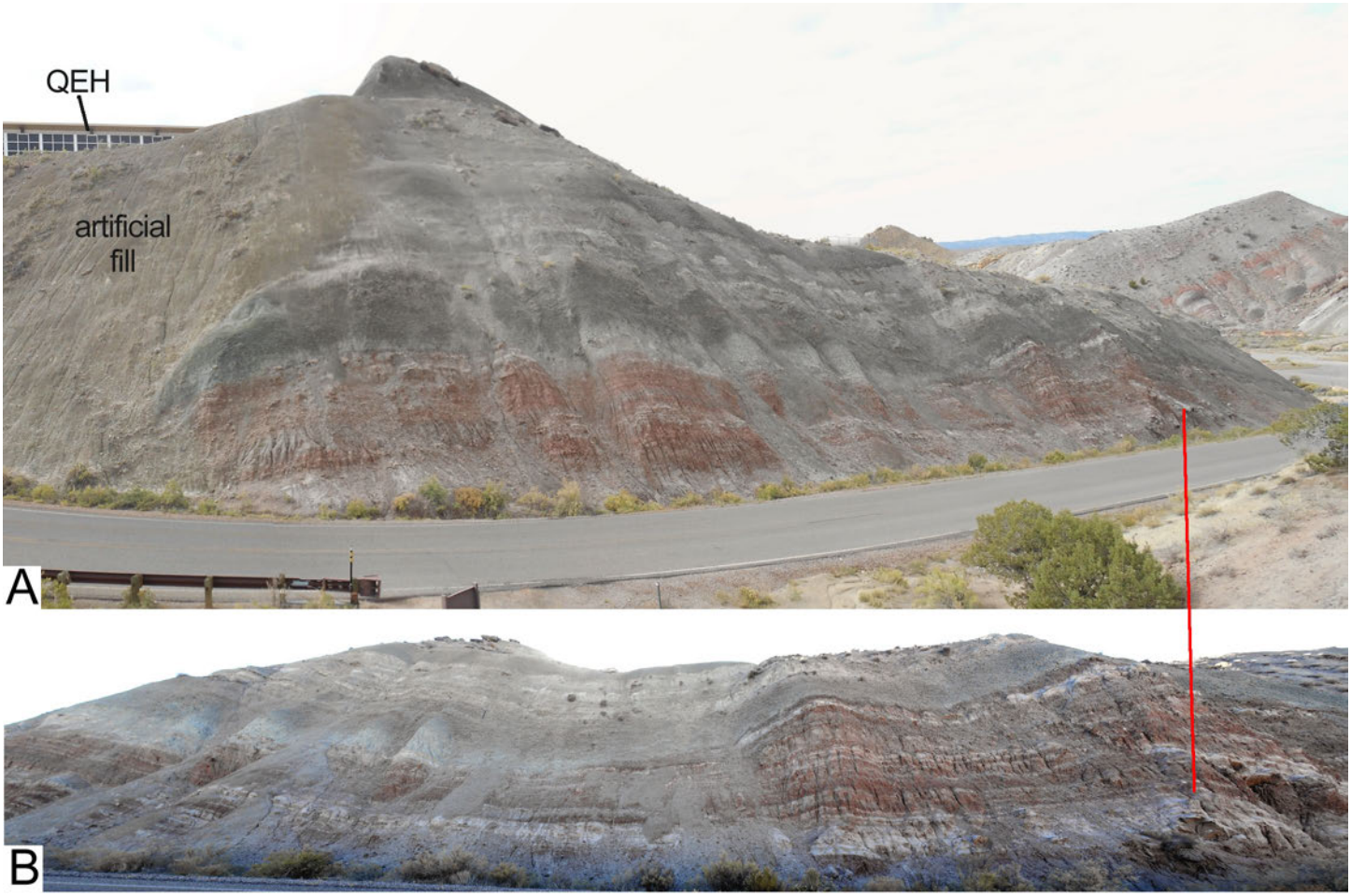

Figure 9. (A) Brushy Basin on the north side of the QEH, showing the lower red and white unit overlain by the gray unit. (B) Another view showing the red and white unit grading into channel sandstone. The red line connects the same sandstone bed (40.4411°N., -109.3014°W.).

LITHOFACIES DESCRIPTION

Sandstone Facies

The distribution of sandstone lenses in the Brushy Basin Member within the study area is depicted in Figure 3A. Although there are a few isolated lenticular sandstone bodies, most sandstone occurs in a narrow interval 3 to 9 m thick, forming a discontinuous ridge created by the Quarry Sandstone extending eastward from the QEH (Figures 3B, 3D, and 6). This sandstone bed can be traced westward to Douglass Draw, although erosion has not yet made it a prominent ridge (Figure 3C). The bases of the sandstone bodies are typically scoured into the underlying strata, resulting in abrupt contacts (Figure 3E). These underlying strata generally consist of sandy mudstone or muddy sandstone, which is generally white and easily recognizable from a distance.

The Quarry Sandstone bed dips to the south, with reported values varying as follows: 50° (Hansen et al., 1983), greater than 55° (Brezinski and Kollar, 2018), 60° (E. Douglass correspondence to Assistant Director Douglas Stewart, Carnegie Museum, September 24, 1909), 60 to 70° (Turner and Peterson, 1992a), 62° (Carpenter, 2013), 65° (Boyle, 1938a), and 67° (Untermann and Untermann, 1954; Bilbey, 1992; Lawton, 1977). These differences can be partly explained by the locations where the dips were measured in and around the QEH and in Neilson Draw. Carpenter (2013) measured the dip on the flat sandstone surface on the east side of the QEH, and Boyle (1938a) on the rock face formerly

Figure 10. (A) Jurassic-Cretaceous boundary on the Colorado Plateau at Horse Bench (38.8534°N., -110.2201°W.). (B) Jurassic-Cretaceous boundary near the QEH (40.4402°N., -109.3012°W.). (C) Three carbonate beds (calcretes) near the base of the Cedar Mountain Formation at Douglass Draw (40.4408°N., -109.3081°W.). Abbreviations: Jmb – Brushy Basin Member; Kcm – Cedar Mountain Formation.

present on the west side of the QEH ("Dinosaur Peak"). Other measurements in the vicinity include 48° near the crest of the divide east of the QEH (Hansen et al., 1983); 50° on the east side of Camp Gulch (Rowley et al., 1979) and 62 to 68° east of the QEH along the Quarry Sandstone (Lawton, 1976).

Isolated Sandstone Bodies

Although the emphasis of this study is on the Quarry Sandstone bed, for thoroughness and context, we briefly describe the few isolated lenticular sandstone bodies in the study area that occur below or above the Quarry Sandstone bed. Such isolated bodies are more common in the Brushy Basin Member than in the stacked sandstone bodies that dominate the Salt Wash Member (Currie, 1997; Galli, 2014; Heller et al., 2015).

The isolated sandstone bodies are represented in the study area by two types of lithologies. An example of Type 1 is approximately 27 m above the Salt Wash Member (Figures 11A and 11B). It is light-brown (5YR 5/6) to pale-yellowish-orange (10YR 8/6), coarse-grained to conglomeratic litharenite with quartz predominating as the coarse-grain fraction. The larger granule-to-pebble-size clasts are gray chert and some potassium feldspar. The brown tint is most likely due to iron hydroxide. An example of Type 2 occurs about 10 m below the Cedar Mountain Formation (Figure 11C). It is a litharenite of quartz sand and polychromatic chert conglomerate, much like the Quarry Sandstone, with silica and calcium carbonate cements. These isolated coarse-grained bodies are narrow, and have a width/thickness (w/t) ratio (less than 4:1).

Stacked Sandstone Bodies (Quarry Sandstone)

The Quarry Sandstone, about 43.9 m above the Salt Wash Member, is composed of discontinuous multistory sandstone bodies that are predominantly stacked conglomeratic or coarse- to fine-grained sandstone, and are white (N9) to very light gray (N8). These bodies weather to pale yellowish-orange (10YR 8/6) to pale reddish-brown (10R 5/4) due to the weathering of iron disseminated in pore spaces (Hubert et al., 1996) in conjunction with desert varnish (Figure 12A; see also cover photograph). The geometries of the stacked sandstone bodies are best seen in the QEH, where three major sets are exposed; at least one additional poorly cemented sandstone bed was mostly removed to expose the fossil bones in the lower sandstone for public viewing; this sandstone is mostly described from reports before it was removed beginning in the early 1950s.

The three remaining sandstone beds in the QEH are generally similar except as noted in the following. The lowest sandstone is conglomeratic near the base, fining upwards, and varies in thickness from 0.6 to 1.8 m (Walker, 1943). Fossil bones occur but are mostly widely dispersed. The second and third sandstone beds, treated as a single sandstone by Walker (1943), are conglomeratic or coarse-grained at the base and fine upwards; combined, they vary in thickness from 2.4 to 3

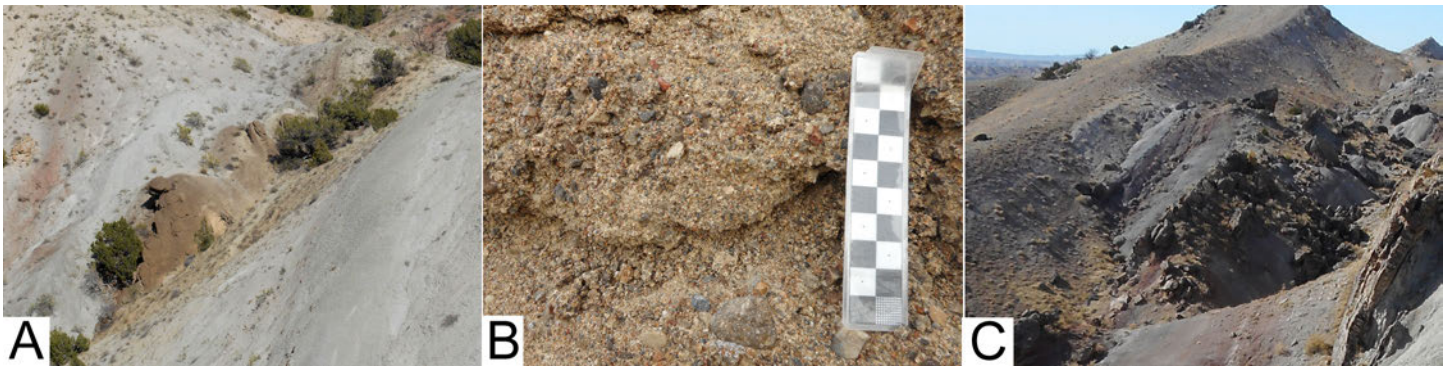

Figure 11. Lenticular sandstone facies. (A) Type 1 brown coarse-grained and conglomeratic litharenite (40.4408°N., -109.2990°W.). (B) Close-up showing quartz sand matrix and pebbles of chert and potassium feldspar. Scale in cm. (C) Type 2 quartz and chert conglomeratic litharenite with silica and carbonate cements.

m. However, as Walker noted, there are two bone levels within this sandstone, implying two depositional cycles, thus it is actually two stacked sandstone beds. On the quarry face today, these sandstone beds are separated by a clay drape, which was not noted by Walker (1943).

The grains of the three sandstone beds are predominantly subrounded to well-rounded, medium- to very-coarse-grained monocrystalline quartz and black chert (approximately 25+%), giving the sandstone a salt-and-pepper appearance (Figure 12B), hence the gray tint from a distance. This litharenite, referred to as a chert arenite by Bilbey et al. (1974), has matrix-supported larger particles that are commonly coarse-sand to pebble-size, angular to subrounded grayish-black (N2) or light-gray (N7) to very light gray (N8) chert (Figure 12C), or subrounded to rounded clasts of carbonate siltstone or mudstone that are occasionally up to cobble size (Figure 12D). These fine-grained clasts (siltstone or mudstone, referred to as devitrified tuff fragments by Bilbey et al., 1974) are less resistant to erosion, creating a pock-marked weathered surface (Figure 12E). Pockets of fine- to medium-grained white (N9) sandstone also occur within the conglomeratic sandstone bodies (Figure 12F). The pockets are often lobate and superficially resemble ball-and-pillow structures but are not connected to underlying mudstone. These do not appear to be transported fine sediment clasts but rather scour infill in the low-pressure, low-velocity recirculation zone on the downstream side of the scour crest during the waning phase of river flow (Figure 12G).

Magnetite is rare, indicating a non-igneous, non-metamorphic source for the sand. Chalcedony and calcite are the predominant cements (Bilbey et al., 1974; Lawton, 1977; Hubert et al., 1996), although potassium ferricyanide staining reveals some ferroan dolomite cement in some sandstone adhering to bones collected by the Carnegie Museum (Carpenter, 2013). Chalcedony is a common sandstone cement where glassy volcanic ash is present because the thermodynamically unstable hydrous silica of the glass shards dissolves and reprecipitates in this more stable form (Worden and Morad, 2000). The abundance of volcanic ash characterizes the mudstone in the Brushy Basin Member and sets it apart from the other members of the Morrison Formation (Keller, 1962; Heller et al., 2015). At Dinosaur National Monument, at least 42 predominantly rhyolitic volcanic ash beds spanning 2.2 million years are present in the Brushy Basin Member both above and below the Quarry Sandstone (Christiansen et al., 2015), thus providing a ready source of soluble silica. Additionally, the chalcedony-cemented sandstones tend to have little interstitial clay because clay inhibits quartz cementation (Worden and Morad, 2000). Large masses of chalcedony occur in sandstone at various places along the Quarry Sandstone.

Bedforms were revealed through erosion and quarrying along bed partings. These include wedge-shaped channel bars having a gently sloped stoss side and steep lee side (Figure 13A); these can be seen in photographs taken during the excavations (Figure 13B). These bedforms are rarely larger than 10 to 30 cm thick. The largest is preserved in the thickest remnant of the Quarry Sandstone today in the west half of the QEH (Figure

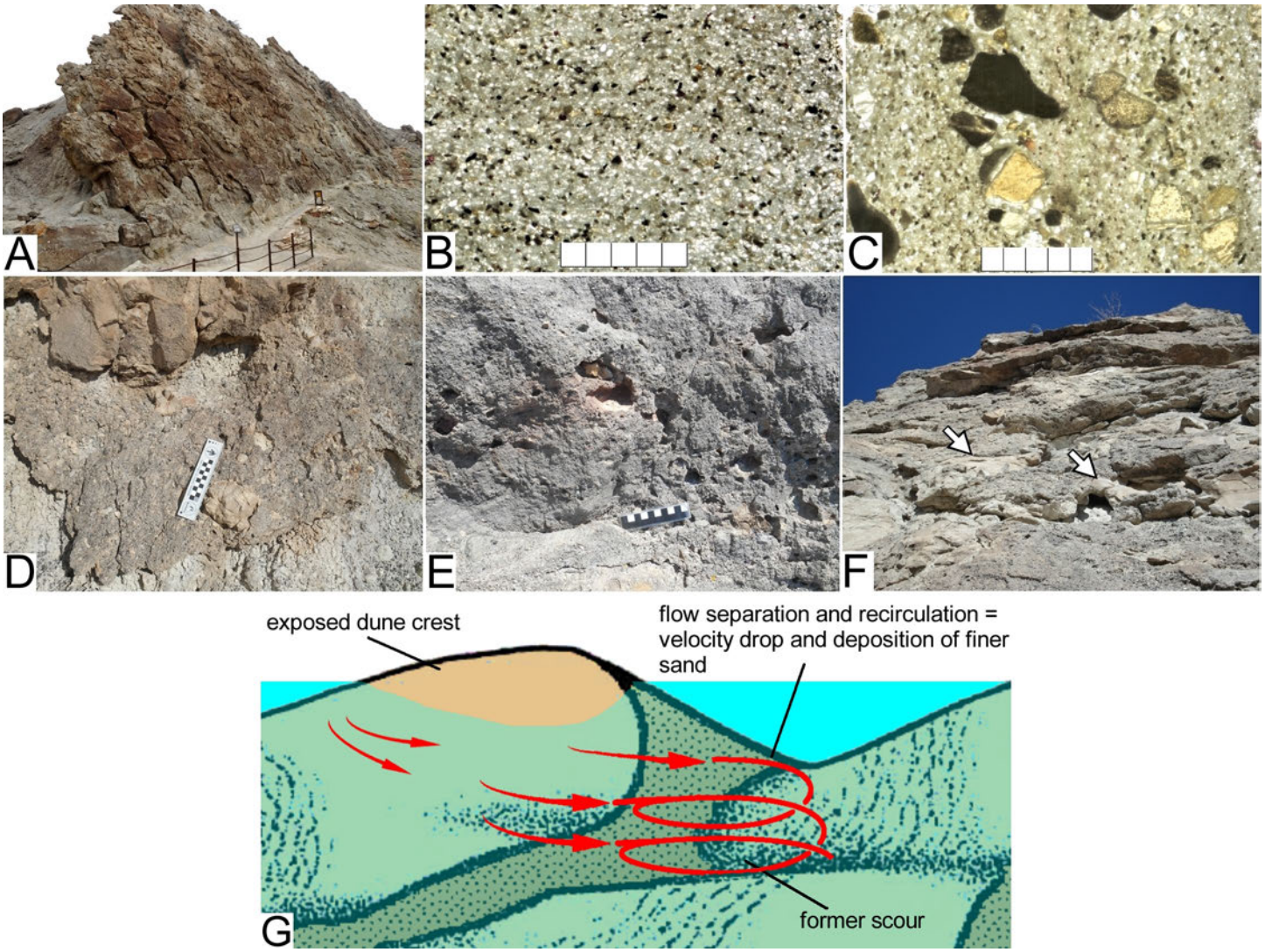

Figure 12. Stacked channel sandstone facies: (A) Weathered Quarry Sandstone at Neilsen Gulch (40.4402°N., -109.2997°W.). (B) Thin section CM70384 is fine- to medium-grained "salt and pepper" sandstone composed of quartz and black chert. Scale in mm. (C) Thin section CM70384 is medium- to coarse-grained quartz and chert sandstone matrix supporting angular to subrounded multicolored chert granules and pebbles. Scale in cm. (D) Carbonate clasts on the east side of the QEH. Scale in cm. (E) Eroded fine-grained clasts creating a pockmarked surface on the east side of the QEH. Scale in cm. (F) Finer-grained sandstone lenses (indicated by arrows) infilling troughs in coarser-grained sandstone at Neilsen Gulch (40.4402°N., -109.2997°W.). (G) Diagram illustrating finer sand deposition in the lee of a dune due to flow separation, recirculation, and velocity drop.

13C). On the west side of the bar, a juvenile sauropod pelvis is preserved standing vertically through the deposit, indicating that sediment deposition was rapid (Figure 13D; Carpenter, 2020a). This mega-bedform is unusual for its height, being about 152 cm, and may have formed as a bank-attached bedform deposited in the thalweg.

The predominant sedimentary structure of the Quarry Sandstone is trough cross-stratification. The tops of these structures can be seen on the top surfaces of the steeply dipping Quarry Sandstone, where the softer mudstone beds have eroded away (Figure 13E). This surface typically preserves troughs in three dimensions, which indicate rapidly waning flows rather than the reworking of bedforms and previously deposited sediments. The same sedimentary structures are seen

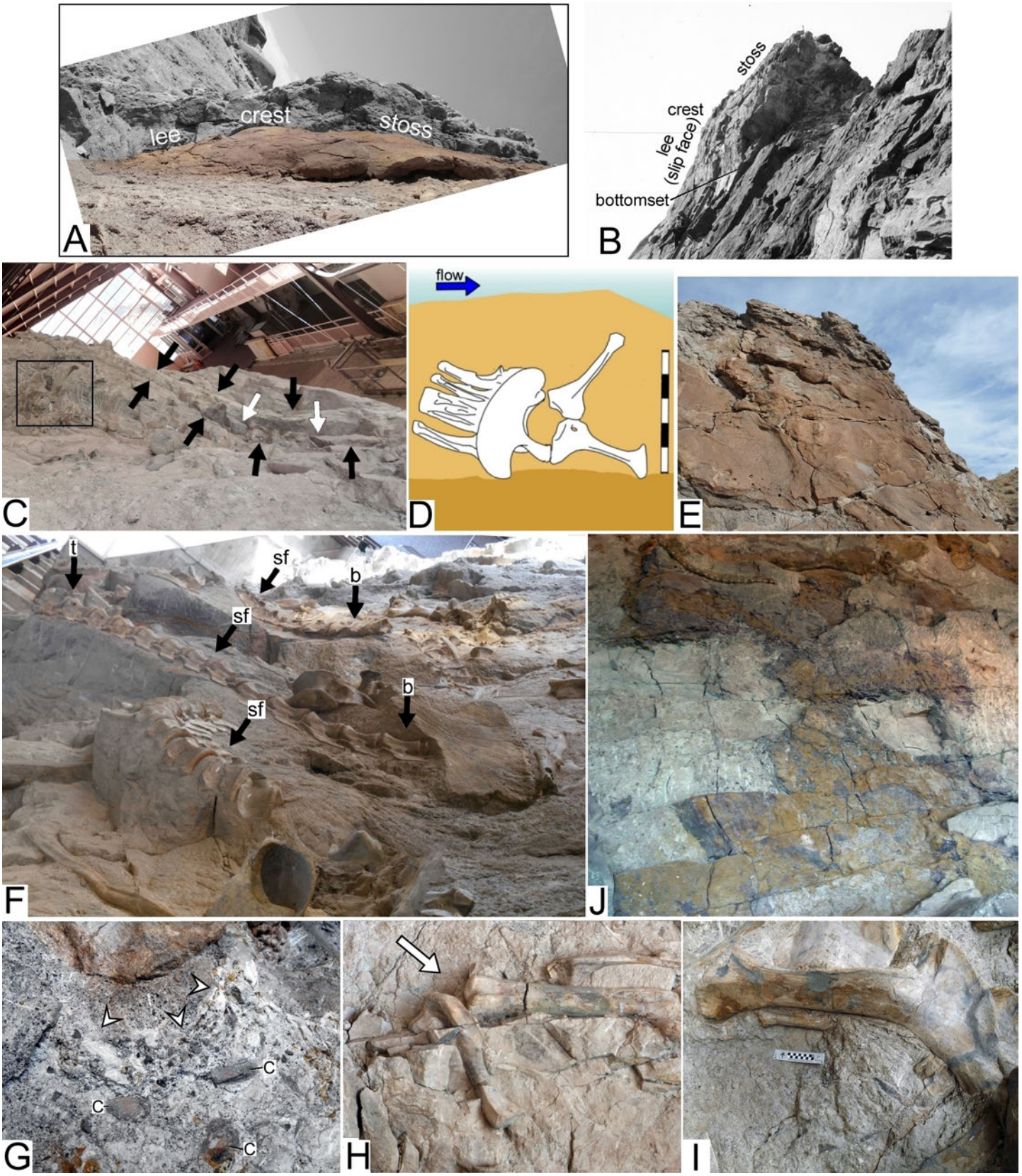

Figure 13 caption is on the following page.

Figure 13 on the previous page. (A) Linguoid dune in profile at Camp Gulch (40.4409°N., -109.3052°W.). (B) Mega-bedform in the quarry was exposed several years earlier by a rockfall noted in a letter by Earl Douglass (November 4, 1916). Photograph taken sometime between 1924–1929 and the bedforms have since been removed in the late 1930s by Works Progress Administration workers. (C) Mega-bedform, 1.52 m tall, on the quarry face. Arrows designate slip faces on the lee side. The box indicates the location of a dinosaur pelvis laying facedown. (D) Sketch showing how the pelvis in (C) was buried standing face down. Scale in dm. (E) Scours and troughs on the top surface of Quarry Sandstone (40.4401°N., -109.2987°W.). (F) Planar face of a straight-crested bedform delineated by strings of dinosaur vertebrae as seen in the QEH. Vertebrae on or near the same slip face (sf) become horizontal on the bed bottom (b). One string of vertebrae is nearly horizontal at the top (t) of the planar dune. Note other scattered horizontal bones on the bed bottom. (G) Infilled scour (indicated by arrows) downstream of the bone. Clam (c) valves are in a stable position in the flow shadow. (H) Upstream inclination (arrow) of large bones due to under scour. Note that the bones cut across the bedding surface. (I) Small bone in the flow shadow of a larger bone (sauropod ischium). Scales in cm. (J) Sideritic stained mud drape at QEH.

in archival photographs of the Quarry Sandstone before their removal during excavation (Figure 13B). High-angled inclined strata (a.k.a. planar stratification) are also present and are best seen on the quarry face where strings of vertebrae are draped over the slip face (Figure 13F); these inclined strata generally range from 10 to 30 cm thick. Finer-grained sandstone atop the bedforms sometimes are horizontally laminated, indicative of high-energy deposition during supercritical flow over the top of bedforms during the waning stage of flow. Also visible on the quarry face are infilled scours. Many of these are adjacent to dinosaur bones as contrasting sediment grains (Figure 13G).

Flume studies have shown that scours form as a result of three-dimensional flow separation (turbulence), creating areas of acceleration and deceleration. The highest values of turbulence occur in regions of highest pressure on the bed in front of and immediately adjacent to an obstacle (Carpenter, 2020a) and indicate regions of flow turbulence (Kirkil and Constantinescu, 2010; Euler and Herget, 2012; Maity and Mazumder, 2014). Helical flow results due to downwards hydrostatic pressure, creating a horseshoe vortex. This vortex plucks or lifts sand grains upwards into the flow, thereby causing bed erosion or scour. Deposition of the transported sand occurs in the flow shadow, a region of flow deceleration and low pressure. If erosion exceeds the depth and width of the obstruction, underscour may result. Upstream scouring may cause bones to dip upstream, thus contributing to their own burial (Figure 13H; Carpenter, 2022). Smaller bones and shells are often found in what was the downstream flow shadow of larger bones (Figure 13I).

The sandstone bodies are separated in places by thin pale yellowish-orange (10YR 8/6), grayish-orange (10YR 7/4), and moderate red (5R 5/4) mottled sideritic mud drapes (Figure 13J) across gently undulatory erosional surfaces that are similar to those within compound bars as revealed by ground-penetrating radar (Sambrook Smith et al., 2006). These drapes were noted by Lawton (1977), Dodson et al. (1980), and Turner and Peterson (1992a).

The uppermost sandstone bed (fourth sandstone bed) is treated separately because little of it remains for study. It was removed because preservation of the fossil bones was generally poor (Museum Geologist Theodore White, memorandum to Superintendent Jess Lombard, October 1, 1963). Archival color photographs and traces remaining in the QEH show that on the west side of the quarry, this sandstone is separated from sandstone 3 by a wedge of purple-tinted muddy sandstone or sandy mudstone (Figure 14A), but it is in contact with sandstone 3 on the east side of the quarry (Figures 14B and 14C). Traces of sandstone 4 east of the QEH are white (N9) to very light gray (N8) and poorly cemented (Figure 14C). Walker (1943, p. 7) reports that this bed was 2.4 to 3 m thick, "composed of a fine to coarse sandstone with considerable clay as a binder [i.e., muddy sandstone]. It also has concretionary masses [recognized as indurated clay balls by Boyle, 1938b] scattered throughout… The matrix composing this … layer is very unstable and weathers rapidly." The sandstone on the east side of the QEH is clayey, medium sand to granule size, poorly sorted, subrounded to rounded, with mudstone

Figure 14. (A) Archival photograph of steeply dipping beds with view of bed tops. The purple mudstone (upper part of photograph) underlies the muddy white sandstone 4 towards the west end of the quarry. (B) Archival photograph showing sandstones 3 and 4 in contact on the east end. The kneeling person in the red circle is pointing to fossil bones. The arrow indicates the general location of (C) today. (C) Remnant of sandstone 4 on the east side of the QEH. (A) and (B) courtesy of the National Park Service, taken in the early 1950s.

or siltstone clasts that are mostly the same color as the sandstone except for an occasional surface stain of pale yellowish-orange (10YR 8/6) or dark yellow-orange (10YR 6/6). Less common clasts are of medium light -gray (N6) with flecks of black organic material. The clasts are 2 to 20 mm in diameter, rarely larger.

Sheet (Tabular) Sandstone Beds

Thin sheet or tabular sandstone beds are present below and above the Quarry Sandstone. Those below are often wedge-shaped and feathering at the edges, and are present on the east side of the QEH below the stacked sandstone beds (Figures 15A and 15B). These thin het-

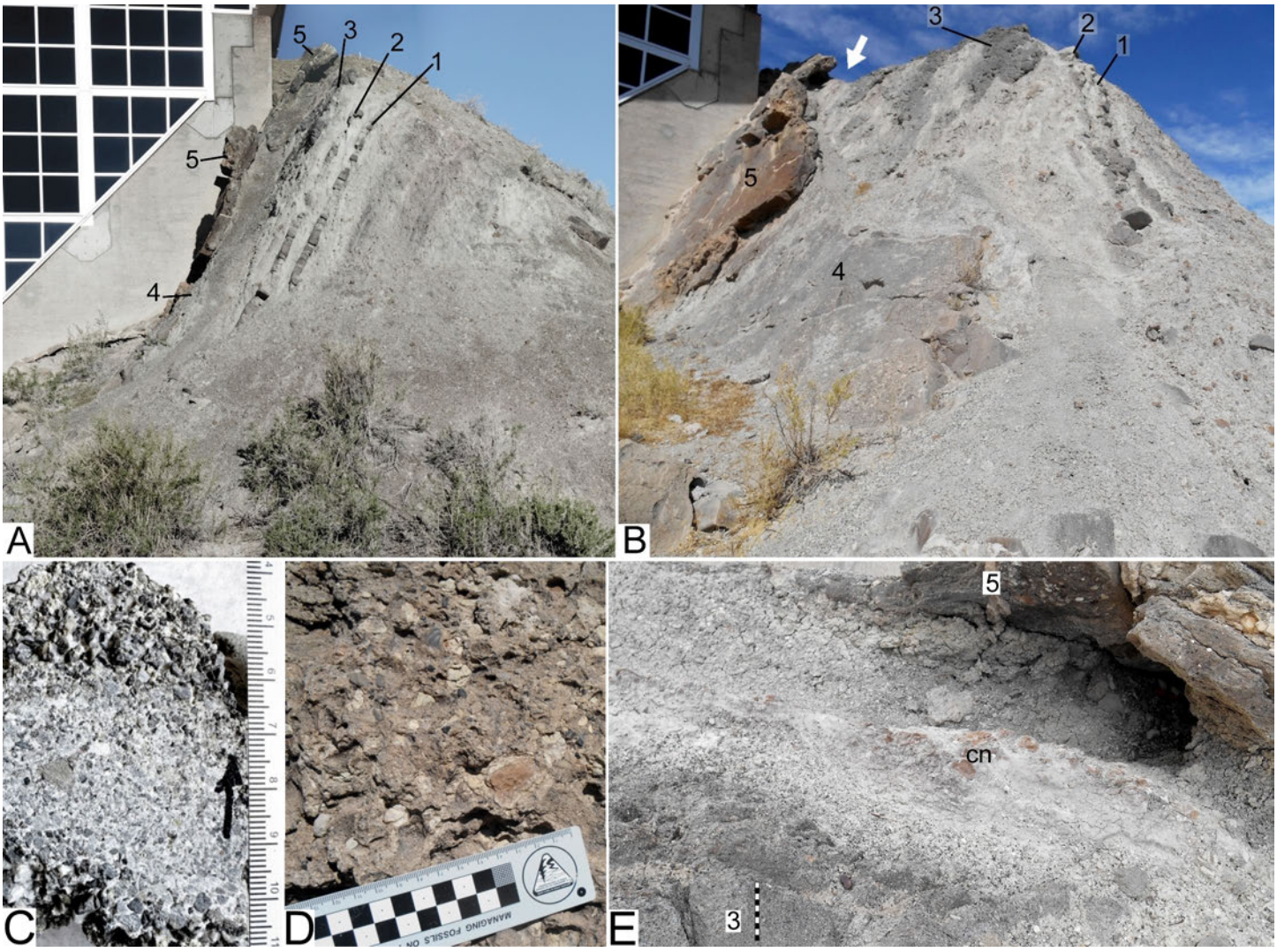

Figure 15. (A) Edge view of tabular sandstone beds (labeled 1 through 5) exposed on the east side of the QEH. Sandstone 3 wedges out downdip, and sandstone 4 wedges out updip. (B) Oblique view of thin-bedded sandstone of (A). The arrow indicates the location of the view in (E). (C) Sectioned sandstone 1, DINO 48398, showing fining upwards, then coarsening upwards within a narrow zone. The arrow indicates upward direction. Scale in mm. (D) Carbonate (orange) and clay (white) pebble conglomerate at the top of sandstone 4. Note pits from eroded clay nodules. (E) Fining upwards from sandstone 3 (labeled 3) to the base of sandstone 5 (labeled 5). Sandstone 4 wedges out and does not extend this far (see B). Carbonate nodules (cn) formed in the muddy sandstone beneath the sandy mudstone below sandstone 5. Scales in cm.

erolithic sandstone wedges have abrupt and sometimes erosional bases, and internally they may exhibit one or more fining and coarsening cycles resulting from fluctuating flows (Figure 15C). These sandstone beds feature increasingly larger clasts from the lowest to the highest bed, with scattered matrix-supported pebbles of subrounded grayish-black (N2) or light-gray (N7) to very light gray (N8) cherts. The upper surfaces may also contain mudstone clasts or pits from clasts that have eroded out (Figure 15D). The lowest sandstone, numbered 1, is underlain by coarsening-upward muddy sandstone beds. The sandstone bodies are separated by white (N9) to very light gray (N8) muddy sandstone lenses that fine upwards (Figure 15E).

Sandstones 1 and 2 (Figures 15A and 15B) are wedge shaped, become thinner in the up-dip direction, as does sandstone 4. Sandstone 3 thins in the down-dip direction on the east side, where it grades into a gravelly or

pebbly white (N2) to light-gray (N7) muddy sandstone. The gravel and pebbles are predominantly grayish-black and light-gray chert. Sandstone 3 can be traced west to a muddy sandstone (see Figure A1 in the Appendix 1) on the west side of the QEH and is used as the datum for correlation. This datum indicates that the base of the Quarry Sandstone is about 1 to 1.5 m lower on the east side of the QEH than on the west (Figures 4 and 10A). Sandstone 5 forms the lowermost bone-bearing sandstone within the QEH, thus showing that these sandstone sheets are intimately linked to the Quarry Sandstone. The five thin sandstone beds are more resistant to erosion, being cemented with silica or calcium carbonate. Whereas the muddy sandstone beds between them erode more easily, leaving the harder sandstone beds projecting where they crop out. Similar thin sandstone beds are present beneath the Quarry Sandstone east of the QEH (Figure 6).

Archival photographs show the now-missing tabular sandstone beds overlying the Quarry Sandstone (Figure 16). This area is now occupied by part of the QEH and a service road. The sandstone beds considered overburden to the underlying bone-bearing sandstone beds were described by geologist Albert Boyle (1938a, p. 13), in charge of their removal, as "fine-grained friable greenish sandstone…" of variable thickness. The abundance of clay in these beds can be inferred by Boyle's observation that "the sandstone sloughs down readily when slightly moistened." The ease of slaking in water was confirmed with a small sample collected on the southwest corner of the QEH. As a result of its ease of weathering and erosion, these sandstone beds originally formed the saddle on the divide between Camp Draw on the west and Neilson Draw on the east and between the silicified Quarry Sandstone and calcrete of the Cedar Mountain Formation (Figure 17).

On the west side of the QEH, the boundaries of many of the stacked sandstone sets are poorly defined in contrast to the sharp base of the overall unit. Here, channel sandstone beds grade laterally with a rapid increase in silt and clay content over a span measured in meters (Figure 18A). In the cross section of the strata visible in the QEH foundation trench, the sandstone is conglomeratic, consisting of rounded mudstone clasts (Figure 18B) or irregular mudstone clasts in a sandstone matrix that also contains floating dark chert pebbles (Figure 18C). These muddy sandstone bodies can be traced outside the QEH as a series of three sheet sandstone beds separated by mudstone (Figure 18D). Dinosaur bones are preserved in these sandstone beds. The most complete bone found recently is a femur (leg bone) oriented parallel to the local shallow flow in a direction away from the sandstone of the quarry (Figure 18E).

The sandstone beds coarsen upwards (Figure 19A) or have an erosional base associated with the distributary channel part of the sheet sandstone beds (Figure 19B). From the quarry wall in the QEH westward, there is a shift from chalcedonic to calcitic cementation of the sandstone as the clay content increases and the clay inhibits chalcedony formation (Figure 18A), resulting in a reduction in resistance to weathering and erosion as seen in Figure 18D. Elsewhere along the ridge, areas of higher clay content are apparent in satellite imagery as light-colored soils and on the ground as gravelly or sandy, very light gray (N8) soils that are commonly vegetated and require trenching to expose the less weathered muddy sandstone.

Mudstone Facies

The mudstone facies are best accessed adjacent to the QEH because construction activity has removed vegetation and soil. Much of the mudstone analysis was conducted there and is representative of the mudstone bracketing the Quarry Sandstone except as noted below. Retallack (1997) proposed names for the paleosols mudstone facies at Dinosaur National Monument, but these have not been widely adopted (e.g., Demko et al., 2004).

On the west side of the QEH is a remnant of "Dinosaur Peak," a topographic high point named by Earl Douglass. The east face is cut perpendicular to the strike, exposing the mudstone beds immediately below the Quarry Sandstone. At 4 m below the Quarry Sandstone, there is an abrupt color and textural change from a silty mudstone to a sandy mudstone unit (Figure 20A). Archival photographs of a less weathered surface show that the lower mudstone had a thin, light-colored ash bed or thin strings of light-colored sandstone (Figure 20B). The lower mudstone (Figures 20C and 21A)

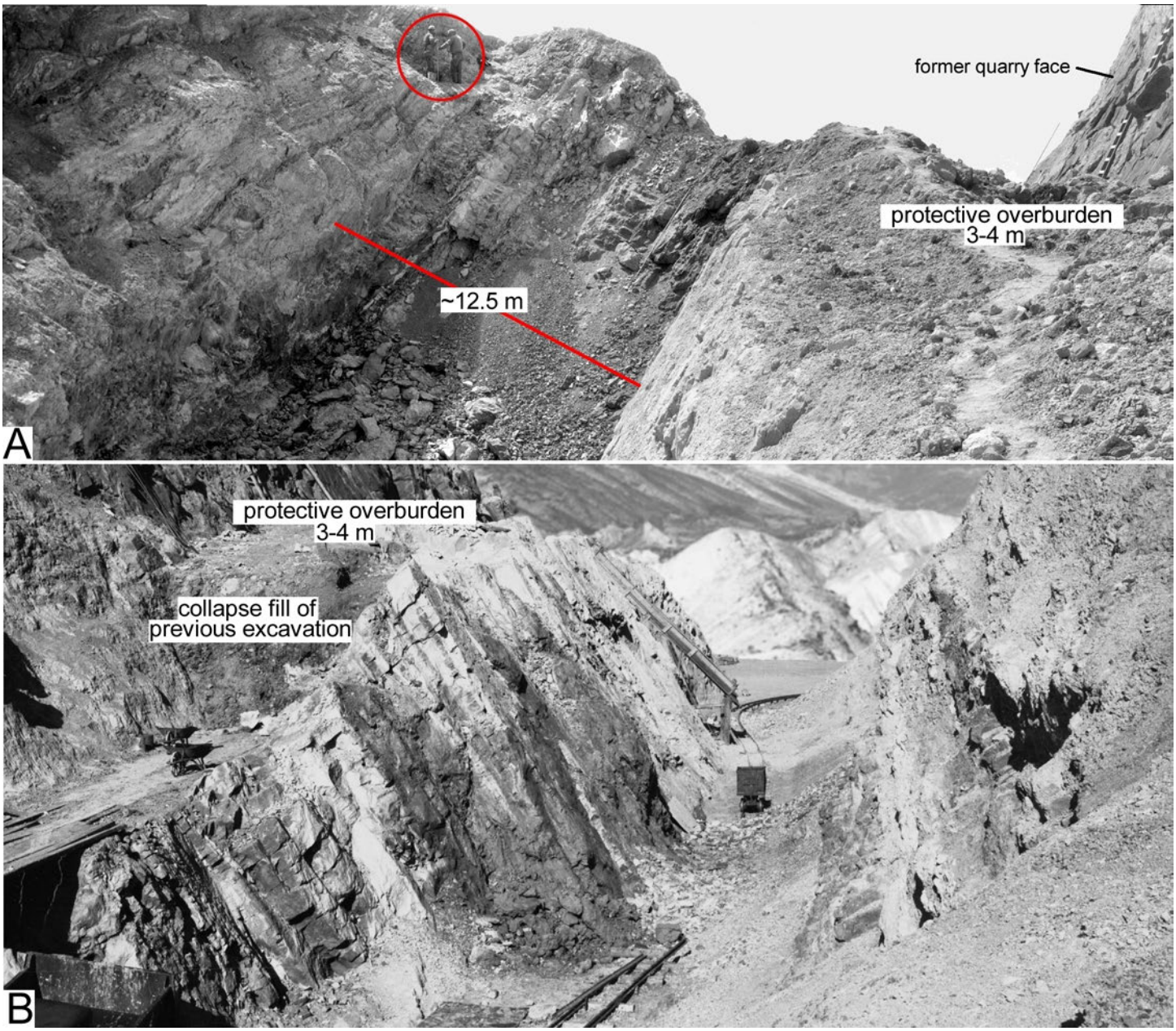

Figure 16. Archival photographs showing the now-missing strata over the Quarry Sandstone. (A) View west with workers in the circle. (B) View east showing part of the bedding in the protective overburden (1938). Photographs by Albert Boyd, courtesy of Uintah County Library Regional History Center.

is predominantly medium dark-gray (N4). In polished cross section, however, the mudstone is polychromatic in color, including pale greenish-yellow (10Y 8/2), pale yellowish-green (10GY 7/2), very light gray (N8) to medium gray (N5), and even a little moderate pink (5R 7/4). These colors accentuate extensive bioturbation, including possible rhizoliths (Figure 21B). The upper sandy and silty mudstone is light gray (N7) (Figure 20D). This sandy mudstone facies correlates with the zone of muddy sandstone and tabular sandstone on the east side of the QEH (Figures 4 and 14).

The upper mudstone shows immature pedogenesis with mottles of grayish-purple (5P 4/3) mudstone that may be mottled up to 50% by diffused light greenish-gray (5G 8/1) redoximorphic iron depletion (Figure 22A). These mottle sizes are in the coarse range (5 to 20

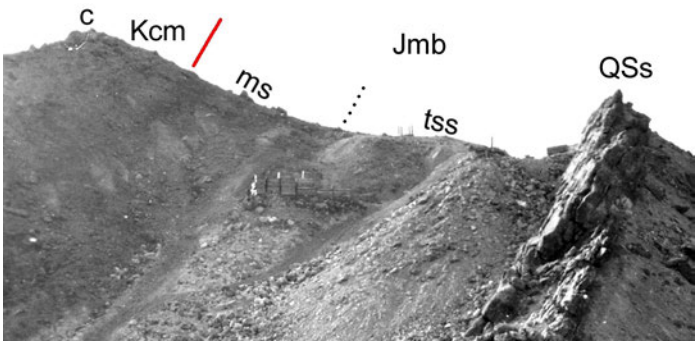

Figure 17. The saddle eroded into muddy tabular sandstones seen in Figure 16. Abbreviations: c – calcrete; Jmb – Brushy Basin Member of the Morrison Formation; Kcm – Cedar Mountain Formation; ms – mudstone facies; QSs – Quarry Sandstone; tss – tabular muddy sandstone region; ms – mudstone. Photograph by Earl Douglass (Carnegie Museum).

mm) of Schoeneberger et al. (2012). Other pedogenesis includes white (N9) redoximorphic iron depletion delineating root traces (Figure 22B). Pedogenesis on the east side of the QEH includes weathered bands of pale-purple (5RP 7/2) below the crevasse splays. Unweathered mudstone, as exposed in trenches, is dusky-purple (5RP 4/2) to grayish-purple (5P 4/2) with streaks of dusky-yellow (5Y 6/4) to very light gray (N8) redoximorphic iron depletions (Figure 22C). Pedogenic alteration is also seen on the southwestern part of the quarry wall in the QEH (Figures 22D and 22E). These diverse examples show that early protosol development is widespread in the mudstone facies. Paleosol carbonates are present and are discussed under Carbonates.

One mineral identified in many of the thin sections (e.g., Appendix 1, Figure A2G) is the green mineral glauconite, or glaucony, as defined by Odin and Létolle (1978) and Odin and Matter (1981), where the proportion of smectitic and micaceous layers is undefined. It is present in both the mudstone and carbonate facies as green and brown grains, some of which are peloidal, suggesting a biogenic origin. Non-biogenic glaucony is most likely from pore-water chemistry altering existing smectite clay (Meunier, 2005), which is abundant in the Brushy Basin Member, rather than from a marine incursion with which it is often associated (Velde, 2014). Furquim et al. (2010) report that glauconite in the Pantanal wetland soils of Brazil is often interstratified with smectite, forming a mixed-layered mineral structure. Its formation is favored by alkaline, saline conditions with high potassium concentrations and reducing environments that stabilize Fe^{3+}. Glauconite crystallizes through neoformation from amorphous silica-rich materials, or via transformation of smectite layers, with its formation varying based on seasonal microenvironmental changes. The mineral was previously reported from the Brushy Basin Member by Craig et al. (1955) and Keller (1958, 1962), who referred to glaucony as "glauconitic mica." A more detailed analysis of various mudstone beds is presented in Appendices 1 and 2.

Tuff Facies

Thin volcanic ash beds are present throughout the Brushy Basin Member, and Christiansen et al. (2015) reported 42 beds in Douglass Draw. These ashes are commonly shades of light gray or white (Figure 23A) and sometimes have a faint pinkish, purplish, or greenish tint, as noted by Turner and Peterson (1991). Internally, the ashes may be structureless, especially if diagenetically altered (Figure 23B), laminated, or composed of accretionary ash pellets (Figure 23C). Another example of ash pellets consists of matrix-supported, 1 to 10 mm ellipsoid-to-spherical pellets distributed randomly throughout the tuff (Figure 23D). These pellets are composed of the same ash that encases them and they lack internal organization. They resemble the AP2 accretionary pellets of Brown et al. (2012), although they lack internal structure, and some are significantly larger. The loss of internal structure might be diagenetic, but retention of the external shape suggests a primary structureless interior.

These AP2 pellets occur in an ash bed immediately underlying sheet-like sandstone 1 adjacent to the Quarry Sandstone on the west side of the QEH (Figure 23E). This tuff is about 70 cm thick and slightly calcareous. Unlike many of the ashes in the study area, there is no siliciclastic detritus, and this clean ash must represent a primary deposit of a large volcanic eruption of an ash-rich plume into a standing body of water. The predominant grain size of the tuff is 9 to 23 μm (fine- to medium-silt size), but a small percentage is 30 to 60 μm (medium- to coarse-silt size). Dispersed throughout

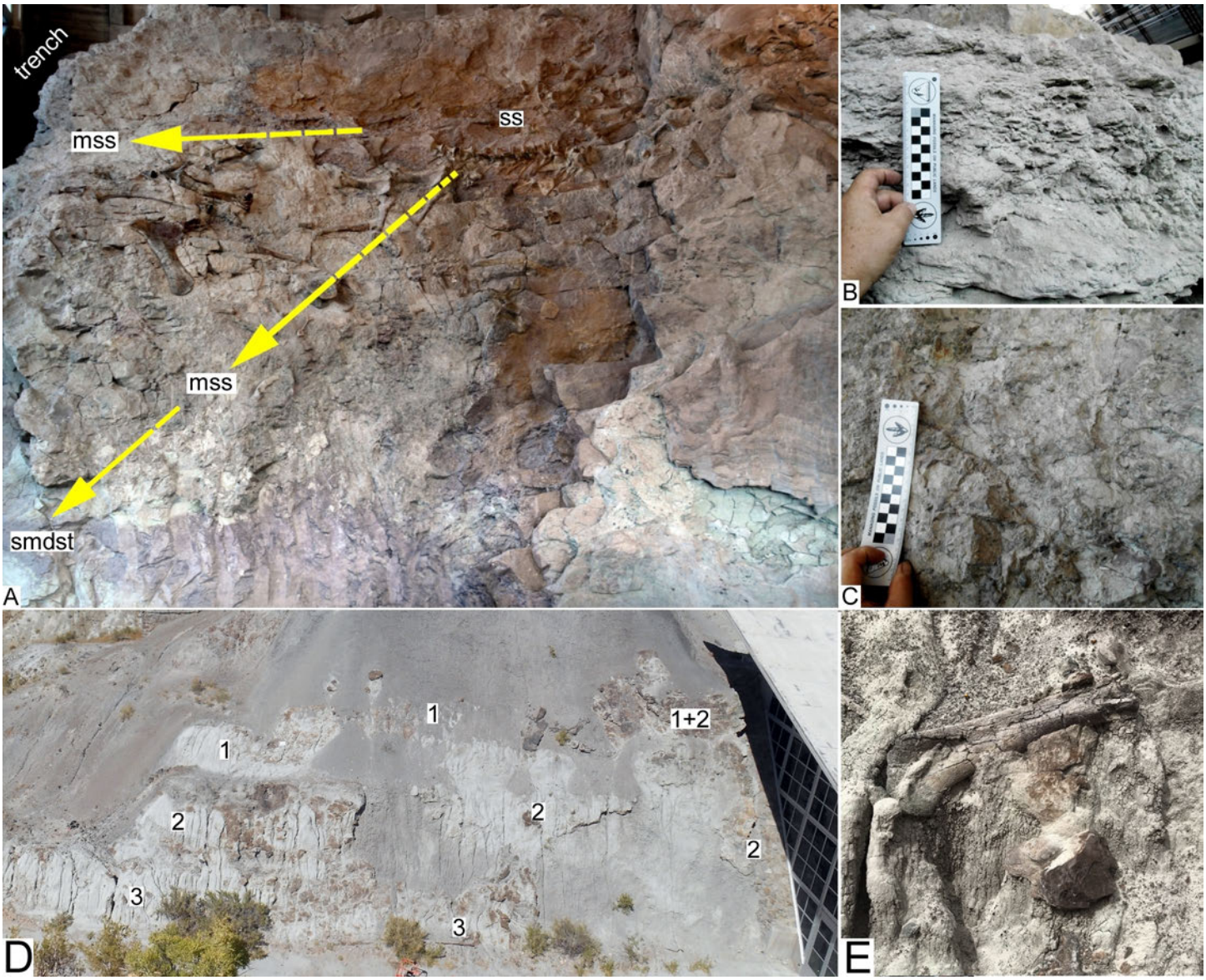

Figure 18. (A) Sandstone (ss) grading rapidly to muddy sandstone (mss) to sandy mudstone (smdst) at QEH. (B) Rounded mud clast conglomerate exposed in the foundation trench that was excavated for the QEH. Scale in cm. (C) Irregular mud clast conglomerate exposed in the foundation trench. Scale in cm. (D) Muddy sheet sandstones (labeled 1, 2, 3) on the west side of the QEH. (E) Long bone (*Stegosaurus* femur) in a splay deposit on the west side of the QEH.

the ash are black minerals, primarily biotite. Zircons are abundant and well preserved (Figure 23F) and gave a weighted mean Th-corrected $^{206}Pb/^{238}U$ CA-ID-TIMS zircon age of 150.77 ± 0.39 Ma (K. Chamberlain, University of Wyoming, personal communication, October 5, 2021). This ash provides the best age yet for the deposition of the Quarry Sandstone, and hence of its preserved dinosaur fauna.

Carbonate Facies

Carbonates faicies includes carbonate beds or nodules in the sandy mudstone facies and as reworked clasts up to 15+ cm in maximum diameter in sandstone beds (Figure 24A). Special attention was given to nodules in mudstone because Dodson et al. (1980), Fiorillo (1994), and Retallack (1997) stated that some of those at Dinosaur National Monument were pedogenic in origin

Figure 19. (A) Rapid coarsening upwards of sandstone 2. Scale in mm. (B) Lenticular bodies (distributary channels) associated with the sheet sandstones of Figure 13D. Scale in dm.

and indicative of well-drained or seasonally dry soils. In addition, Retallack (1997) used the depth to the calcic horizon in the predominately dusky red (10R 3/3), clayey, calcareous paleosols overlying the Quarry Sandstone to estimated rainfall as approximately 600 to 900 mm/yr.

Nodules in mudstone are most commonly 0.75 to 2 cm in diameter and often have abrupt rather than diffuse boundaries with the encasing matrix (Figure 24B). Some of the oriented samples showing original structures indicate an in-situ formation (e.g., Appendix 1, Figure A7A). Carbonate nodules typically erode from the mudstone (Figure 24C) and accumulate as a lag of fragments and whole nodules at the base of slopes. In contrast, limestone beds are thin (about 10 cm) and are best seen on the west side of the QEH (Figure 24D). This limestone tends to erode as large fragments (Figure 24E) and may be the source for the larger carbonate clasts in the sandstone beds. Both carbonate types are predominantly white (N8) or light greenish-gray (5G 8/1) to medium light-gray (N6) or even grayish-purple (5P 4/2). Most carbonates have a weathered surface of pale yellow-orange (10YR 8/6) to grayish-orange (10YR 7/4) caused by the oxidation of iron within the carbonate.

Dodson et al. (1980) noted the carbonate horizons that they identified as calcretes in "red" or "purple" paleosols as well as in "gray-green" mudstone. Only nodules from the mudstone beds weathered "gray-green" on the east side of the QEH were examined by thin section. Some of these contained diplostracan branchiopods, ostracods, and rare charophytes. The fact that many of the diplostracan and ostracods are fragments or single valves, and some valves are at an angle relative to the bedding plane of oriented rock samples, suggests that these are mostly allochthonous fossil assemblages (e.g., Appendix 1, Figure A4).

Diagenetic events observed in cross-sections and thin sections of the carbonates include septarian cracks infilled with calcite or quartz (Appendix 1, Figure A4A) and pedogenetic fracturing (Appendix 1, Figure A5A). Thin section analysis (Appendix 1) indicates that the allochems in the carbonate facies are dominated by ostracod fossil fragments and complete or nearly complete shells (e.g., Appendix 1, Figure A4C). This and the abundance of calcareous mudstone suggest that the limestones were deposited in relatively quiet water. Grains observed in the carbonate facies are predominantly quartz, with rare grains of other minerals that suggest their igneous origin. Grains are mostly silt-sized or smaller and in such great abundance as to qualify the limestones as being silty. In contrast, Lawton (1976, p. 5) noted that many of the lenticular limestone beds in her samples were "clean," presumably meaning free of siliciclastics. Lawton (1976) did note, however, that one limestone body contained "calcite-coated micro-mudballs and irregular blocky clasts of silt and clay in calcite and chalcedony cement." We also noted the presence of mud clasts in some of our samples. See Appendix 1 and Appendix 2 for additional photographs and descriptions.

INTERPRETATION OF LITHOFACIES

Isolated lenticular conglomeratic sandstone bodies are encased in sandy mudstone and we interpret them as fill of single-threaded channels. The sandy mudstone

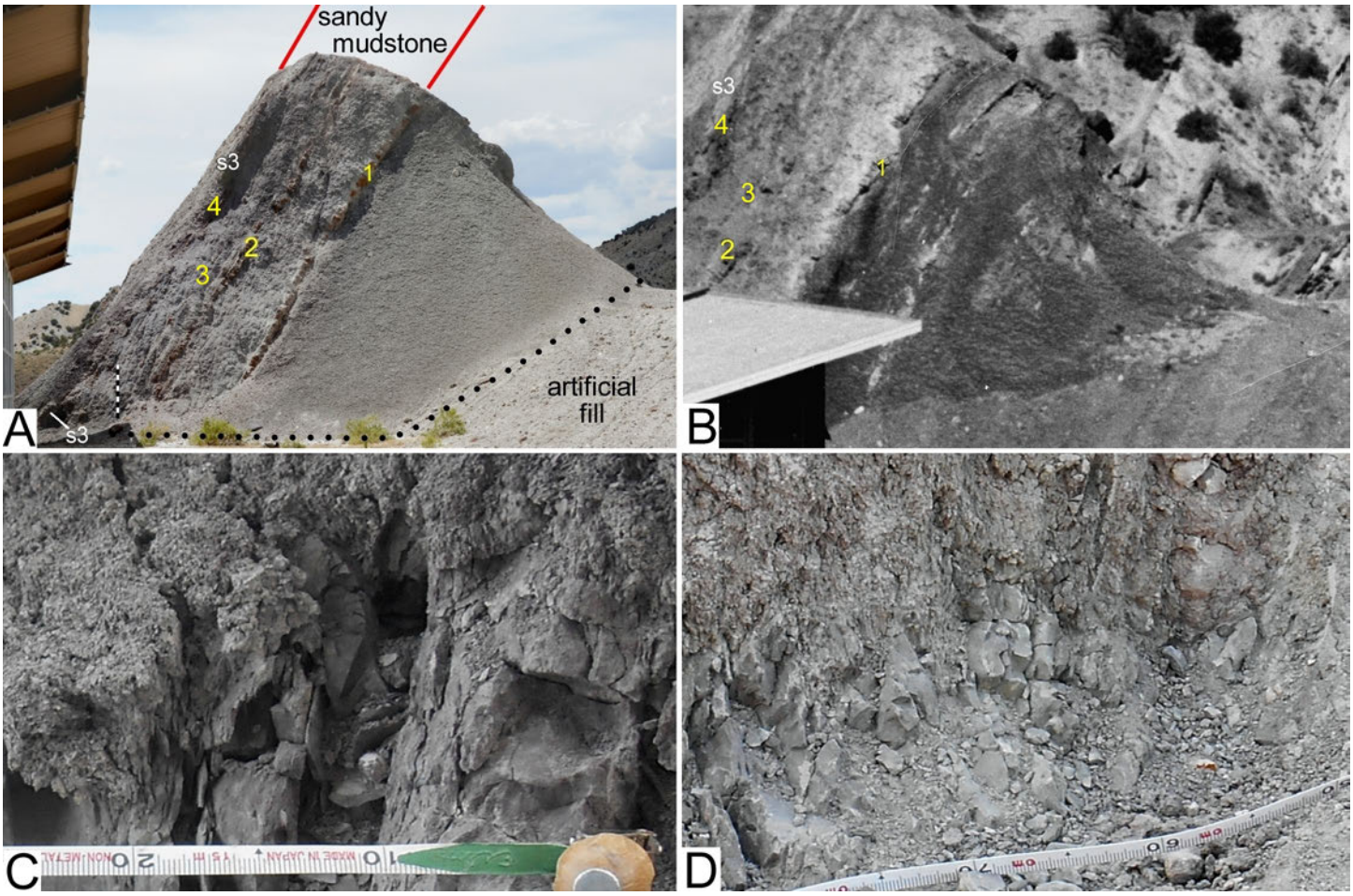

Figure 20. (A) Abrupt facies change from a lower clay-rich mudstone to an upper sandy and silty mudstone at Dinosaur Peak, west side of the QEH. Also present are three limestone beds (labeled 1, 2, 3). Abbreviation: s3 correlates with sandstone 3 on the east side (see Figure 15). Scale in decimeters. (B) Historic photograph (around 1958) showing lenses of sandstone and carbonate in the unweathered gray mudstone. Compare with (A). Photograph courtesy of National Park Service. (C) Pedogenic mottling (protosol) with colors saturated to bring out differences. (D) Detail of blocky sandy and silty mudstone. Scales in B through D in cm.

are interpreted as proximal overbank deposits. However, the poor exposure due to the steep dip and in-situ weathering makes it difficult to determine whether lateral accretions are present or if the proximal overbank deposits are levee or crevasse splay deposits.

The lowest thin tabular and wedge-shaped sandstone in the context of the muddy sandstone are interpreted as a succession of crevasse splay deposits preceding an avulsion and redirection of the river that deposited the Quarry Sandstone. The different directions of wedging are expected as the loci of the crevasse splay deposition shift with each event (Burns et al., 2019). Of the upper, now missing, bedded tabular sandstone bodies (Figure 16), little can be said because those beds cannot now be examined. A proposal has been submitted to trench through the access road around to the west side of the QEH to provide this important information.

Several lines of evidence taken together, rather than any single feature, indicate that the Quarry Sandstone consists of stacked braided (multichannel) fluvial deposits: (1) the sandstone bodies are sheetlike, having high width-to-thickness ratios characteristic of multithread rivers (Labourdette, 2011); (2) vertical accretion of sandstone sheets separated by gently undulating erosional surfaces represents stacked compound bars similar to those of the South Saskatchewan River (Sambrook

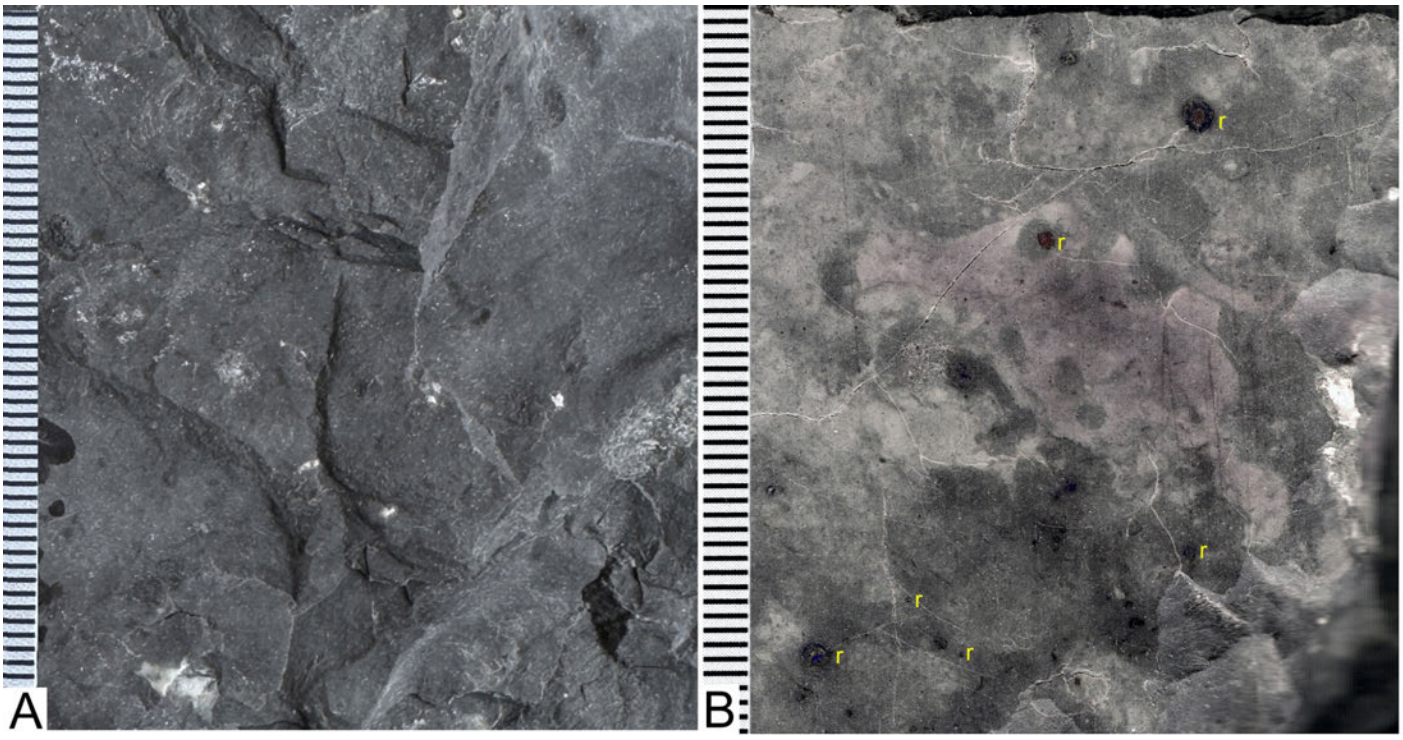

Figure 21. (A) Detail of smectitic lower mudstone (DINO 48397). (B) Polished surface of (A) showing extensive bioturbation and possible rhizoliths (labeled r). Scale in mm.

Smith et al., 2006); (3) the coarse sand to cobble grain-size fraction ranges up to 1 cm in diameter (rarely greater than 10 cm), excluding the transported greater than 160-cm dinosaur limb bones, but the sand grains typically range from 0.5 to 1 mm in diameter with D50 1 mm (Carpenter, 2013); (4) the generally clean sands indicate turbulent flow or bed reworking that winnowed out clay particles; (5) the presence of pockets of fine-grain slack-water deposits in otherwise coarse-grained sandstone, which are mostly associated with troughs (Lynds and Hajek, 2006); (6) the abrupt transition from coarse-grain sandstone to fine-grain sandstone and thin clay drapes over undulating erosional surfaces indicates a rapid drop in transport energy associated with flashy discharge; (7) the presence of three-dimensional bars (mega-bedforms); and (8) the lack of lateral accretion deposits, which are more typical of sinuous single-threaded rivers. Trough cross-stratification and planar stratification are not included as evidence because both also are present in single-channel sinuous river deposits and crevasse splays (Brierley, 1996; Bridge, 2003). These multiple lines of evidence align with modern alalogues of the complex subsurface architecture and history of sandy braided river deposits revealed by ground-penetrating radar of the Saskatschewan River, deposits in Canada (Sambrook Smith et al., 2006).

The correlation between grain size/channel depth (grain size D50 = 1 mm; depth = approximately 1 m for the Quarry Sandstone) and slope (Paola and Mohring, 1996; Friend and Dade, 2005) suggests that the river depositing the Quarry Sandstone had a paleoslope of 10^{-3} to 10^{-4} with bedload dominating. This projected paleoslope is close to the 1.1×10^{-3} estimated for the Morrison depositional environment by Trampush et al. (2013), whereas Lawton (1976) concluded the channel gradient at the quarry as 3.8×10^{-4}. The paleoslope methods of Lynds et al. (2014) were not used because these were developed for sandy suspended-load rivers with maximum grain size of less than 0.5 mm and D50 is significantly less; these values are significantly less than the 1 mm D50 of the Quarry Sandstone.

Peak discharge most likely occurred during seasonal rains, resulting in overbank flooding and floodplain inundation. Paleocurrent data for the Quarry Sandstone

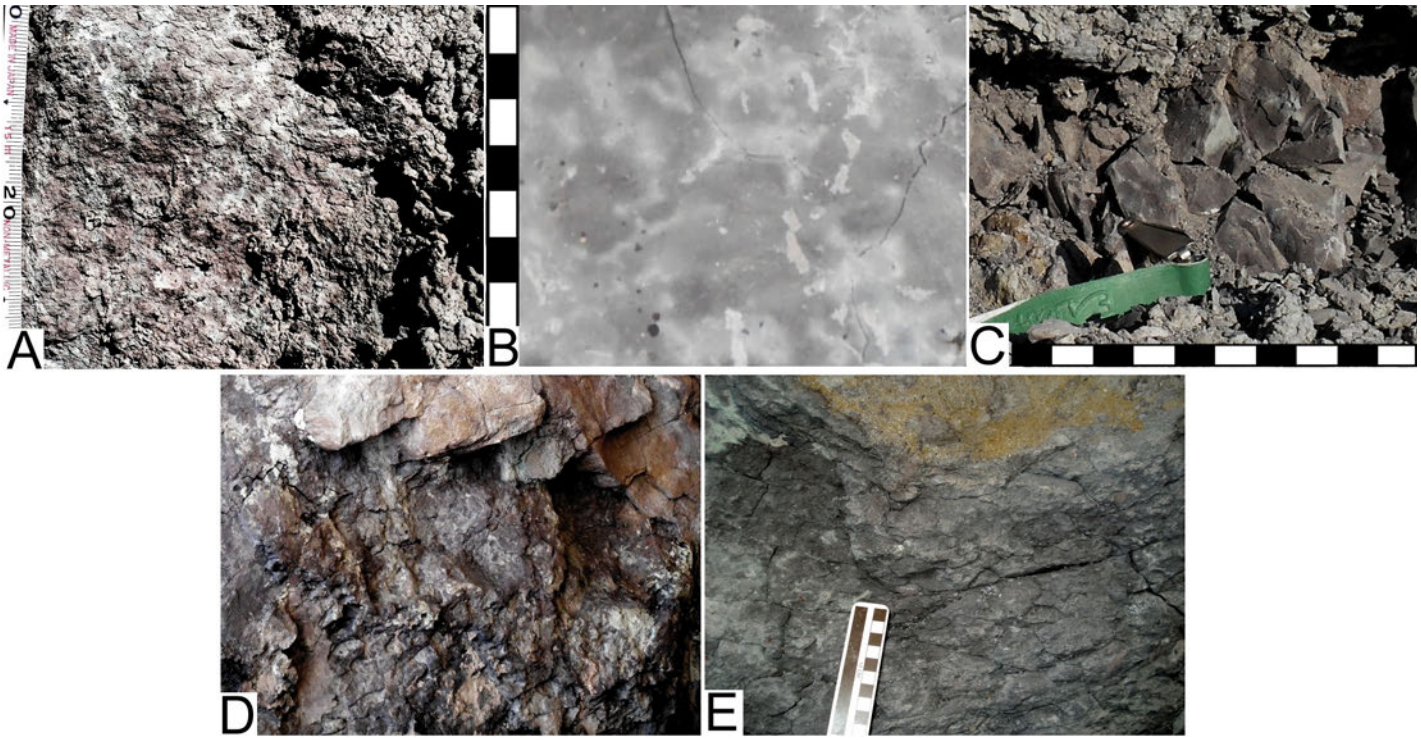

Figure 22. Diverse examples of pedogenesis in mudstone beds of the study area. (A) Light-colored mottles in reddish mudstone (color enhanced). (B) Rhizoliths in gray calcareous mudstone. (C) Rhizoliths and light-colored mottles in gray to brown mudstone (color enhanced). (D) Light-colored mottles in purple mudstone on the west end of the QEH (color enhanced). (E) Light gray and dark gray mottles in mudstone on the west end of the QEH. Scales in cm.

from sedimentary structures (Figure 25A), unionid clam long-axes (Figure 25B), and dinosaur limb bones (Figure 25C) indicate the overall flow was toward the southeast. The greater vector spread of the limb bones is because some bones tend to roll perpendicular to the current, and some bones are trapped against the upstream side of bone piles or jams (Carpenter, 2013). Perhaps the best paleocurrent indicators are the long whip-like tails of diplodocid sauropods (Figures 25D and 25E). These rope-like structures offered little resistance to water flow, as has been demonstrated experimentally in a water flume (Carpenter, 2020b).

Few of the channel sandstone bodies in the Quarry Sandstone have distinctive lateral margins or show an abrupt change in lithology or grain size that could represent the incised channel margin or bank. Most of the sandstone bodies show diffuse margins marked by a rapid increase in clay content, coincidental with a change from sandstone to muddy sandstone (Figure 18A) to sandy mudstone in which grains up to 2 mm may be suspended. This lack of well-defined or absent margins implies a fluvial system of frequent spillage sedimentation building the confining banks (Lewin and Ashworth, 2014; Lewin et al., 2017). Such systems are typical for non-montane braided or multithreaded river systems with their complex of active and inactive channels on the braid plain. These inactive channels may convey water at high river stage, resulting in pockets of finer sand sediments in otherwise coarse-grained deposits.

On outcrop, the transition from well-cemented, erosion-resistant channel sandstone to more easily eroded muddier sandstone typically takes place over a span of a few meters. This transition zone is not uniform, as local variation in clay content and cementation is reflected in the differential erodibility of the sandstone, such as seen on the west side of the QEH both within the building and adjacent to it (Figure 18B). These transitional sandstone bodies typically are fine-grained distally and are interpreted to be the proximal overbank facies, predominantly spillage sedimentation of levees and crevasse splay deposits (e.g., Cazanacli and Smith, 1998;

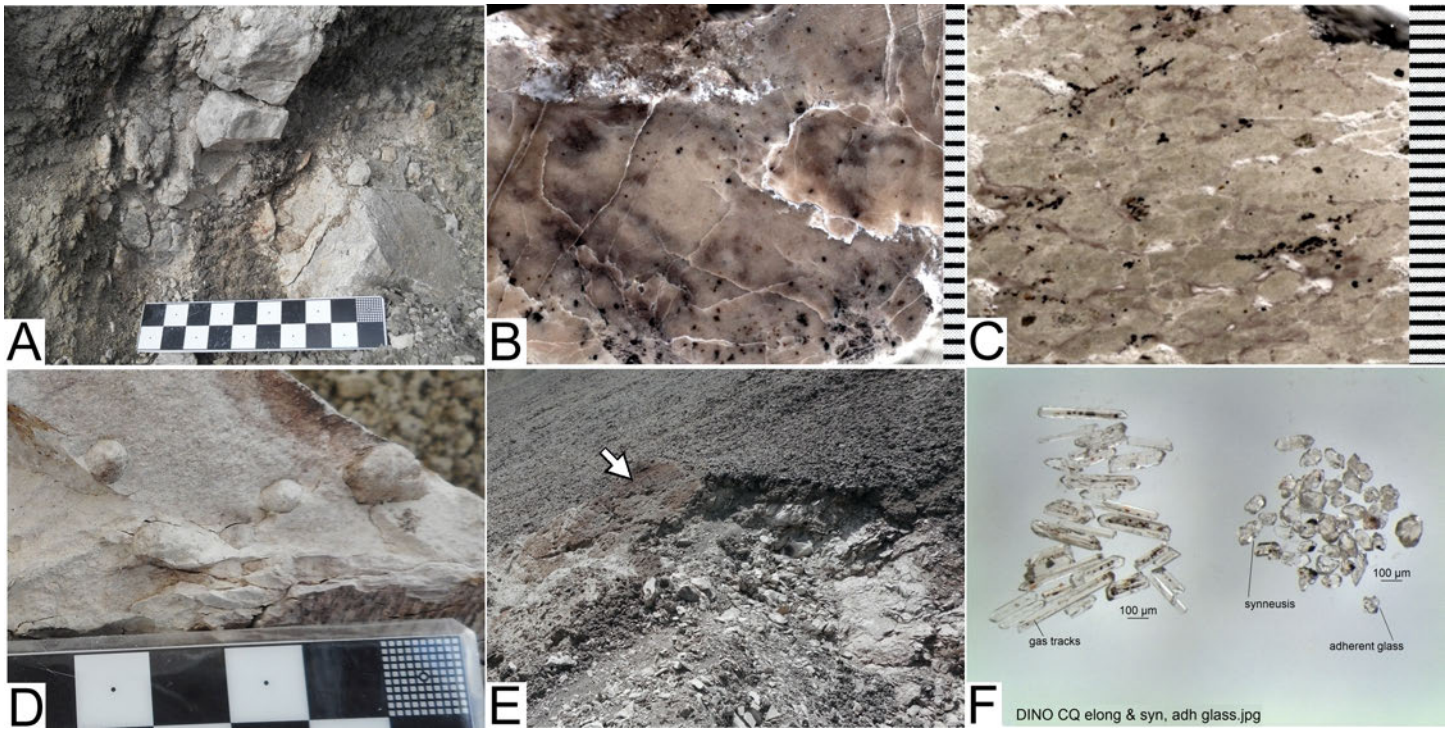

Figure 23. (A) Thin bed of volcanic ash in Douglass Draw. (B) Structureless diagenetically altered silicified ash from the right side of (A), DINO 48399. (C) Oriented compressed pellets of accretionary ash from the left side of (A), DINO 48400. (D) Matrix-supported Type AP2 accretionary pellets from (E). (E) Ash immediately below sandstone 1 of Figure 18D. (F) Example of pristine zircons from (E). Courtesy of K. Chamberlain, University of Wyoming.

Hudson, 2005; Alexander and Fielding, 2006; Lewin et al., 2017). The coarseness of these proximal overbank deposits is most commonly associated with fluvial systems having highly variable discharge (Alexander and Fielding, 2006).

Levee and crevasse splay deposits share similar criteria (e.g., sharp bases, distal thinning, and fining), and distinguishing them is made more difficult by the limited exposure of the Quarry Sandstone on the steeply dipping cross sections. The radiating paleocurrent pattern of crevasse splays, which is not known to occur in levees, has been identified on the west side of the QEH where two sandstone beds merge in a small area corresponding to a breakout point in a levee (Figure 18D). The main distributary channels of these splays are seen in cross section (Figure 19B) and prograding into the flood basin, evident by the coarsening upwards (Figure 19A).

Although levees tend to be well-drained because of their elevation above the bottomland, the absence of mature paleosols in any of the proximal sediments implies high rates of vertical accretion. Dinosaur bones occur in the transitional sandstone beds, but their sizes decrease away from the channel, corresponding to a decrease in flow velocity. The burial of these bones was probably due to downstream progradation of the levees during floods (Johnston et al., 2019).

The finer-grained mudstone and bedded limestone are interpreted to be floodplain and lacustrine deposits distal to the levee and crevasse splay deposits, hence representing the distal overbank facies. The floodplain deposits are drab gray (N6 to N3) calcic Gleysols with some carbonate nodules and some lacustrine limestone, as indicated by their microfossils. Many of the diplostracans in the limestone consist of only one valve of the bivalved carapace, which furthermore may be broken, indicating turbulent fluvial transport across the floodplain prior to deposition in topographic lows (i.e., areas of negative relief). Retallack (1997) referred to these gray mudstone beds as periodically waterlogged paleosols.

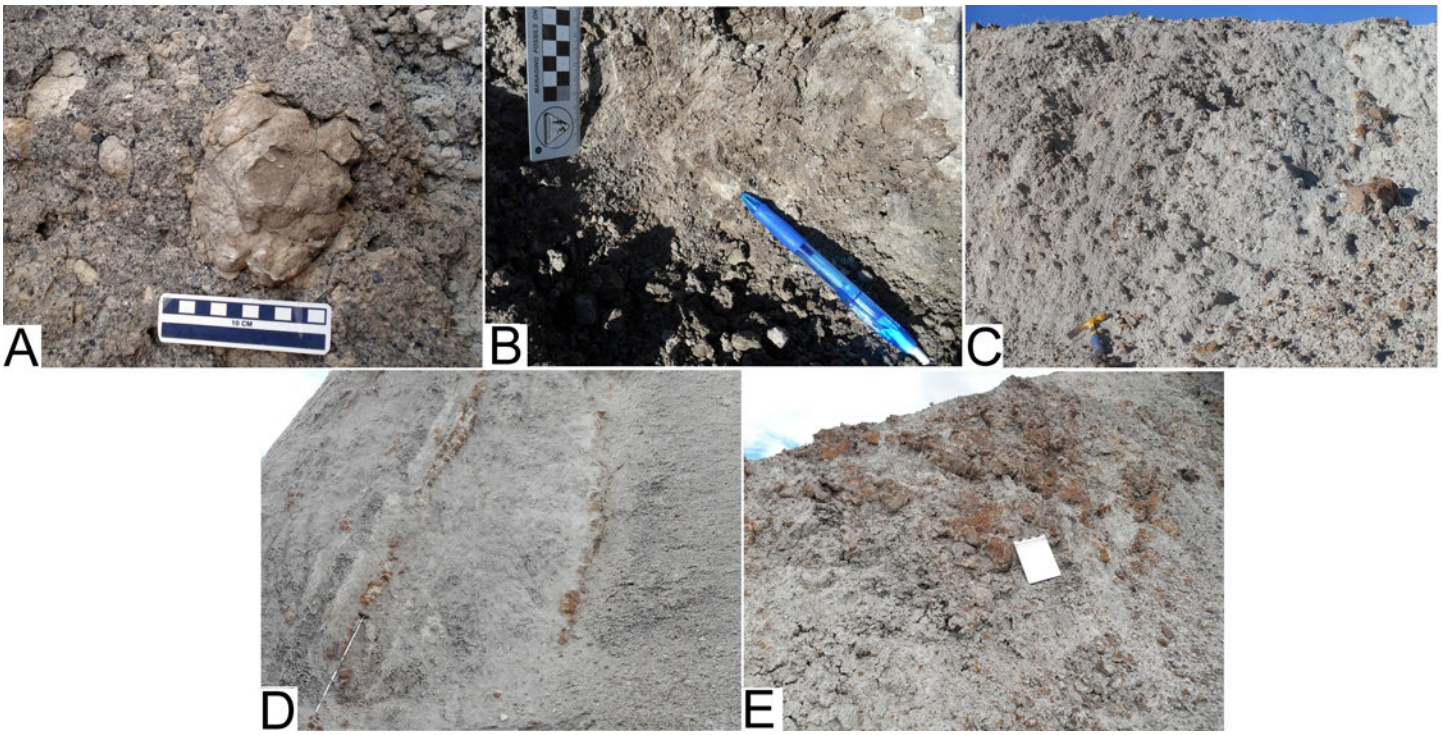

Figure 24. Carbonates. (A) Large reworked carbonate in Quarry Sandstone near the QEH. Scale in cm. (B) Nodule in situ at the tip of a pen, with an abrupt boundary with mudstone on the east side of the QEH. Scale in cm. (C) Nodules eroding in situ from mudstone, showing their relative density. Hammer for scale. (D) Edge view of multiple limestone beds. The upper right bed correlates with (E). Jacob staff with alidade holder (1.25 m) for scale. These beds are also seen in Figure 20A. (E) Eroding surface of limestone bed at Dinosaur Peak, west side of the QEH. Aluminum clipboard for scale.

In contrast, the absence of clay or siliciclastic grains in the Quarry ash indicates airfall sedimentation into a floodplain pond rather than fluvial transport of the ash into a topographic low. Brown et al. (2012) noted that historic eruptions reaching the tropopause typically have a distal region of increased fallout composed of aggregates of ash. They identified several, mostly hydrometeor mechanisms for accretionary formation. The size of the largest pellets in the QVC tuff suggests a late-stage formation most likely involving water droplets. The distal mass deposition maxima of modern eruptions reaching the tropopause may be hundreds of kilometers from the volcano. For example, the centroid for the distal deposition maxima for the 1980 Mount Saint Helens eruption was 500 km downwind (Brown et al., 2012). For the ash at Dinosaur National Monument, the source is believed to have been the Mohave volcanic center about 680 km to the southwest (Hart et al., 2005; Christiansen et al., 2015).

DEPOSITION ENVIRONMENT OF THE QUARRY SANDSTONE

Accommodation

The unusually wide Quarry Sandstone within the Brushy Basin Member has been previously noted by several researchers (Bilbey et al., 1974; Lawton, 1977; Turner and Peterson, 1992a; Carpenter, 2013; Brezinski and Kollar, 2018). The average paleocurrent trend is roughly perpendicular to the 1.5-km-wide exposure of these stacked and amalgamated sandstone beds suggesting the sandstone represents a broad fluvial system with multiple channels. Recent studies of similar wide stacked and amalgamated sandstone beds emphasize the critical roles of both accommodation and sediment supply (e.g., Labourdette, 2011; Sharma et al., 2023). Accommodation, closely tied to sediment accumulation, refers to the "thickness" of sediment deposited over time (Muto and Steel, 2000). Sediment supply refers to

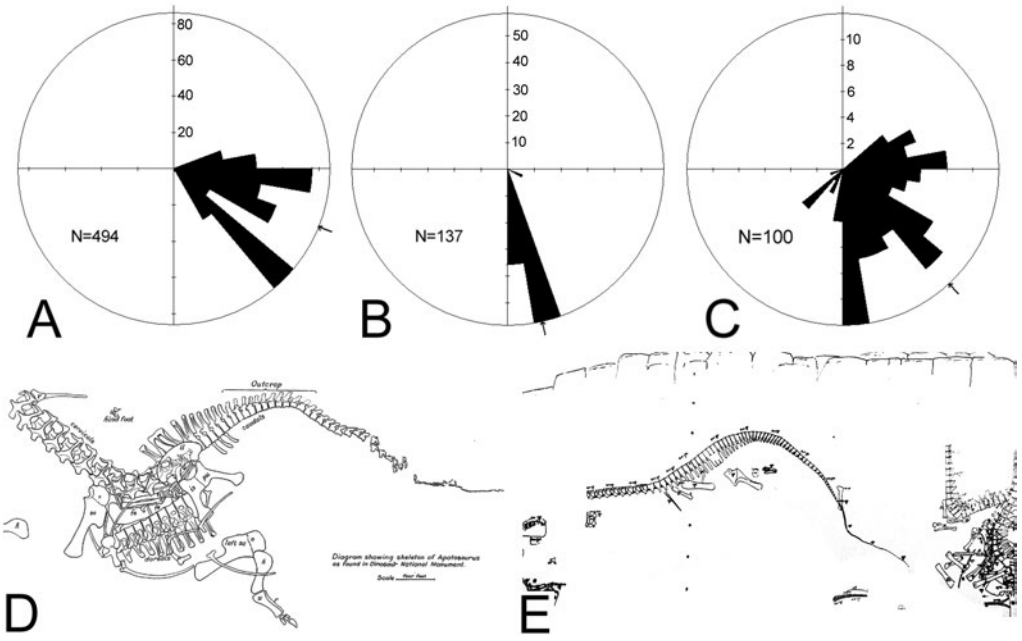

Figure 25. Quarry Sandstone paleocurrent based on (A) sedimentary structures; (B) long axis of unionid bivalves; (C) dinosaur limb bones. Arrow at margins indicates the axis of the mean. Quarry excavation maps showing the effects of flowing water on long whip-tailed sauropods recovered from the Quarry Sandstone; (D) *Apatosaurus* from Gilmore (1936); (E) *Diplodocus*, unpublished from Earl Douglass (Carnegie Museum). Data for (A) and (B) provided by Fred Peterson, U.S. Geological Survey.

the "volume" of sediment deposited within a given period. Accommodation is primarily controlled by tectonic processes such as basin uplift or subsidence, along with changes in eustatic or local base level. Sediment supply is influenced by erosion rates associated with uplift and climate in the catchment area (Allen, 2017; Caracciolo et al., 2020).

Sediment transfer through a sediment routing system from its origin to its final deposition site is governed by both allogenic and autogenic processes. These influences are evident in the variations observed in sedimentary successions, including changes in channel distribution, channel density, and the width of river channels and channel belt deposits. The resulting deposition continuum can range from low-density narrow shoe-string channels encased in finer overbank deposits, reflecting high accommodation-to-sediment supply ratios (A/S), to high-density interconnected tabular channels indicative of low A/S ratios (Bridge and Leeder, 1979; Huerta et al., 2011). These A/S ratios remain consistent even when accounting for variables such as compaction (Bridge and Mackey, 1993).

Several studies illustrate the role of basin subsidence as a major factor influencing the A/S ratio. For example, Labourdette (2011) in an in-depth study of the Eocene Olson Member of the Escanilla Formation in the Ainsa Basin of northern Spain, reported that variations in basin subsidence during the Eocene were the primary drivers of accommodation space for sediment deposition. During periods of slow subsidence, low accommodation caused braided channels to laterally stack, forming wide multichannel belts. Conversely, during periods of faster subsidence, high accommodation resulted in narrower and thicker single-threaded channels.

In the Morrison Formation of the Colorado Plateau, variations in accommodation space have been linked to shifts in fluvial system dynamics and sedimentary facies distributions. Heller et al. (2015) noted an inverse relationship between channel-belt stacking and floodplain aggradation in the Upper Jurassic Morrison Formation of Utah, USA, linking this to basin subsidence and accommodation. They associated the density of channel stacking with avulsion frequency, which is coupled with the sedimentation rate in the channel belt (Heller and Paola, 1996; Heller et al., 2015).

Whereas subsidence fluctuations in a basin are a major method of altering accommodation space, changes can also occur during the inversion of an intracratonic rift. This possibility has not been previously considered for the Morrison Formation, but we explore it here to account for the unusual Quarry Sandstone, given its proximity to the inverted Uinta rift, which now forms the core of the Uinta Mountains (Dehler and Sprinkel, 2005). The Uinta Mountains, a product

of the Late Cretaceous Laramide orogeny, have a core composed of the Neoproterozoic-aged Uinta Mountain Group, which was deposited in mixed marine, deltaic, and braided river environments within a failed rift (Dehler and Sprinkel, 2005). This intracratonic rift represents an early phase in the breakup of the Rodinia supercontinent along the western margin of Laurentia. The rift was bounded by inward-dipping normal faults produced by crustal extension on the north and south. Modeling suggests that during later contraction these faults were reactivated as reverse faults, and additional faults were created, including low-angle thrust faults (Pinto et al., 2010). The Uinta Mountain rift basin experienced several contractional events between the late Neoproterozoic and Late Cretaceous (Hansen, 1986a, 1986b; Stone, 1993; Sprinkel, 2014), as evidenced by angular unconformities in formations around the Uinta Mountains (Williams, 1953; Sprinkel, 2014). Contraction during the Cenozoic led to the formation of numerous synclines and anticlines flanking the eastern Uinta Mountains (Hansen, 1986a, 1986b). One of these, the Split Mountain anticline, formed between the Asphalt Ridge thrust fault to the south and the Island Park normal fault to the north, represents a reactivation of an older anticline developed during the Late Jurassic, as discussed below.

The compressional forces acting against the Uinta rift were oblique, directed toward the northeast (Johnston and Yin, 2001; Ashby et al., 2005). These oblique forces likely resulted from the movement of the Colorado Plateau driven by the Farallon subduction (Sassi et al., 2012). Paleomagnetic data indicate that the Colorado Plateau has moved 160 km ± 36 km since the Triassic (Erskine, 2001), accompanied by a clockwise rotation of approximately 9° during the Jurassic relative to a Euler pole on the North American continent (Steiner, 2003). This movement was probably episodic, as suggested by the different paleopole positions of the lower and upper Morrison Formation (Steiner, 2003) and the episodic growth of the Mexico-Alaska megashear zone (Anderson, 2015).

Modeling suggests that oblique compression of one block relative to another can produce transpressional uplift or an anticline (Dewey et al., 1998). Bally (1984) previously predicted an asymmetrical "petit inversion" anticline adjacent to the bounding fault of an inverted rift (Figure 26A). Additionally, in Bally's (1984) model, syn-sedimentation would prevent the anticline from breaching the surface. Although not explicitly stated, Bally's figure shows a reduction in accommodation space above the anticline, which would influence sediment deposition by any fluvial system flowing over it. Similar situations were reported by Peterson (1980, 1984) from the Henry Mountains basin, Utah (see DISCUSSION).

We propose that an example of "petit inversion" of Bally (1984) as a proto-Split Mountain anticline likely influenced the deposition of the Quarry Sandstone,

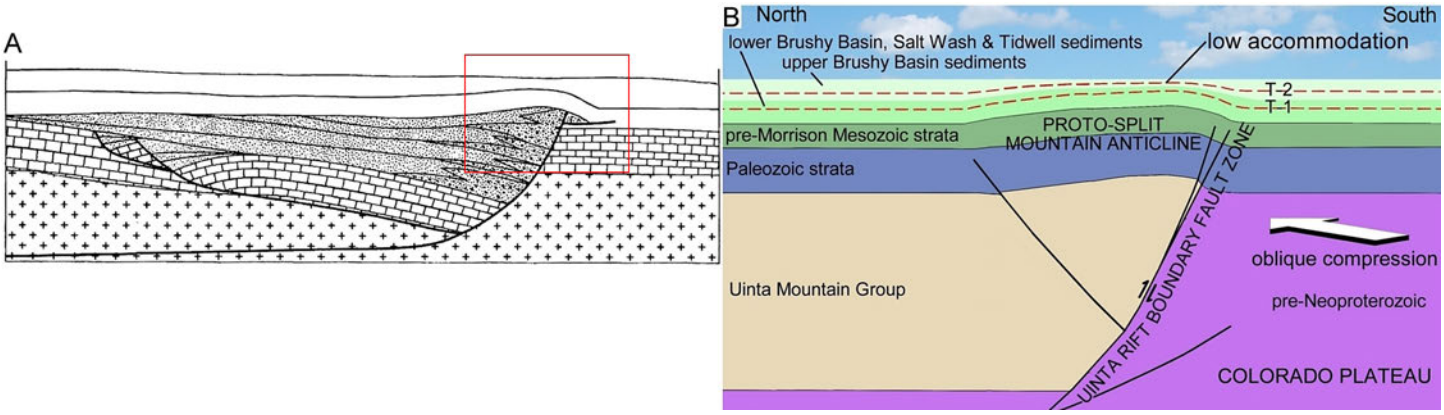

Figure 26. (A) Small anticline due to a "petit inversion" of a rift margin as predicted by Bailey (1984, Figure 4). (B) Transpressive rift inversion caused by the Colorado Plateau during the latter part of the Late Jurassic. The effects on local sedimentation by the proto-Split Mountain anticline are visible in the accommodation space. T-1 represents pre-uplift with no change in accommodation space; unit thickness is uniform. Uplift begins between T-1 and T-2, starting to reduce accommodation space over the anticline; peak reduction by T-2.

based on the thinning of the Brushy Basin Member (Figure 26A) along a north-south transect (Figure 27B). In contrast, a thickening in the underlying Middle Jurassic Curtis Formation suggests that the "petit inversion" had not yet occurred at that time (Figure 27C). The thickness of the Morrison Formation members indicates that the compression event and resulting transpressional uplift began after the deposition of the Tidwell Member sediments, making the event younger than the 156.84 ± 0.59 Ma $^{40}Ar/^{39}Ar$ date from the Tidwell Member at Rainbow Draw (locality 2 on Figure 27B; Trujillo and Kowallis, 2015). It is likely that the transpressional uplift began during the deposition of the Brushy Basin Member, resulting in the Morrison Formation being 40 to 45 m thinner near the uplift than it is to the north or south. The location of the proto-Split Mountain anticline near the southern boundary fault of the Uinta rift aligns with Bally's (1984) prediction, as the peak compression force on the inversion block dissipates from peak pressure near the boundary fault. Additionally, this asymmetrical compression loading results in an asymmetrical anticline, with the steeper side facing the compression loading.

The proto-Split Mountain anticline contributed to the shifting of multiple active and semi-active channels. The rapid reduction in accommodation is evidenced by the abrupt transition from isolated lenticular sandstone bodies to laterally interconnected braided river channel belt deposits of the Quarry Sandstone (Figure 6). This connection results from channel avulsions, spillage, overlapping of channel deposits, and spillage cannibalism due to the lateral mobility of the channels (Labourdette, 2011; Colombera and Mountney, 2021). The frequent avulsions were likely the result of aggradation of the channels, the availability of steeper alternative flow paths in the adjacent floodplains, and in some cases to the presence of large dinosaur bone accumulations. Bone and carcasses probably had the same effect as wood in fluvial systems by increasing channel roughness, altering flow hydraulics, and decreasing sediment transport (Cadol and Wohl, 2011; Spreitzer et al., 2012). The accumulation of bones and carcasses forming large jams (Figure 28) in the channels may have also contributed to avulsions by obstructing the channels, directing flow toward the unstable margins much the same way as log jams can trigger avulsions (Phillips, 2012). Brummer and Montgomery (2006) noted that the presence of boulders covering 20% of the riverbed was enough to cause channel widening during floods. Log jams can initiate multi-channel patterns by diverting flow to a secondary path (Sear et al., 2010; Cadol and Wohl, 2011), and carcasses (see Figure 1 in Carpenter, 2020a) and bone jams have been shown to have that effect (Carpenter, 2020b).

Channel obstacles also act as sediment traps by increasing frictional flow resistance and causing turbulent eddies that reduce flow velocity and sediment transport competence (Carpenter, 2020a). Thus, bones behave much like boulders on the riverbed by constituting a major roughness element imparting form drag on flow (Ferguson, 2007). The result is the deposition of sediment in the channel (Spreitzer et al., 2021; Chen et al., in press). This deposition is greater during floods, where the added suspended mass and increased viscosity enhance the logjam's ability to slow down the flow (Chen et al., in press); bone jams would have the same effect.

The sudden change in fluvial styles near the QEH began around 150.77 ± 0.39 Ma, as indicated by volcanic ash immediately below the Quarry Sandstone and represented by the T2 timeline in Figure 26B. The duration of the anticline's subsurface uplift and the time until accommodation space was restored to pre-uplift conditions remain unknown, but it likely took thousands of years based on the local thickness of the Brushy Basin Member and its depositional duration of less than 2 million years (Christiansen et al., 2015).

The Quarry Sandstone shows little confined flow due to avulsions and overlapping proximal overbank flow (levees and splays) across the floodplain until channels were re-established elsewhere. Mud pebble clasts from bank or levee collapse, matrix-supported coarse grains, and weakly developed paleosol mottling are common. It lacks the lateral accretion or other features characteristic of meandering rivers, such as those identified below.

A similar situation of lateral mobility leading to the formation of a new braid plain can be observed in the gravelly braided Blaeberry River, British Coloumbia, Canada (Figure 29). In this case, a crevasse splay preceded the avulsion event, indicating bank instability, but

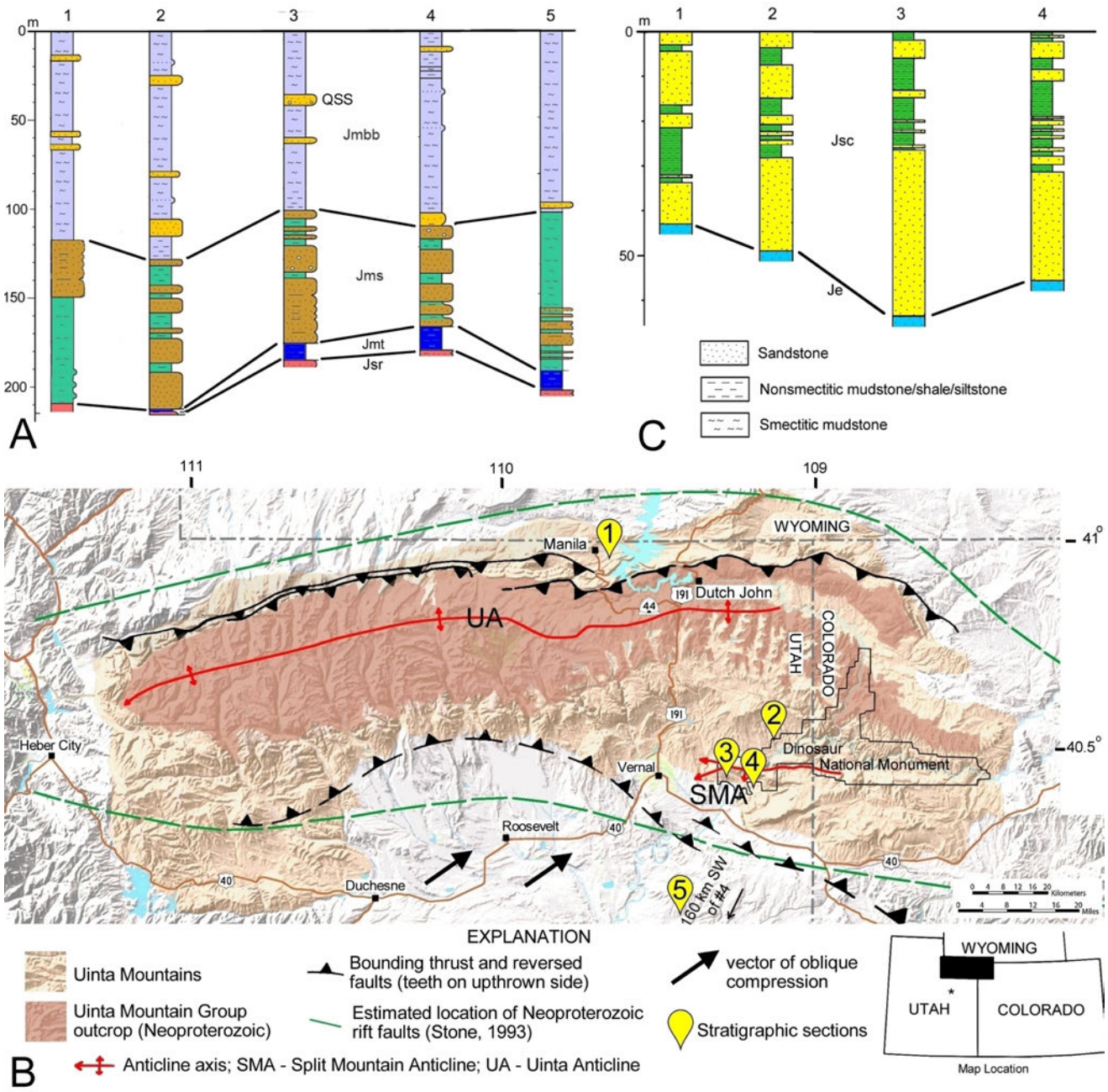

Figure 27. Rift inversion impact on accommodation space is observed by (A) thinning of the Morrison Formation over the proto-Split Mountain anticline. Redwater Member, Stump Formation (Jsr); Tidwell Member, Morrison Formation (Jmt); Salt Wash Member, Morrison Formation (Jms); Brushy Basin Member, Morrison Formation (Jmbb); Quarry Sandstone (QSS). (B) Map of northern Utah showing the boundaries of the Uinta rift, location of measured sections, and the axis of the Split Mountain anticline today. (C) Pre-rift inversion influence on the deposition of the underlying Curtis Member, Stump Formation (Jsc); Entrada Sandstone (Je).

the avulsion occurred farther upstream, creating a new braid plain parallel to the old one. Whether an erosive breach becomes a crevasse splay or leads to an avulsion is determined by the balance between erosion and deposition processes, influenced by factors such as floodplain erodibility, vegetation, and water surface slope (Nienhuis et al., 2018). A wide zone of interconnectivity is visible in the vicinity of the avulsion, highlighting the importance of spillage, especially crevasse splays, in connectivity between channels (Columbera and Mountney, 2021).

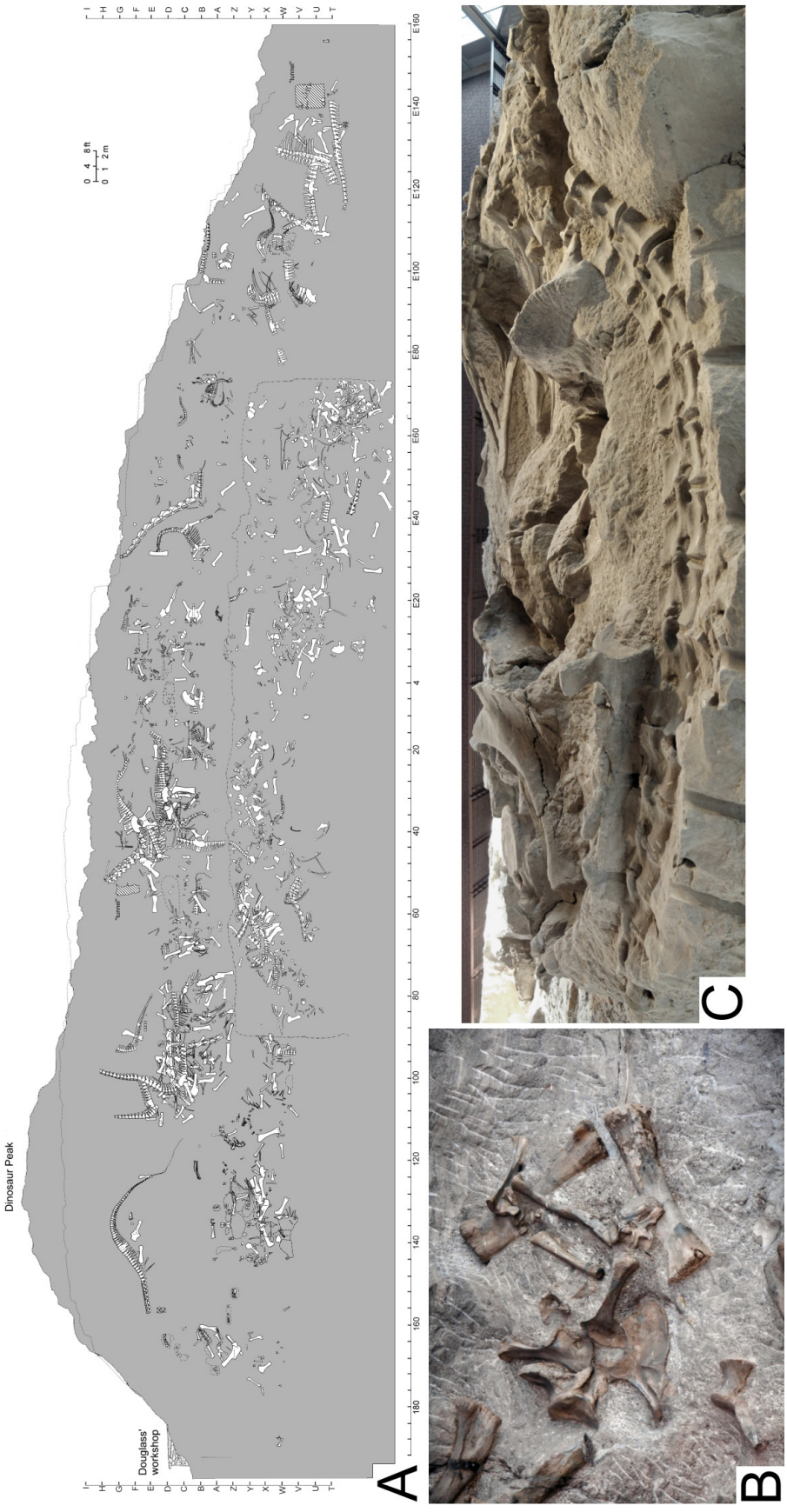

Figure 28. Bone clusters or "bone jams," analogous to log jams, undoubtedly impacted water flow and caused sediment deposition. (A) Bone jams surrounded by barren or nearly barren rock. (B) Example of a small bone jam. (C) Downstream view of a bone jam.

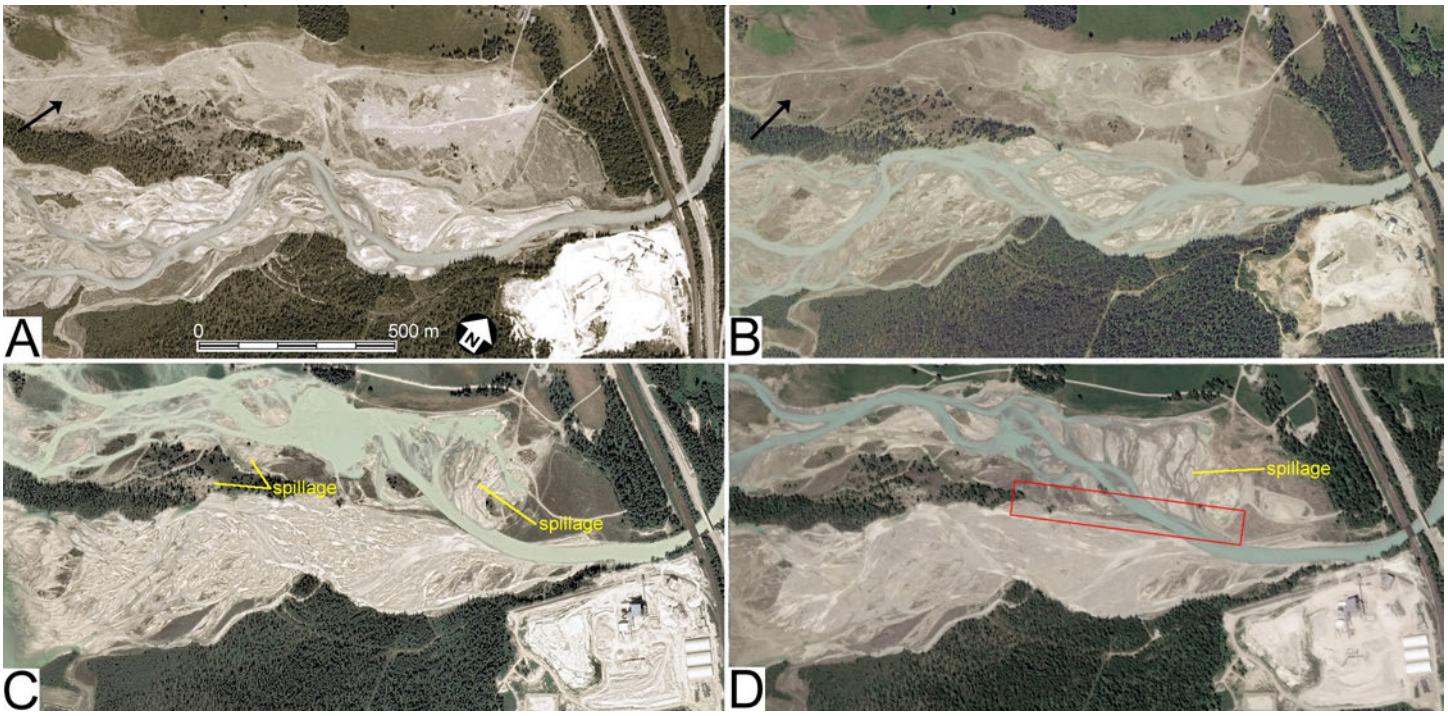

Figure 29. Relocation of a braided river channel over time as a model for the Quarry Sandstone, Blaeberry River, British Columbia (51.4264°N., -117.0709°W.). (A) Pre-avulsion with crevasse splay sediment (arrow). Image date: 2004. (B) Pre-avulsion with recolonization of the crevasse splay surface by vegetation (arrow and similar brown patterns). Image date: June 25, 2015. (C) Post-avulsion in spring 2019, showing the abandonment of the previous braid plain. Note the extensive reworking by shallow flow of the previous braid plain from the spring flood prior to complete abandonment. Image date: September 4, 2019. (D) Fully established new braid plain. A wide region of interconnectivity between the two braid plains is marked by a red box. Image date: August 2022. Images: (A) through (C) Google Earth; (D) Bing Maps.

To test the hypothesis that the Quarry Sandstone resulted from a loss of accommodation space due to the activity of a proto-Split Mountain anticline, we examined sandstone beds along the western periphery of Split Mountain, which provides a nearly continuous exposure of the Morrison Formation from the QEH (Figure 30A). Our objective was to identify a sandstone body located upstream of the proto-Split Mountain anticline. The search criteria included stratigraphic placement near the middle of the Brushy Basin Member, a similar conglomeratic salt-and-pepper lithology, and the presence of dinosaur bones with comparable preservation. Although several sandstone bodies were identified, only two met all these criteria.

One such sandstone body is 6.9 km west of the QEH (Figures 30B and 30C), whereas the other is 8.6 km northwest of the QEH (Figures 30D and 30E). The western sandstone represents an infilled thalweg on the cut bank side of a single-threaded river, with a paleocurrent direction of 182° as determined from the axis of the thalweg. This sandstone body measures approximately 70 m wide perpendicular to its axis. The northwestern sandstone, on the other hand, is a cross section of a single-threaded river deposit featuring accretionary deposits on the eastern side and the thickest sandstone on the west. The paleocurrent direction for this sandstone body is around 145°. The entire sandstone body, including the accretionary deposits, is 232 m wide, with the main body forming a resistant ridge measuring about 157 m in width.

The northwestern sandstone body exhibits paleocurrents that suggest it served as the upstream segment for both the western sandstone and the Quarry Sandstone. It may have been the source of sediment for both at different times. As the upstream segment to the Quarry Sandstone, a sinuous single-threaded river likely transitioned into a multithreaded system as it crossed the proto-Split Mountain anticline and then possibly

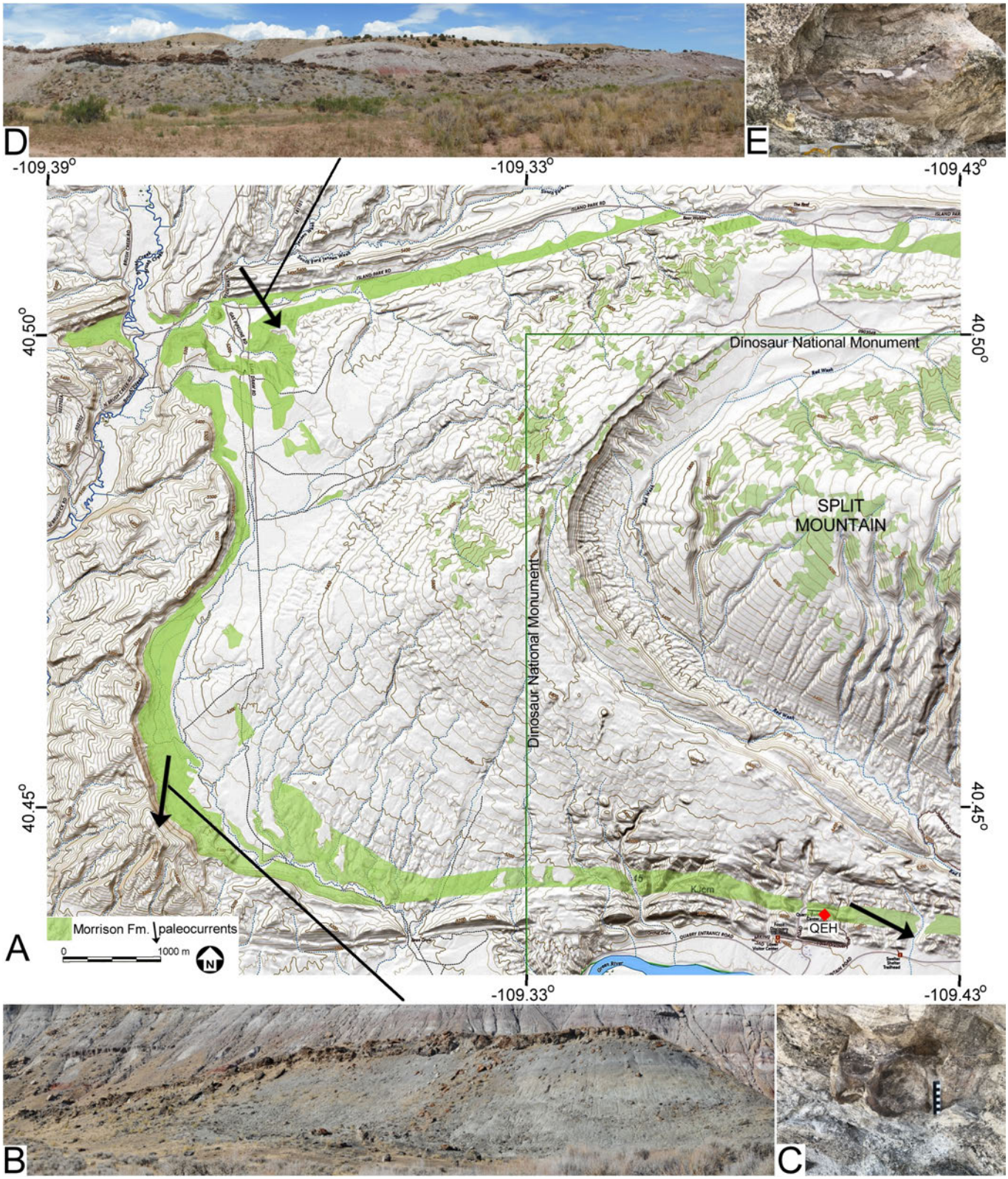

Figure 30. (A) Distribution of the Morrison Formation around the western end of Split Mountain. Two sandstone bodies match the lithology of the Quarry Sandstone. (B) Outcrop of the western sandstone with (C) a sauropod vertebra (scale in cm). (D) Outcrop of the northwestern sandstone with (E) a sauropod limb fragment (hammer head length approximately 17 cm). Abbreviation: QEH – Quarry Exhibit Hall. Base map from Topozone.

reverted to a single-threaded river afterward. Such tripartite transitions are observed in modern rivers (e.g., Figure 31).

Depositional Model

A hypothetical paleoenvironmental cross section from channel to floodplain is presented in Figure 32 (see also Carpenter, 2023). The vegetation is mostly based on palynomorphs recovered by F. Peterson (U.S. Geological Survey) west of the QEH along Camp Draw (Turner and Peterson, 1991) and reported by Litwin et al. (1998). Megafloral specimens include the ginkgophyte, *Czekanowskia*, from a fine-grained, horizontally laminated sandstone interbedded in the Ridge Sandstone, and a cycadeoid log fragment eroded from the Ridge Sandstone. These taxa plus other non-vertebrate fossils are given in Table 1.

We interpret the Quarry Sandstone channel facies as a braided river whose deposits are not well differentiated laterally from the proximal overbank facies, reflecting the rapid deceleration of overbank flow and deposition of coarse-grained sediment. Flume work suggests that wide braided rivers that are not laterally constrained—i.e., have minimal bank cohesion, produce a stable channel when width is about 24 times depth (Warburton, 1996). This is apparently controlled by grain size (Paola and Mohrig, 1996) and the development of natural levees thus lead to self-containment (Cazanacli and Smith, 1998). We propose a similar

Figure 31. Example of a sinuous, single-threaded river transitioning to a multithreaded river and back to a sinuous, single-threaded river. Flow is toward the left. Blaeberry River, British Columbia (51.4265°N., -117.0507°W.). Imagery date: October 11, 2021, Google Earth.

Table 1. Non-vertebrate fossils from the study area (see Gregson et al., 2024, Table 1 for vertebrates). The plants were used to reconstruct the habitat shown in Figure 32. Palynoflora marked with * from Ash (1994); Litwin et al. (1998). Invertebrates from Schudack et al. (1998), Schudack unpublished (taxa updated by Benjamin Sames, personal communications, April 11, 2022), Good (2004), Lucas and Kirkland (1998).

- Kingdom Plantae
  - Division Charophyta
    - Family Characeae
      - *Aclistochara bransoni*
      - *Aclistochara latisulcata*
      - *Alistochara madleri*
      - *Aclistochara miniscula*?
      - *Aclistochara obovata*
      - *Latochara /atitruncata*
      - *Latochara* sp.
      - *Peckisphaera verticillata*
      - *Porochara arguta*
      - *Porochara kimmeridgensis*
    - Family Clavatoraceae
      - *Echinochara* sp.
  - Division Polypodiophyta
    - Family Equisetaceae
      - *Equisetum* sp.
  - Division Pteriodophyta
    - Family Umkomasiaceae
      - *Pteruchipollenites microsaccus**
    - Family Osmundaceae
      - *Todisporites minor* *
  - Division unknown
    - Bennettitales (family and genus unknown)
  - Division Pinophyta
    - Family Araucariaceae
      - *Callialasporites trilobatus* *
      - *Callialasporites*. cf *C. rugularus* *
    - Family Podocarpaceae
      - *Microcachrydites antarcticus* *
      - *Parvisaccites* sp. *
      - *Rugubivesiculites* sp. *
  - Division Ginkgophyta
    - Family Czekanowskiaceae
      - *Czekanowskia* sp.
- Kingdom Animalae
  - Class Bivalvia
    - Family Unionidae
      - *Vetulonaia* sp.
      - genus unidentified
  - Class Ostracoda
    - Family Cyprididae
      - *Candona* sp.
    - Family Limnocytheridae
      - *Bisulcocypris pahasapensis*
      - *Helmdachia petersoni*
    - Family incertae sedis
      - *Cetacella* sp.
  - Class Branchiopoda
    - Family Cyzicidae
      - *Lioestheria* sp.

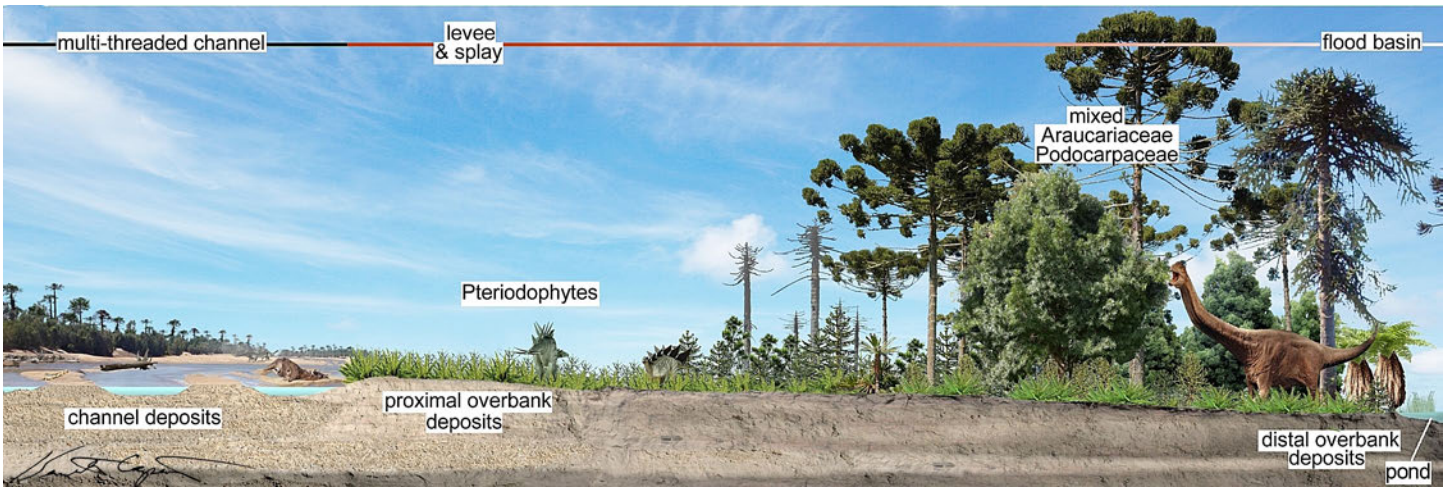

Figure 32. Reconstructed cross section from channel to floodplain, with inferred distribution of vegetation. No scale implied.

mechanism was in operation with the Quarry Sandstone fluvial system.

The absence of interbedded paleosols in the proximal overbank suggests that flood disturbances and sediment deposition were frequent enough to maintain a continuously disturbed habitat colonized by polypodiopsid pteridophytes (ferns and tree ferns), known as pioneer species today (Walker and Sharpe, 2010). Slower-growing tree seedlings attempting to establish themselves were likely smothered by sediment, along with older established trees, as the crevasse splays prograded, as indicated by the presence of dead trees. The coarseness and white color of the sediments suggest well-drained, oxidizing soil with limited organic carbon buildup. Overbank facies sediments become finer-grained distally, with immature paleosols and rhizoliths in the B-horizon indicating sedimentation hiatuses in the range of decades rather than hundreds of years (Kraus, 1987; Burns et al., 2019).

The absence of large rhizoliths of tree roots in the Morrison Formation has long been a mystery. Trees are known to have been present in the vicinity of the Quarry Sandstone, as evidenced by a log on the quarry face (Figure 33A). The absence of large tree tap-roots in paleosols of this study may be explained by conifers generally having shallow, horizontal roots (Figure 33B), as a result of which trees commonly topple, exposing their shallow roots (Figure 33C). Decomposition of the roots by insects, especially termites known from the Morrison (Hasiotis, 2004), and saprophagic activity could have removed the evidence of large, horizontal roots over time (see Gee, 2023).

The vegetation in this area consisted of a mixed riverine conifer-dominated forest of two species of araucariacean, three species of podocarpacean, and the ginkgophyte *Czekanowskia*, with an understory of shade-tolerant ferns. Today, such trees inhabit moist, well-drained soils in humid climates. Cycadeoids were also present, as evidenced by a section of log from the channel facies.

In the flood basin, there were small water bodies that primarily received water sporadically from overland flow (crevasse splay drainage, floods, rain). Longer-lasting water bodies probably also received groundwater seepage flowing through the coarser sediments of crevasse splays. Fragmentary or single microcrustacean valves, some angled relative to the bedding plane of oriented rock samples, suggest the presence of some allochthonous assemblages. Additionally, branchiopod diversity is very low in bulk samples of matrix collected by F. Peterson (Turner and Peterson, 1991) along a transect west of the QEH having only one or two species, suggesting a similarity to modern stressed ecosystems. The brecciation of some lacustrine carbonates indicates pedogenetic episodes in the flood basin.

DISCUSSION

Our analysis of the Quarry Sandstone and its surrounding strata provides a foundation for reassessing

Figure 33. (A) Fossil log on the quarry face in the QEH (approximately 3 m in length). (B) Conifer showing laterally directed roots that provide a broad base for support. (C) Root mass of a toppled conifer showing the absence of major taproots.

prior studies of the sedimentology of the Morrison Formation at Dinosaur National Monument. Consistent with earlier research, we interpret the Quarry Sandstone as the product of braided river systems accompanied by finer-grained overbank deposits (e.g., Lawton, 1977; Turner and Peterson, 1992a; Carpenter, 2013). Traditional interpretations of braided rivers often regarded associated overbank or vertical accretion deposits as volumetrically insignificant (e.g., Miall, 1977; Cant and Walker, 1978; Walker and Cant, 1984). This perspective emerged primarily from studies of valley-confined or incised braided rivers, in which frequent channel shifts reworked overbank deposits, leaving behind only erosional remnants (Cant and Walker, 1978; Bridge, 2003, p. 157).

However, such interpretations are inconsistent with the stratigraphic record, which often reveals extensive overbank deposits associated with braided river systems. Examples include the Atcotas Formation of Spain (Arche and Lopez-Gomez, 1999), the Cutler Formation of New Mexico (Eberth and Miall, 1991), the Escanilla Formation of Spain (Bentham et al., 1993), and the Salt Wash Member of the Morrison Formation on the Colorado Plateau (Robinson and McCabe, 1998). The volume of finer-grained floodplain deposits in braided river systems correlates strongly with rates of basin aggradation (e.g., Bentham et al., 1993; Robinson and McCabe, 1998; Labourdette, 2011). Consequently, the relative thickness of vertical accretion deposits is no longer considered a primary criterion for distinguishing between meandering and braided river deposits (e.g., Miall, 2014).

Additionally, proximity to orogenic mountains fronts does not necessarily dictate the development of braided river systems, as demonstrated by the 1899 topographical map of the Platte River near Columbus, Nebraska (U.S. Geological Survey, 1899). This map illustrates that, prior to channelization and dam construction, the Platte River was braided nearly 700 km downstream from the Hartville uplift in eastern Wyoming. This was also demonstrated by Holbrook and Allen (2020), who noted that the lower reaches of the Missouri River were braided prior to damming and channelization. Finally, Bridge at al. (1998) described the braided part of the Calamus River, which originates in the Sand Hills of western and central Nebraska, not from any orogenic front. These and other studies support the prevalence of braided rivers, which are now recognized as being as common as meandering rivers globally (Miall, 2014, p. 39).

In a significant departure from the consensus that the Quarry Sandstone represents channel deposits, Brezinski and Kollar (2018) interpreted the Quarry Sandstone as a crevasse splay complex, which consists of multiple genetically related splay and crevasse-channel fill elements formed in an interfluve wetland or lake. They based their analogy on a distributary channel of the clay and silt Mississippi River Delta (Figure 34A), as described and illustrated by Coleman and Prior (1982). Brezinski and Kollar (2018) identified the Quarry Sandstone as being composed of numerous laterally continuous and upward-coarsening sandstone bodies, which they interpreted as distributary mouth bars within cre-

Figure 34. (A) Distribution channels (center below arrow) on the lower Mississippi River delta, serving as a model for the Quarry Sandstone as cited by Brezinski and Kollar (2018). The arrow indicates the direction of flow of the Mississippi River. (B and C) Crevasse splay development, Columbia River, British Columbia (50.9358°N., -116.4079°W.). (A) Early phase (Yandex Maps, undated). (B) 2004 (Google Earth). Note that most sediment is deposited proximally, with an increase in sediment divergence as the splay grows.

vasse splays. These bars were cut by trough cross-bedded and upward-fining sandstone lenses, which they identified as distributary channels. They proposed that the 130-m-wide quarry bed was formed within one of these channels.

There is a moderate to strong correlation between crevasse splay width and parent channel width (Millard et al., 2017; Columbera and Mountney, 2021; Rahman et al., 2022). Typically, channel widths are found to be about two to four times the width of associated splays. Using this information, a rough estimation of the Quarry Sandstone's parent river width, based on a 130-m-wide splay, would suggest a river width of approximately 260 to 520 m. This range accounts for the variability in correlations observed across different fluvial systems, including sediment supply, floodplain gradient, and river morphology. However, no suitable body of sandstone is present to the west or north of the Quarry Sandstone, making the crevasse splay or complex of multiple splays interpretation for the Quarry Sandstone questionable.

During the formation of a crevasse or breach in the levee, spillage into the floodplain results in a divergence of currents from the crevasse, which is recorded in the preserved sediments even for lobate splays (Columbera and Mountney, 2021). This divergence is crucial for developing wide and lobate splays (Figures 34B and 34C; Millard et al., 2017). However, no segment of the Quarry Sandstone preserves paleocurrents that can be backtraced to a crevasse splay. Furthermore, coarser sediments in modern crevasse splays are deposited closer to the breakout point as the transport capacity of the unconfined flow rapidly decreases, while finer materials are carried farther away (Millard et al., 2017; Burns et al., 2019). The deceleration of crevasse water is even more rapid in standing water, such as swamps and lakes, which would restrict the dispersal of coarse grains and large bones to the most proximal part of the splay. The Quarry Sandstone shows no major reduction in the size or abundance of the coarse fraction at its western and eastern extremities when compared with the dinosaur quarry (Figure 35).

The rapid drop in transport competence as the crevasse water spills onto the floodplain often causes the healing of the breach (Hajek and Wolinsky, 2012). This breach healing also occurs when log or debris jams develop at the mouth of the breach, acting as barriers that reduce water flow and sediment transport, thereby allowing sediment deposition to fill the crevasse. This phenomenon contributes to the difficulty of explaining how large bones could get into the distributary channel of a crevasse splay without the bone jams healing the crevasse.

Our work updates the previous work of Peterson (1980, 1984), who had identified paleo-anticlines based on localized thinning of the Salt Wash Member of the Morrison Formation in southern Utah. In discussing the effects of these subsurface paleo-anticlines on syn-deposition, Peterson considered the paleo-anticlines as slight barriers to braided river flow, result-

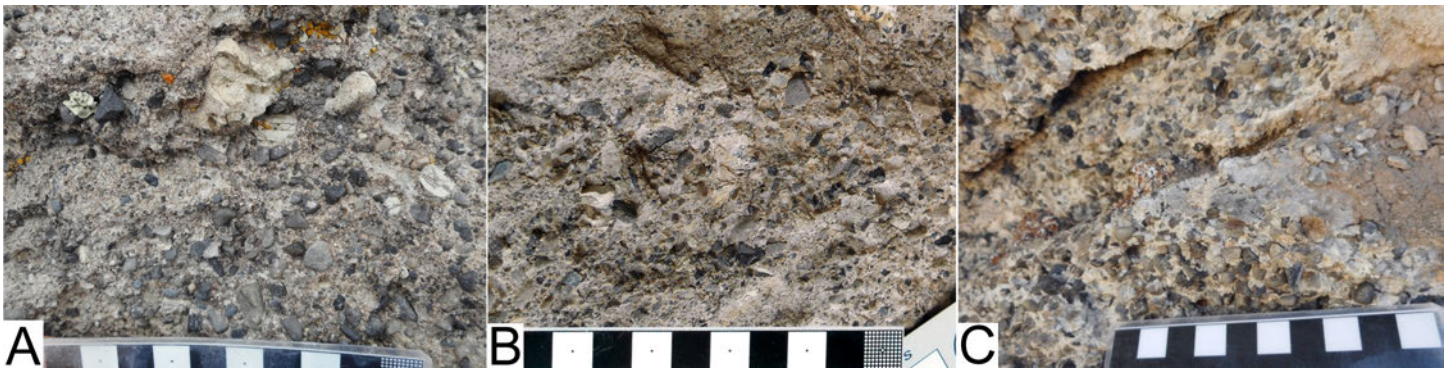

Figure 35. Comparison of the Quarry Sandstone at (A) the western end in Douglass Draw, (B) on the quarry face in the QEH, and (C) the eastern end near Swelter Shelter Draw, showing the absence of distal fining expected of a crevasse splay. Scales in cm.

ing in coarser sediments being preferentially trapped in the paleo-synclines because the streams lacked the transport energy to move the sediments over the paleo-anticlines. Winnowed fine-grained sediments were deposited on and beyond the paleo-anticlines. However, unresolved issues remain, including: (1) how did paleo-synclines downstream received coarse-grained sediments if they were trapped at the most upstream paleo-syncline-paleo-anticline pairs; (2) how did sedimentation rates maintain a delicate balance to trap coarse grains in the paleo-synclines without forming lakes; and (3) why did the restricted flow over the anticlines not actually increase in transportation capacity due to increased velocity? Peterson (1980, 1984) postulated that the paleo-anticlines were located near the position of modern anticlines and suggested that the modern anticlines were a Laramide reactivation of the paleo-anticlines.

Our research on the Quarry Sandstone and accommodation space associated with the proto-Split Mountain anticline suggests that the loss of accommodation space due to the paleo-anticlines can be shown by localized thinning of strata and the lateral aggregation and lateral interconnectedness of braided channel sandstone bodies. This interpretation suggests that switching the placement of the paleo-anticlines and paleo-synclines as determined by Peterson (1980, 1984) would resolve many of the problems with his model, and the matter becomes one of accommodation space, a concept that was not well-developed during Peterson's time.

CONCLUSION

This comprehensive study of the Quarry Sandstone within the Morrison Formation provides critical insights into the depositional environment, sedimentological processes, and the geological influences that shaped this unique sedimentary deposit. By synthesizing new data and reassessing previous interpretations, this study reinforces the view that the Quarry Sandstone represents braided river deposits, characterized by multithreaded channels and dynamic fluvial processes and the high width-to-thickness ratios of the sandstone bodies.

Our research challenges the alternative interpretation proposed by Brezinski and Kollar (2018), which suggested that the Quarry Sandstone formed as a crevasse splay complex. By critically evaluating the correlation between crevasse splay width and parent channel width, and by examining the distribution of coarse sediments and paleocurrents, this study refutes the crevasse splay hypothesis, instead favoring a model of stacked braided river deposits influenced by tectonic activity.

This study also highlights the role of tectonic features, particularly paleo-anticlines, in influencing sediment deposition within the Morrison Formation. The proposed proto-Split Mountain anticline likely played a significant role in shaping the Quarry Sandstone by reducing accommodation space, leading to the lateral aggregation of braided channel sandstone bodies and frequent avulsions. This tectonic influence aligns with the earlier work of Peterson (1980, 1984), who suggested that paleo-anticlines influenced local sediment transport.

Furthermore, this study provides a nuanced understanding of the complex interactions between accommodation space, sediment supply, and tectonic processes, illustrating how these factors collectively influenced the depositional patterns within the Morrison Formation. By revisiting and refining previous models, this research not only resolves longstanding questions about the formation of the Quarry Sandstone but also contributes to a broader understanding of fluvial dynamics in ancient, tectonically active regions.

ACKNOWLEDGMENTS

Our study builds upon the foundational work at Dinosaur National Monument (1990–1993) by Christine Turner, U.S. Geological Survey, and the late Fred "Pete" Peterson (1933–2019), U.S. Geological Survey. We are grateful to Pete for his discussions on the Morrison Formation and for sharing his stratigraphic sections from Dinosaur National Monument, which were used in Figures 5 and 6. We also thank Kevin Chamberlain, Department of Geology and Geophysics, University of Wyoming, for providing the calculated radiometric age. Thin sections were prepared by Wagner Petrographic, Lindon, Utah. We extend our thanks to Manja Hethke, Institute of Geological Sciences, Freie Universität Berlin, and Benjamin Sames, Department of Geodynamics and Sedimentology, University of Vienna, for providing information on the late Michael Schudack's, Institut für Paläontologie, Freie Universität Berlin, ostracod and charophyte collection from Dinosaur National Monument. Thanks to Diane Iverson, Sue Ann Bilbey, and Evan Hall (Uinta Paleontological Associates, Inc.) for sharing the Earl Douglass photographs. Fieldwork was conducted under National Park Service Scientific Research and Collecting Permits DINO-2019-SCI-0028, DINO-2020-SCI-0010, and DINO-2021-SCI-0008; we thank ReBecca Hunt-Foster of Dinosaur National Monument for her assistance in expediting the permitting process. We thank Isaac Allred, Brigham Young University-Idaho; Tom Chidsey, Utah Geological Survey; John Foster, Utah Field House of Natural History State Park Museum; ReBecca Hunt-Foster, Dinosaur National Monument; William Lund, Utah Geological Survey; Theresa Schwartz, U.S. Geological Survey; Douglas Sprinkel, Azteca Geosolutions; and Jianqiao Wang, Colorado School of Mines, for their constructive reviews.

This is the ninth installment in a series by the senior author on Dinosaur National Monument.

REFERENCES

Alexander, J., and Fielding, C.R., 2006, Coarse-grained floodplain deposits in the seasonal tropics—towards a better facies model: Journal of Sedimentary Research, v. 76, p. 539–556.

Allen, P.A., 2017, Sediment routing systems—the fate of sediment from source to sink: New York, Cambridge University Press, 407 p.

Anderson, T.H., 2015, Jurassic (170–150 Ma) basins—the tracks of a continental-scale fault, the Mexico-Alaska megashear, from the Gulf of Mexico to Alaska, *in* Anderson, T.H., Didenko, A.N., Johnson C.L., Khanchuk, A.I., and MacDonald, J.H., Jr. editors, Late Jurassic margin of Laurasia—a record of faulting accommodating plate rotation: Geological Society of America Special Paper 513, p. 107–188.

Arche, A., and López-Gómez, J., 1999, Subsidence rates and fluvial architecture of rift-related Permian and Triassic alluvial sediments of the southeast Iberian Range, eastern Spain, *in* Smith, N.D., and Rogers, J., editors, Fluvial sedimentology VI: International Association of Sedimentologists, Special Publication 28, p 283–304.

Ash, S., 1994, First occurrence of *Czekanowskia* (Gymnospermae, Czekanowskiales) in the United States: Review of Palaeobotany and Palynology v. 81, p. 129–140.

Ashby, J.M., Geissman, J.W., and Weil, A.B., 2005, Has the eastern end of the Uinta Mountains been bent?—paleomagnetic and fault kinematic assessment, *in* Dehler, C.M., Pederson, J.L., Sprinkel, D.A., and Kowallis, B.J., editors, Uinta Mountain geology: Utah Geological Association Publication 33, p. 285–319.

Bally, A.W., 1984, Tectogenèse et sismique réflexion: Bulletin de la Société Géologique de France, 7, 279–285.

Bentham, P.A., Talling, P.J., and Burbank, D.W., 1993, Braided stream and flood-plain deposition in a rapidly aggrading basin—the Escanilla Formation, Spanish Pyrenees, *in* Best, J.L. and Bristow, C.S., editors, Braided rivers: Geological Society (London) Special Publication 75, p. 177–194.

Bilbey, S.A., 1992, Stratigraphy and sedimentary petrology of the Upper Jurassic–Lower Cretaceous rocks at Cleve-

land–Lloyd Dinosaur Quarry with a comparison to the Dinosaur National Monument Quarry, Utah: Salt Lake City, University of Utah, Ph.D. dissertation, 295 p.

Bilbey, S.A., Kerns, R.L., and Bowman, J.T., 1974, Petrology of the Morrison Formation, Dinosaur Quarry Quadrangle, Utah: Utah Geological and Mineral Survey Special Studies 48, 15 p.

Blair, T.C., and McPherson, J.G., 1999, Grain-size and textural classification of coarse sedimentary particles: Journal of Sedimentary Research, v. 69, p. 6–19.

Boyle, A.C., 1938a, Report relating to status of project, Dinosaur National Monument, Jensen, Utah: Unpublished report, National Park Service, 55 p.

Boyle, A.C., 1938b. Master plan data: Unpublished draft manuscript, National Park Service, 9 p.

Brezinski, D.K., and Kollar, A.D., 2018, Origin of the Carnegie Quarry Sandstone (Morrison Formation, Jurassic) at Dinosaur National Monument, Jensen, Utah: PALAIOS, 33, 94–105.

Bridge, J.S., 2003, Rivers and floodplains—forms, processes, and sedimentary record: Oxford, United Kingdom, Blackwell Publishing, 491 p.

Bridge, J.S., and Leeder, M.R., 1979, A simulation model of alluvial stratigraphy: Sedimentology, v. 26, p. 617–644.

Bridge, J.S., and Mackey, S.D., 1993, A revised alluvial stratigraphy model, *in* Marzo, M. and Puigdefábregas, C., editors, Alluvial sedimentation: International Association of Sedimentologists Special Publication, v. 17, p. 317–336.

Bridge, J.S., Collier, R., and Alexander, J.A.N., 1998. Large-scale structure of Calamus River deposits (Nebraska, USA) revealed using ground-penetrating radar: Sedimentology, v. 45, p. 977–986.

Brierley, G.J., 1996, Channel morphology and element assemblages—a constructivist approach to facies modeling, *in* Carling, P.A., and Dawson, M.R., editors, Advances in fluvial dynamics and stratigraphy: Chichester, United Kingdom, Wiley, p. 263–298.

Brown, R.J., Bonadonna, C., and Durant, A.J., 2012, A review of volcanic ash aggregation: Physics and Chemistry of the Earth, v. 45, p. 65–78.

Brummer, C.J., and Montgomery, D.R., 2006, Influence of coarse lag formation on the mechanics of sediment pulse dispersion in a mountain stream, Squire Creek, North Cascades, Washington, United States: Water Resources Research, v. 42, no. 7, W07412, https://doi:10.1029/2005WR004776.

Burns, C.E., Mountney, N.P., Hodgson, D.M., and Colombera, L., 2019, Stratigraphic architecture and hierarchy of fluvial overbank splay deposits: Journal of the Geological Society (London), v. 176, p. 629–649.

Cadol, D., and Wohl, E., 2011, Coarse sediment movement in the vicinity of a logjam in a neotropical gravel-bed stream: Geomorphology, v. 128, p. 191–198.

Cant, D.J., and Walker, R.G., 1978, Fluvial processes and facies sequences in the sandy braided South Saskatchewan River, Canada: Sedimentology, v. 25, p. 625–648.

Cazanacli, D., and Smith, N.D., 1998, A study of morphology and texture of natural levees—Cumberland Marshes, Saskatchewan, Canada: Geomorphology, v. 25, p. 43–55.

Caracciolo, L., Chew, D., and Andò, S., 2020, Sediment generation and sediment routing systems: Earth Science Reviews, v. 207, 103221, https://doi.org/10.1016/j.earscirev.2020.103221.

Carpenter, K., 2013, History, sedimentology, and taphonomy of the Carnegie Quarry, Dinosaur National Monument: Annals of Carnegie Museum, v. 81, p. 153–232.

Carpenter, K., 2018, Rocky start of Dinosaur National Monument (USA), the world's first dinosaur geoconservation site: Geoconservation Research, v. 1, no. 1, p.1–20.

Carpenter, K., 2020a, Hydraulic modeling and computational fluid dynamics of bone burial in a sandy river channel: Geology of the Intermountain West, v. 7, p. 97–120, https://doi.org/10.31711/giw.v7.

Carpenter, K., 2020b, Use of scaled dinosaur bones in taphonomic water flume experiments: The Science of Nature, v. 107, no. 15, 8 p., https://doi.org/10.1007/s00114-020-01673-2.

Carpenter, K., 2022, The lithostratigraphic Tidwell Member of the Morrison or Summerville Formations (Upper Jurassic)—who, what, where, when?: Geology of the Intermountain West, v. 9, p. 49–114, https://doi.org/10.31711/giw.v9.

Carpenter, K., 2023, Reconstructing the floodplain paleogeography associated with the Quarry River, Dinosaur National Monument, Utah, USA, *in* Kirkland, J.I., Hunt-Foster, R., and Loewen, M., editors, 14th symposium on Mesozoic terrestrial ecosystems and biota: Anatomical Record, v. 306, Supplement 1, p. 65–67.

Carpenter, K., Chure, D., and Kirkland, J.I., editors, 1998,

The Morrison Formation—an interdisciplinary study: Modern Geology, v. 22, p. 1–533; v. 23, p. 1–506.

Cazanacli, D., and Smith, N.D., 1998, A study of morphology and texture of natural levees—Cumberland Marshes, Saskatchewan, Canada: Geomorphology, v. 25, p. 43–55.

Chen, J., Fei, G., Zhao, W., Wang, X., Wang, J., Xu, W., Yang, F., Zong, J., and Chen, X., in press, Blockage characteristics of large wood and its influence on sediment deposition: Social Science Research Network, http://dx.doi.org/10.2139/ssrn.4593638.

Christiansen, E.H., Kowallis, B.J., Dorais, M.J., Hart, G.L., Mills, C.N., Pickard, M., and Parks, E., 2015, The record of volcanism in the Brushy Basin Member of the Morrison Formation—implications for the Late Jurassic of Western North America, *in* Anderson, T.H., Didenko, A.N., Johnson, C.L., Khanchuk, A.I., and MacDonald, J.H., Jr., editors, Late Jurassic margin of Laurasia—a record of faulting accommodating plate rotation: Geological Society of America, Special Paper 513, http://doi:10.1130/2015.2513(11).

Chure, D., Britt, B.B., Whitlock, J.A., and Wilson, J.A., 2010, First complete sauropod dinosaur skull from the Cretaceous of the Americas and the evolution of sauropod dentition: Naturwissenschaften, v. 97, p. 379–391.

Coleman, J.M., and Prior, D.B., 1982, Deltaic environments of deposition, *in* Scholle, P.A., and Spearing, D., editors, Sandstone depositional environments: American Association of Petroleum Geologists Memoir 31, p. 139–178.

Colombera, L., and Mountney, N.P., 2021, Influence of fluvial crevasse-splay deposits on sandbody connectivity—lessons from geological analogues and stochastic modelling: Marine and Petroleum Geology, v. 128, p.105060.

Cope, E.D., 1877, On a carnivorous dinosaur from Dakota Beds of Colorado: U.S. Geological and Geographical Survey Bulletin, v. 3, no. 4, p. 805–806.

Craig, L.C., Holmes, C.N., Cadigan, R.A., Freeman, V.L., Mullens, T.E., and Weir, G.W., 1955, Stratigraphy of the Morrison and related formations, Colorado Plateau region, a preliminary report: U.S. Geological Survey Bulletin, v. 1009-E, p. 125–168.

Craig, L.C., Holmes, C.N., Freeman, V.L., Mullens, T.E., and Weir, G.W., 1977, Map showing thickness of the Morrison Formation and thickness and generalized facies of the members of the Morrison Formation in the Colorado Plateau region, Sheet 1—isopach and facies map of Salt Wash Member of the Morrison Formation: U.S. Geological Survey Open-File Report 77-516, scale 1:1,000,000.

Currie, B.S., 1997, Sequence stratigraphy of nonmarine Jurassic–Cretaceous rocks, central Cordilleran foreland-basin system: Geological Society of America Bulletin, v. 109, p. 1206–1222.

Danise, S., and Holland, S.M., 2018, A sequence stratigraphic framework for the Middle to Late Jurassic of the Sundance seaway, Wyoming—implications for correlation, basin evolution, and climate change: The Journal of Geology, v. 126, p. 371–405.

Dawson, J.C., 1970, The sedimentology and stratigraphy of the Morrison Formation (Upper Jurassic) in northwestern Colorado and northeastern Utah: Madison, University of Wisconsin, Ph.D. dissertation, 125 p.

Dehler, C.M., and Sprinkel, D.A., 2005, Revised stratigraphy and correlation of the Neoproterozoic Uinta Mountain Group, northeastern Utah, *in* Dehler, C.M., Pederson, J.L., Sprinkel, D.A., and Kowallis, B.J., editors, Uinta Mountain geology: Utah Geological Association Publication 33, p. 17–30.

Demko, T.M., Currie, B.S., and Nicoll, K.A., 2004, Regional paleoclimatic and stratigraphic implications of paleosols and fluvial/overbank architecture in the Morrison Formation (Upper Jurassic), Western Interior, USA, *in* Turner, C.E., Peterson, F., and Dunagan, S., editors, Reconstruction of the extinct ecosystem of the Upper Jurassic Morrison Formation: Sedimentary Geology, v. 167, p. 115–135.

Dewey, J.F., Holdsworth, R.E., and Strachan, R.A., 1998, Transpression and transtension zones, *in* Holdsworth, R.E., Strachan, R.A., and Dewey, J.E, editors, Continental transpressional and transtensional tectonics: The Geological Society (London), Special Publication 135, p. 1–14.

Dodson, P., Behrensmeyer, A.K., Bakker, R.T., and McIntosh, J.S., 1980, Taphonomy and paleoecology of the dinosaur beds of the Jurassic Morrison Formation: Paleobiology, v. 6, p. 208–232.

Dunagan, S.P., and Turner, C.E., 2004, Regional paleohydrologic and paleoclimatic settings of wetland/lacustrine depositional systems in the Morrison Formation (Upper Jurassic), Western Interior, USA. *in* Turner, C.E., Peterson, F., and Dunagan, S., editors, Reconstruction of the extinct ecosystem of the Upper Jurassic Morrison Formation: Sedimentary Geology, v. 167, p. 269–296.

Eberth, D.A., and Miall, A.D., 1991, Stratigraphy, sedimen-

tology and evolution of a vertebrate-bearing, braided to anastomosed fluvial system, Cutler Formation (Permian-Pennsylvanian), north-central New Mexico: Sedimentary Geology, v. 72, p. 225–252.

Ehlers, E.G., and Blatt, H., 1982, Petrology—igneous, sedimentary, and metamorphic: New York, W.H Freeman, 732 p.

Erskine, M.C., 2001, Colorado Plateau tectonostratigraphic unit, *in* Erskine, M.C., Faulds, J.E., Bartley, J.M., and Rowley, P.D., editors, The geologic transition, high plateaus to great basin—a symposium and field guide: Utah Geological Association Publication 30, p. 39–58.

Euler, T., and Herget, J., 2012, Controls on local scour and deposition induced by obstacles in fluvial environments: Catena, v. 91, p. 35–46.

Ferguson, R., 2007, Flow resistance equations for gravel-and boulder-bed streams: Water Resources Research, v. 43, no. 5, W05427, p. 1–12, https://doi:10.1029/2006WR005422.

Fiorillo, A.R., 1994, Time resolution at Carnegie Quarry (Morrison Formation), Dinosaur National Monument, Utah; implications for dinosaur paleoecology: Contributions to Geology, University of Wyoming, v. 30, p. 149–156.

Foster, J.R., and Lucas, S.G., editors, 2006, Paleontology and geology of the Upper Jurassic Morrison Formation: New Mexico Museum of Natural History and Science Bulletin 36, 249 p.

Friend, P.F., and Dade, W.B., 2005, Transport modes and grain-size patterns in fluvial basins, *in* Blum, M.D., Marriott, S.B., and Leclair, S.F., editors, Fluvial sedimentology VII: International Association of Sedimentologists Special Publication 35, p. 397–407.

Furquim, S.A.C., Barbiero, L., Graham, R.C., de Queiroz Neto, J.P., Ferreira, R.P.D., and Furian, S., 2010, Neoformation of micas in soils surrounding an alkaline-saline lake of Pantanal wetland, Brazil: Geoderma, v. 158, p. 331–342.

Galli, K.G., 2014, Fluvial architecture element analysis of the Brushy Basin Member, Morrison Formation, western Colorado, USA: Volumina Jurassica, v. 12, no. 2, p. 69–106, https://doi: 10.5604/17313708.1130130.

Gee, C.T., 2023, Elucidating ecological interactions between trees, insects, fungi, and dinosaurs in the Upper Jurassic biota of the Morrison Formation, *in* Kirkland, J.I., Hunt-Foster, R., Loewen, M., editors, 14th Symposium on Mesozoic terrestrial ecosystems and biota: Anatomical Record, v. 306, Supplement 1, p. 109–111.

Gilmore, C.W., 1936, Osteology of *Apatosaurus*, with special reference to specimens in the Carnegie Museum: Memoirs of the Carnegie Museum, v. 11, p. 175–301.

Good, S.C., 2004, Paleoenvironmental and paleoclimatic significance of freshwater bivalves in the Upper Jurassic Morrison Formation, Western Interior, USA., *in* Turner, C.E., Peterson, F., and Dunagan, S., editors, Reconstruction of the extinct ecosystem of the Upper Jurassic Morrison Formation: Sedimentary Geology, v. 167, p. 163–176.

Gregson, J.D., Chure, D.J, Sprinkel, D.A, and Hunt-Foster, R., 2024, Geology of Dinosaur National Monument, Utah-Colorado, *in* Sprinkel, D.A., Chidsey, T.C., Jr., Anderson, P.B., and Willis, G.C., editors, Geology of Utah's parks and monuments (fourth edition): Utah Geological Association Publication 28, p. 217–249.

Hajek, E.A., and Wolinsky, M.A., 2012. Simplified process modeling of river avulsion and alluvial architecture—connecting models and field data: Sedimentary Geology, v. 257, p. 1–30.

Hansen, W.R., 1986a, History of faulting in the eastern Uinta Mountains, Colorado and Utah, *in* Stone, D.S., editor, New interpretations of northwest Colorado geology: Rocky Mountain Associations of Geologists Symposium, p. 5–17.

Hansen, W.R., 1986b, Neogene tectonics and geomorphology of the eastern Uinta Mountains in Utah, Colorado, and Wyoming: U.S. Geological Survey Professional Paper 1356, 78 p.

Hansen, W.R., Rowley, P.D., and Carrara, P.E., 1983, Geologic map of Dinosaur National Monument and vicinity, Utah and Colorado: U.S. Geological Survey Miscellaneous Investigation Series, Map I-1407, scale 1:50,000, 1 sheet.

Hasiotis, S.T., 2004, Reconnaissance of Upper Jurassic Morrison Formation ichnofossils, Rocky Mountain region, USA—paleoenvironmental, stratigraphic, and paleoclimatic significance of terrestrial and freshwater ichnocoenoses, *in* Turner, C.E., Peterson, F., and Dunagan, S., editors, Reconstruction of the extinct ecosystem of the Upper Jurassic Morrison Formation: Sedimentary Geology, v. 167, p. 177–268.

Hayden, A.T., and Lamb, M.P., 2020, Fluvial sinuous ridges of the Morrison Formation, USA—meandering, scarp retreat, and implications for Mars: Journal of Geophysi-

cal Research—Planets, v. 125, p.e2020JE006470, https://doi.org/10.1029/2020JE006470.

Heller, P.L., and Paola, C., 1996, Downstream changes in alluvial architecture; an exploration of controls on channel-stacking patterns: Journal of Sedimentary Research, v. 66, p. 297–306.

Heller, P.L., Ratigan, D., Trampush, S., Noda, A., McElroy, B., Drever, J. and Huzurbazar, S., 2015, Origins of bimodal stratigraphy in fluvial deposits—an example from the Morrison Formation (Upper Jurassic), Western USA: Journal of Sedimentary Research, v. 85, p. 1466–1477.

Holland, S.M., and Wright, S.N., 2020, The unconformity that isn't—a sequence-stratigraphic reinterpretation of the J-5 unconformity and the Redwater–Windy Hill–Morrison transition in Wyoming, USA: Journal of Geology, v. 128, p. 247–274.

Hubert, J.F., Panish, P.T., Chure, D.J., and Prostak, K.S., 1996, Chemistry, microstructure, petrology, and diagenetic model of Jurassic dinosaur bones, Dinosaur National Monument, Utah: Journal of Sedimentary Research, v. 66, p. 531–547.

Hudson, P.F., 2005, Natural levees, *in* Trimble, S.W., editor, Encyclopedia of water science: Boca Raton, CRC Press, p. 763–767.

Huerta, P., Armenteros, I., and Silva, P.G., 2011, Large-scale architecture in non-marine basins—the response to the interplay between accommodation space and sediment supply: Sedimentology, v. 58, p. 1716–1736.

Johnston, G.H., David, S.R., and Edmonds, D.A., 2019, Connecting fluvial levee deposition to flood-basin hydrology: Journal of Geophysical Research—Earth Surface, v. 124, p. 1996–2012.

Johnston, R.E., and Yin, A., 2001, Kinematics of the Uinta fault system (southern Wyoming and northern Utah) during the Laramide orogeny: International Geology Review, v. 43, p. 52–68.

Keller, W.D., 1958, Glauconitic mica in the Morrison Formation in Colorado, *in* Swineford, A., editor, National Conference on Clays and Clay Minerals, 5th Proceedings: National Academy of Sciences–National Research Council Publication, p. 120–129.

Keller, W.D., 1962, Clay minerals in the Morrison Formation of the Colorado Plateau: U.S. Geological Survey Bulletin, v. 1150, 90 p.

Kirkil, G., and Constantinescu, G., 2010, Flow and turbulence structure around an in-stream rectangular cylinder with scour hole: Water Resources Research, v. 46, w11549, 20 p., https://doi:10.1029/2010WR009336.

Kirkland, J.I., and Madsen, S.K., 2007, The Lower Cretaceous Cedar Mountain Formation, eastern Utah—the view up an always interesting learning curve, *in* Lund, W.R., editor, Field guide to geological excursions in southern Utah: Geological Society of America Rocky Mountain Section 2007 Annual Meeting, Grand Junction Geological Society and Utah Geological Association Publication 35, 108 p.

Kirkland, J. I., Suarez, M., Suarez, C., and Hunt-Foster, R., 2016, The Lower Cretaceous in east-central Utah—the Cedar Mountain Formation and its bounding strata: Geology of the Intermountain West, v. 3, p. 101–228.

Kjemperud, A.V., Schomacker, E.R., and Cross, T.A., 2008, Architecture and stratigraphy of alluvial deposits, Morrison Formation (Upper Jurassic), Utah: American Association of Petroleum Geologists Bulletin, v. 92, p. 1055–1076.

Kraus, M.J. 1987, Integration of channel and floodplain suites; II, vertical relations of alluvial paleosols: Journal of Sedimentary Research, v. 57, p. 602–612, https://doi.org/10.1306/212F8BB6-2B24-11D7-8648000102C1865D.

Labourdette, R., 2011, Stratigraphy and static connectivity of braided fluvial deposits of the lower Escanilla Formation, south central Pyrenees, Spain: American Association of Petroleum Geologists Bulletin, v. 95, p. 585–617.

Lawton, R., 1976, Taphonomy and paleohydraulics: Morrison Formation—northeastern Utah: Santa Cruz, University of California, senior thesis, 68 p.

Lawton, R., 1977, Taphonomy of the dinosaur quarry, Dinosaur National Monument: Rocky Mountain Geology, v. 15, p. 119–126.

Lazar, O.R., Bohacs, K.M., Schieber, J., Macquaker, J.H.S., and Demko, T.M., 2022, Mudstone nomenclature, *in* Bohacs K.M., and Lazar, O.R., editors, Sequence stratigraphy—applications to fine-grained rocks: American Association of Petroleum Geologists Memoir 126, p. 21–34.

Lewin, J., and Ashworth, P.J., 2014, The negative relief of large river floodplains: Earth-Science Reviews, v. 129, p. 1–23.

Lewin, J., Ashworth, P.J., and Strick, R.J., 2017, Spillage sedimentation on large river floodplains: Earth Surface Processes and Landforms, v. 42, no. 2, p. 290–305.

Litwin, R.J., Turner, C.E., and Peterson, F., 1998, Palynological

evidence on the age of the Morrison Formation, Western Interior U.S., *in* Carpenter, K., Chure, D., and Kirkland, J.I., editors, The Morrison Formation—an interdisciplinary study: Modern Geology, v. 22, p. 297– 319.

Lucas, S.G., and Kirkland, J.I., 1998, Preliminary report on conchostraca from the Upper Jurassic Morrison Formation, Western United States, *in* Carpenter, K., Chure, D., and Kirkland, J.I., editors, The Morrison Formation—an interdisciplinary study: Modern Geology, v. 22, p. 415–422.

Lynds, R., and Hajek, E., 2006, Conceptual model for predicting mudstone dimensions in sandy braided-river reservoirs: American Association of Petroleum Geologists Bulletin, v. 90, p. 1273–1288.

Lynds, R.M., Mohrig, D., Hajek, E.A., and Heller, P.L., 2014, Paleoslope reconstruction in sandy suspended-load dominant rivers: Journal of Sedimentary Research, v. 84, p. 825–836.

Macquaker, J.H., and Adams, A.E., 2003, Maximizing information from fine-grained sedimentary rocks—an inclusive nomenclature for mudstones: Journal of Sedimentary Research, v. 73, p. 735–744.

Maidment, S.C., and Muxworthy, A., 2019, A chronostratigraphic framework for the Upper Jurassic Morrison Formation, Western USA: Journal of Sedimentary Research, v. 89, p. 1017–1038.

Maity, H., and Mazumder, B.S., 2014, Experimental investigation of the impacts of coherent flow structures upon turbulence properties in regions of crescentic scour: Earth Surface Processes and Landforms, v. 39, p. 995–1013.

Marsh, O.C., 1877, Notice of a new and gigantic dinosaur: American Journal of Science, Third Series, v. 15, p. 87–88.

Meunier, A., 2005, Clays in sedimentary environments, *in* Meunier, A., editor, Clays: New York, Springer, p. 295-327.

Meyers, V.L., Matthews, N.A., and Breithaupt, B.H., 2009, Late Jurassic pterosaur and sauropod tracks from the Seminoe Reservoir Tracksite, Wyoming, *in* Foss, S.L., Calvin, J.L., Brown, T., Kirkland, J.I., and Santucci, V.L., editors, Proceedings of the Eighth Conference on Fossil Resources Abstract: Bureau of Land Management, Utah State Office, Salt Lake City, 161 p.

Meyers, V.L., and Breithaupt, B.H., 2014, *Pteraichnus saltwashensis* tracks and trackways in the Upper Jurassic Windy Hill Sandstone of Wyoming: New Mexico Museum of Natural History and Science Bulletin 62, p. 235–248.

Miall, A.D., 1977, A review of the braided-river depositional environment: Earth Science Reviews, v. 13, p. 1–62.

Miall, A.D., 2014, Fluvial depositional systems: Cham, Springer International Publishing, 316 p.

Millard, C., Hajek, E., and Edmonds, D.A., 2017, Evaluating controls on crevasse-splay size—implications for floodplain-basin filling: Journal of Sedimentary Research, v. 87, p. 722–739.

Mullens, T.E., and Freeman, V.L., 1957, Lithofacies of the Salt Wash Member of the Morrison Formation, Colorado Plateau: Geological Society of America Bulletin, v. 68, p. 505–526.

Munsell, 2009, Rock-color chart: Grand Rapids, Michigan, USA, 9 p.

Muto, T., and Steel, R.J., 2000, The accommodation concept in sequence stratigraphy—some dimensional problems and possible redefinition: Sedimentary Geology, v. 130, p. 1–10.

Nienhuis, J.H., Törnqvist, T.E., and Esposito, C.R., 2018, Crevasse splays versus avulsions—a recipe for land building with levee breaches: Geophysical Research Letters, v. 45, p. 4058–4067, https://doi.org/10.1029/2018GL077933.

Odin, G.S., and Létolle, R., 1978, Glauconitic and close or mistaken aspects; sedimentological significance: Bulletin de la Société Géologique de France, v. 20, p. 553–558.

Odin, G.S., and Matter, A., 1981, De glauconiuarum origine: Sedimentology, v. 28, p. 611–641.

O'Sullivan, R.B., 1984, The base of the Upper Jurassic Morrison Formation in east-central Utah: U.S. Geological Survey Bulletin, v. 1561, 17 p.

Owen, D.E., Turner-Peterson, C.E., and Fishman, N.S., 1989, X-ray diffraction studies of the <0.5 mm fraction from the Brushy Basin Member of the Upper Jurassic Morrison Formation, Colorado Plateau: U.S. Geological Survey Bulletin, v. 1808-G, p. G1–G25.

Owen, A., Nichols, G.J., Hartley, A.J., Weissmann, G.S., and Scuderi, L.A., 2015, Quantification of a distributive fluvial system—the Salt Wash DFS of the Morrison Formation, SW USA: Journal of Sedimentary Research, v. 85, p. 544–561.

Owen, A., Nichols, G.J., Hartley, A.J., and Weissmann, G.S., 2017, Vertical trends within the prograding Salt Wash distributive fluvial system, SW United States: Basin Research, v. 29, p. 64–80.

Paola, C., and Mohrig, D., 1996, Palaeohydraulics revisited—palaeoslope estimation in coarse-grained braided rivers: Basin Research, v. 8, p. 243–254.

Peterson, F., 1980, Sedimentology of the uranium-beating Salt Wash Member and Tidwell Unit of the Morrison Formation in the Henry and Kaiparowits basins, Utah, *in* Picard, M.D., editor, Henry Mountains symposium: Utah Geological Association Publication 6, p. 305–322.

Peterson, F., 1984, Fluvial sedimentation on a quivering craton—influence of slight crustal movements on fluvial processes, Upper Jurassic Morrison Formation, western Colorado Plateau: Sedimentary Geology, v. 38, p. 21–49.

Peterson, F., 1988, Stratigraphy and nomenclature of Middle and Upper Jurassic rocks, western Colorado Plateau, Utah and Arizona—revisions to stratigraphic nomenclature of Jurassic and Cretaceous rocks of the Colorado Plateau: U.S. Geological Survey Bulletin, v.1633-B, p. B13–B56.

Peterson, F., 1994, Sand dunes, sabkhas, streams, and shallow seas; Jurassic paleogeography in the southern part of the Western Interior basin, *in* Caputo, M.V., Peterson, J.A., and Franczyk, K.J., editors, Mesozoic systems of the Rocky Mountain region, USA: Society for Sedimentary Geology (SEPM), Rocky Mountain Section Special Publication, p. 233–272.

Phillips, J.D., 2012, Log-jams and avulsions in the San Antonio River delta, Texas: Earth Surface Processes and Landforms, v. 37, p. 936–950.

Pinto, L., Muñoz, C., Nalpas, T., and Charrier, R., 2010, Role of sedimentation during basin inversion in analogue modelling: Journal of Structural Geology, v. 32, p. 554–565.

Pipiringos, G.N., 1968, Correlation and nomenclature of some Triassic and Jurassic rocks in south-central Wyoming: U.S. Geological Survey Professional Paper 594-D, 26 p.

Potter, P.E., Maynard, J.B., and Depetris, P.J., 2005, Mud and mudstones—introduction and overview: Berlin, Germany, Springer-Verlag, 297 p.

Rahman, M.M., Howell, J.A., and MacDonald, D.I., 2022, Quantitative analysis of crevasse-splay systems from modern fluvial settings: Journal of Sedimentary Research, v. 92, p.751–774.

Retallack, G.J., 1997, Dinosaurs and dirt, *in* Wolberg, D., and Stump, E., editors, Dinofest II: Philadelphia Academy of Sciences, Philadelphia, p. 345–359.

Robinson, J.W., and McCabe, P.J., 1998, Evolution of a braided river system—the Salt Wash Member of the Morrison Formation (Jurassic), in southern Utah, *in* Shanley, K.W., and McCabe, P.J., editors, Relative role of eustasy, climate and tectonism in continental rocks: Society for Sedimentary Geology (SEPM) Special Publication, v. 59, p. 93–107.

Rowley, P.D., Kinney, D.M., and Hansen, W.R., 1979, Geologic map of the Dinosaur Quarry quadrangle, Uintah County, Utah: U.S. Geological Survey Geologic Quadrangle Map GQ-1513, scale 1:24,000, 1 p.

Sambrook Smith, G.H., Ashworth, P.J., Best, J.L., Woodward, J., and Simpson, C.J., 2006, The sedimentology and alluvial architecture of the sandy braided South Saskatchewan River, Canada: Sedimentology, v. 53, p. 413–434.

Sassi, W., Guiton, M.L.E., Leroy, Y.M., Daniel, J.M., and Callot, J.P., 2012, Constraints on bed scale fracture chronology with a FEM mechanical model of folding—the case of Split Mountain (Utah, USA): Tectonophysics, v. 576, p. 197–215.

Schoeneberger, P.J., Wyosocki, D.A., Benham, E.C., and Soil Survey Staff, 2012, Field book for describing and sampling soils, version 3.0: Lincoln, Nebraska, National Research Conservation Service, National Soil Survey Center, 300 p.

Schudack, M.E., Turner, C.E., and Peterson, F., 1998, Biostratigraphy, paleoecology and biogeography of charophytes and ostracodes from the Upper Jurassic Morrison Formation, Western Interior, USA, *in* Carpenter, K., Chure, D., and Kirkland, J.I., editors, The Morrison Formation—an interdisciplinary study: Modern Geology, v. 22, p. 379–414.

Sear, D.A., Millington, C.E., Kitts, D.R., and Jeffries, R., 2010, Logjam controls on channel—floodplain interactions in wooded catchments and their role in the formation of multi-channel patterns: Geomorphology, v. 116, p. 305–319.

Sharma, N., Whittaker, A.C., Adatte, T., and Castelltort, S., 2023, Water discharge and sediment flux intermittency in the fluvial Escanilla Formation, Spain—implications for changes in stratigraphic architecture: Nature, Scientific Reports, v. 10, p. 245–259.

Spreitzer, G., Tunnicliffe, J., and Friedrich, H., 2021, Ef-

fects of large wood (LW) blockage on bedload connectivity in the presence of a hydraulic structure: Ecological Engineering, v. 161, 106156, p. 1–17, https://doi.org/10.1016/j.ecoleng.2021.106156.

Sprinkel, D.A., 2014, The Uinta Mountains—a tale of two geographies and more: Utah Geological Survey, Survey Notes, v. 46, no. 3, p. 1–4.

Sprinkel, D.A., 2019, The curious case of the Green River in the Uinta Mountains: Utah Geological Survey, Survey Notes, v. 51, no. 3, p. 9–11

Sprinkel, D.A., Bennis, M., Gray, D.E., and Gee, C.T., 2019, Stratigraphic setting of fossil log sites in the Morrison Formation (Upper Jurassic) near Dinosaur National Monument, Uintah County, Utah, USA: Geology of the Intermountain West, v. 6, p. 61–76.

Sprinkel, D.A., Madsen, S.K., Kirkland, J.I., Waanders, G.L., and Hunt, G.J., 2012, Cedar Mountain and Dakota Formations around Dinosaur National Monument—evidence of the first incursion of the Cretaceous Western Interior Seaway into Utah: Utah Geological Survey Special Study 143, 21 p.

Steiner, M.B., 2003, A cratonic Middle Jurassic paleopole—Callovian-Oxfordian stillstand (J-2 cusp), rotation of the Colorado Plateau, and Jurassic North American apparent polar wander: Tectonics, v. 22, 1020, https://doi:10.1029/2001TC001284.

Stokes, W.L., 1944, Morrison Formation and related deposits in and adjacent to the Colorado Plateau: Bulletin of the Geological Society of America, v. 55, p. 951–992.

Stone, D.S., 1993, Tectonic evolution of the Uinta Mountains—palinspastic restoration of a structural cross section along latitude 109° 15', Utah: Utah Geological and Mineral Survey Miscellaneous Publication 93-8, 19 p.

Trampush, S.M., McElroy, B.J., and Heller, P., 2013, Application of paleoslope reconstruction method to the Jurassic Morrison Formation in southeast Utah [abs.]: American Geophysical Union, Fall Meeting Abstracts, p. EP53B-0830.

Trujillo, K.C., 2006, Clay mineralogy of the Morrison Formation (Upper Jurassic–?Lower Cretaceous), and its use in long distance correlation and paleoenvironmental analysis, *in* Foster, J.R., and Lucas, S.G., editors, Paleontology and geology of the Upper Jurassic Morrison Formation: New Mexico Museum of Natural History and Science Bulletin 36, p. 17–23.

Trujillo, K.C, and Kowallis, B.J., 2015, Recalibrated legacy $^{40}Ar/^{39}Ar$ ages for the Upper Jurassic Morrison Formation, Western Interior, U.S.A.: Geology of the Intermountain West, v. 2, p. 1–8.

Turner, C.E., and Peterson, F., 1991, Sedimentology and stratigraphy of the Morrison Formation in Dinosaur National Monument: University of Wyoming–National Park Service Research Center Annual Report, v. 15, art. 17, 3 p.

Turner, C.E., and Peterson, F., 1992a, Sedimentology and stratigraphy of the Morrison Formation in Dinosaur National Monument, Utah and Colorado: Annual Report to the National Park Service, 85 p.

Turner, C.E., and Peterson, F., 1992b, Sedimentology and stratigraphy of the Morrison Formation in Dinosaur National Monument: The University of Wyoming–National Parks Service Research Station Annual Reports, v. 16, p. 86–91.

Turner, C.E., and Peterson, F., 1993, Fluvial sedimentology of the Carnegie Quarry, Upper Jurassic Morrison Formation, Dinosaur National Monument, Utah [abs.]: Fifty-Third Annual Meeting, Society of Vertebrate Paleontology, v. 13, no. 3, p. 60A–61A.

Turner, C.E., and Peterson, F., editors, 1998, The Morrison Formation extinct ecosystems project final report: National Park Service Technical Information Center, 594 p.

Turner, C.E., and Peterson, F., 1999, Biostratigraphy of dinosaurs in the Upper Jurassic Morrison Formation of the Western Interior, U.S.A., *in* Gillette, D.D., editor, Vertebrate paleontology of Utah: Utah Geological Survey Miscellaneous Publication 99-1, p. 77–114.

Turner, C.E., Peterson, F., and Dunagan, S., 2004, Reconstruction of the extinct ecosystem of the Upper Jurassic Morrison Formation: Sedimentary Geology, v. 167, p. 111–355.

U.S. Geological Survey, 1899, David City quadrangle topographic sheet, scale: 1:125,000, https://ngmdb.usgs.gov/ht-bin/tv_browse.pl?id=6f9c0252b070c3b9c7edac48f8f-8d49a.

Untermann, G.E., and Untermann, B.R., 1954, Geology of Dinosaur National Monument and vicinity, Utah-Colorado: Utah Geological and Mineralogical Survey, Bulletin 42, 229 p.

Velde, B., 2014, Green clay minerals, *in* Mackenzie, F.T., editor, Sediments, diagenesis and sedimentary rocks: Treatise on Geochemistry, v. 9, p. 351–364.

Walker, L.R., and Sharpe, J.M., 2010, Ferns, disturbance and succession, *in* Mehltreter, K., Walker, L.R., and Sharpe, J.M., editors, Fern ecology: Cambridge University Press, 444 p.

Walker, M.V., 1943, Part 1 – General studies and investigations—a report on studies and investigations at Dinosaur National Monument relative to an interpretative and museum development program: Unpublished report, National Park Service, 21 p.

Walker, R.G., and Cant, D.J., 1984, Sandy fluvial systems—facies models 3: Geoscience Canada Reprint Series, v. 1, p. 71–89.

Warburton, J., 1996, Active braidplain width, bed load transport and channel morphology in a model braided river: Journal of Hydrology (New Zealand), v. 35, p. 259–285.

Weissmann, G.S., Hartley, A.J., Scuderi, L.A., Nichols, G.J., Davidson, S.K., Owen, A., Atchley, S.C., Bhattacharyya, P., Chakraborty, T., Ghosh, P., Nordt, L.C., Michel, L., and Tabor, N.J., 2013, Prograding distributive fluvial systems—geomorphic models and ancient examples, *in* Dreise, S.G., Nordt, L.C., and McCarthy, P.J., editors, New frontiers in paleopedology and terrestrial paleoclimatology: Society for Sedimentary Geology (SEPM) Special Publication 104, p. 131–147.

Williams, N.C., 1953, Late pre-Cambrian and early Paleozoic geology of western Uinta Mountains, Utah: American Association of Petroleum Geologists Bulletin, v. 37, p. 2734–2742.

Worden, R.H., and Morad, S., 2000, Quartz cementation in oil field sandstones—a review of the key controversies, *in* Worden, R.H., and Morad, S., editors, Quartz cementation in sandstones: International Association of Sedimentologists Special Publication, v. 29, p. 1–20.

Wroblewski, A.F.J., and Morris, E.A., 2022, Unconformity generation and the shift from storm-dominated to tide-dominated processes in a Jurassic retroarc foreland basin—insights from ichnology: The Depositional Record, v. 9, p. 253–299.

APPENDIX 1

Appendix 1 is attached to the PDF. It includes photographs and photomicrographs showing details of the various lithologies applicable to this study. Grain and fossil content are included. Details included in the Appendix 1 figure captions are presented in chart form in Appendix 2.

APPENDIX 2

Appendix is attached to the PDF amd is a spreadsheet summarizing details of Appendix 1 figure captions.